A SOFT-BODY INTERCONNECT FOR

SELF-RECONFIGURABLE MODULAR ROBOTS

by

Min Ying

A Thesis

Submitted to the Faculty

of the

WORCESTER POLYTECHNIC INSTITUTE
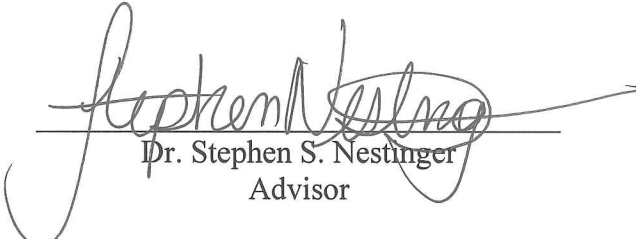
in partial fulfillment of the requirements for the

Degree of Master of Science

in
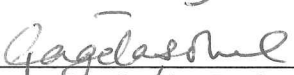
Mechanical Engineering

April 2014

APPROVED:

_____   _____
Dr. Stephen S. Nestinger   Dr. Gregory S. Fischer
Advisor   Committee Member

_____   _____
Dr. Cagdas D. Onal   Dr. Raghvendra Cowlagi
Committee Member   Graduate Representative

Abstract

Disaster support and recovery generally involve highly irregular and dangerous environments. Modular robots are a salient solution to support search and rescue efforts but are still limited to do their reliance on a rigid structure design. To enhance flexibility and resilience to damage, a soft-body interconnection mechanism for self-reconfigurable modular robotic systems has been developed. The soft-body interconnection mechanism utilizes elastomeric polymers instead of a rigid body. Hence, it is capable of deforming under extreme loads without damage. This thesis presents the work completed towards the realization of a soft-body interconnection mechanism. The functional requirements of the soft-body mechanism were broken down into two separate modules for extension and capture. An initial simulation demonstrated the inability of using a simulated model made of hypo-elastic materials as a basis for design. Hence, an iterative design process was used to develop an initial extension and capture soft-body mechanisms that conformed to the desired performance parameters. An empirical study which varied multiple structural parameters was then completed with the initial extension and capture soft-body mechanisms as a basis for the modified designs. The data from the study was correlated with measured performance data with resulted in diagrams useful for the optimal design of soft-body extension and capture mechanisms. The use of the diagrams for design was demonstrated in the design and development of a soft-body interconnection mechanism for an in-house designed small hard shell modular robot system.

Acknowledgements

Firstly, my deepest gratitude goes to my thesis advisor, Prof. Stephen S. Nestinger, for all of the time and effort he has put into helping me edit my thesis and for his invaluable support, guidance, and patience throughout this project.

I would like to thank Prof. R. Cowlagi, Prof. G. Fischer and Prof. C. Onal for being my defense committee members and offering professional suggestions to my thesis.

Thanks to Prof. C. Onal, Prof. Hou and Dr. Hera that helped me to solve countless difficulties I met during the research.

The big thanks and warm feelings are given to the staff of ME department and my lab-mates who have been encouraging me, accompanying me and helping me at all time.

Finally, the greatest thanks and deepest love are presented to my parents. There love and support which accompany me at every time every moment is always becoming the infinite power I have both physically and spiritually.

Table of Contents

List of Figures

viii

List of Tables

Chapter 1

Introduction

In the aftermath of unfortunate urban disasters, including earthquakes, hurricanes, fires or even terrorist attacks, survivors may be injured, trapped or unconsciousness and unable to get to safety or seek medical attention on their own. Under these circumstances, the main priority for Urban Search and Rescue teams is to quickly find the survivors before they reach critical condition. Unfortunately, the environment is extremely unstructured and chaotic with rubble scattered throughout. Due to the dangers or structural collapse and other safety concerns, it is best not to send humans into these environments. Instead of putting more humans at risk, robotic systems can play an integral part in these types of emergency response scenarios where time is critical and the environment is highly irregular. Among various robotic systems, the reconfigurable modular robot system is a salient solution since a modular approach enables mobile robots to reconfigure, which is

essential for tasks that are difficult for fixed-shape robots, let alone humans. Introducing robotic systems into search and rescue operations, especially reconfigurable modular robot systems, can greatly benefit search and rescue support teams, provide an opportunity for robots to play a pivotal support role and improve the level of civil and military technology.

Most modular robotic systems are built with rigid structures and interconnection mechanisms. However, robots operating in treacherous environments can be heavily damaged due to falling concrete, high temperature or heavy dust. Hence, it is desirable to have compliant, low cost and easily reproducible robotic systems. With the development of soft-body robotic technologies in recent years[1][2][3][4], there is a high potential to intersect the concept of modular robotic systems with soft-body materials to produce a robotic system capable of modifying their overall structural configuration while being able to maneuver through highly cluttered and constrained environments. The soft-body robots have certain advantage of low costs [5], simple manufacturing process [6] and though the soft material has a lower stiffness than metal, the soft material can reduce the damage of impact with obstacles as well as other robots [7].

1.1   Modular Robots

Indoor robotics systems are usually constrained by their programming and structural geometry. They repeat their tasks in a well-defined and structured environment. For robots operating outdoors, the ability to change their shape is of great benefit due to the unpredictable environment. Self-reconfiguring modular robots form a cluster of robotic systems composed of multiple, simple homogeneous or heterogeneous units that can

reconfigure to change the overall cluster structure. They also have self-repair functionality in which the system is able to determine if any defective component exists within the cluster and replace them with new units. These kinds of novel features are expected to have various advantages for operations such as rescue, search, transportation and maintenance in unstructured environments. Over the last two decades, various types of modular reconfigurable robot systems have been prototyped and tested [8][9][10][11][12].

Reconfigurable robot systems are generally classified into three architectures [13]: chain, lattice, and mobile. In Chain Architectures, the modular robots connect together in a chain shape. Each chain attaches to the other modules at one or more points. Some locomotion of chain robots has already been achieved such as slithering like a snake [14], rolling like a tank tread or walking like a spider [15]. In the Lattice Architecture, the modular robots are arranged and connect by moving into position on a virtual cubic or hexagonal grid. Lattice Architectures usually offer simpler planning and control since the modules may only move to neighboring positions instead of any arbitrary position. In the Mobile Architecture, the modular robots can attach and detach themselves, and connect at new locations to form new configurations such as complex chains or lattices.

Self-reconfiguring modular robots comprise of several to potentially millions of modules. These kinds of systems, like cells in a human body, are few in type but many in number. They provide three key features: versatility, robustness, and low cost [13]. The versatility is easy to witness: a modular system holds tens or hundreds of modules and

may contain thousands of possible configurations. However, to put them together as a useful system is the key point. The complexity of programming and control issues due to the coordination and collaboration between every unit in the system should also be considered. Since the modular robots are interchangeable in the system, the robustness of modular robot system is initially high. However, the overall number of modules is a factor: the more of them there are, the more likely some of them may fail. One main cost advantage of self-reconfiguring modular robots is mass production of just one or a few robot types, which lowers manufacturing costs. Another is dividing complex machines into dozens of simple units, saving time and human resources in the design process.

1.2 Soft Robotics

Conventional robotic systems usually made of rigid materials such as steel and aluminum and are exploited in many successful applications [16][17][18]. However, the study of soft bodied robots, which generally make use of soft, elastic, and flexible materials, are now drawing more attention. Over the last 20 years, researchers have developed soft robots that provide new capabilities relative to traditional hard robots [19][20][21][22][23]. The most commonly used hard robots have multiple flexible joints connected by stiff links. Each joint provides one degree of freedom: either simple rotation or translation [24]. These robots usually perform limited actions with high precision with the help of advanced sensors and feedback control loops in well-defined environments. Meanwhile, soft robots have distributed deformation with a theoretically infinite number of degrees of freedom. This leads to a hyper-redundant configuration space wherein the

robot tip can attain every point in the three-dimensional workspace with an infinite number of robot shapes or configurations [25].

Soft robots have additional advantages over hard robots, such as displaying large strain deformation in normal operation which allow them to squeeze through openings smaller than their nominal dimensions, and generating little resistance to compressive forces which reduces potential damage when contacting obstacles [7]. These factors make them ideal to maneuver through highly cluttered and constrained environments.

1.3 Related Work

This section introduces some related work on reconfigurable mechanisms for modular robots and the current development, simulation and actuation of soft-body robots.

1.3.1 Mechanism for Self-Reconfigurable Modular Robots

Many kinds of modular robots have been developed. However, only a few reconfigurable mechanism types have been studied.
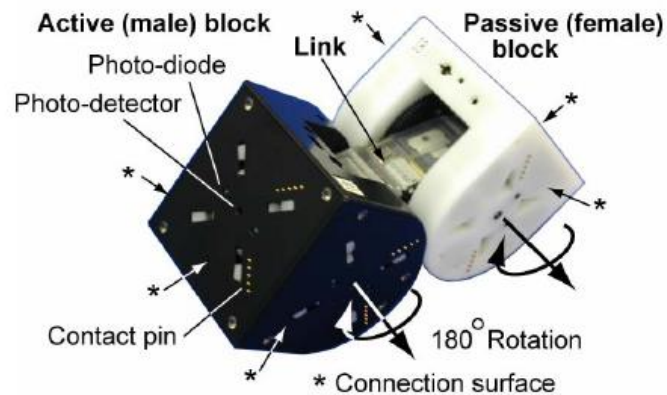
Figure 1: The M-TRAN III module [26]

5

In general, reconfigurable modular robots use a lock-like mechanism to interconnect robot modules. One example is M-TRAN [26], shown in Figure 1. An M-TRAN III module is comprised of two blocks and one link. Each block has three connection surfaces. The two blocks differ in gender and a connection surface of an active (male) block can connect mechanically with a passive (female) block. The mechanical connector is designed based on latch connectors. There are four hooks that extend from any of the three surfaces of the active block and hold another module at the surface of its passive block. The active block has three such mechanisms, each driven by a DC motor.
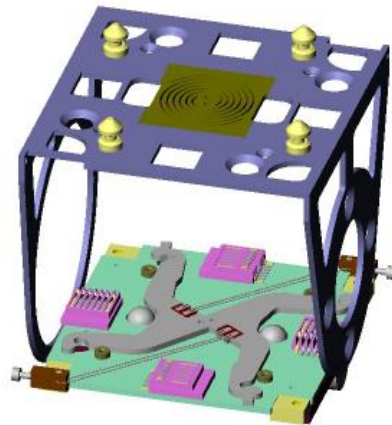
Figure 2: A rendering of back side of connection plate of the PolyBot G2 [27]

Another example is PolyBot, the modular robot being developed at Xerox PARC [27], which is a chain base reconfigurable robot. It has grooved pins and holes that repeat at intervals about the center on the surface and electromechanical latches under software control protruding from the opposite face. The connection surface is hermaphroditic. Hence, any connection surface can mate with another connection surface. This varies from some other reconfigurable robots, like M-TRAN, where attaching is conditional due

to having the gender based module interfaces. With PolyBot, when two modules are attached together, the grooved pins on one plate penetrate through the holes in the other plate. The hook-like latch is engaged in the groove on the pin to lock the modules rigidly together. The structure of the latch is quite simple as shown in Figure 2. It rotates about the center of the interface and has four legs which engage the grooves of the pins and hold them tight. There are two pieces of Shape Memory Alloy (SMA) wire mechanically connected to latch plate. When the wires are heated, they will contract and cause the latch to rotate. Then the latch will loosen the hold of the pins and the detaching process will be complete.
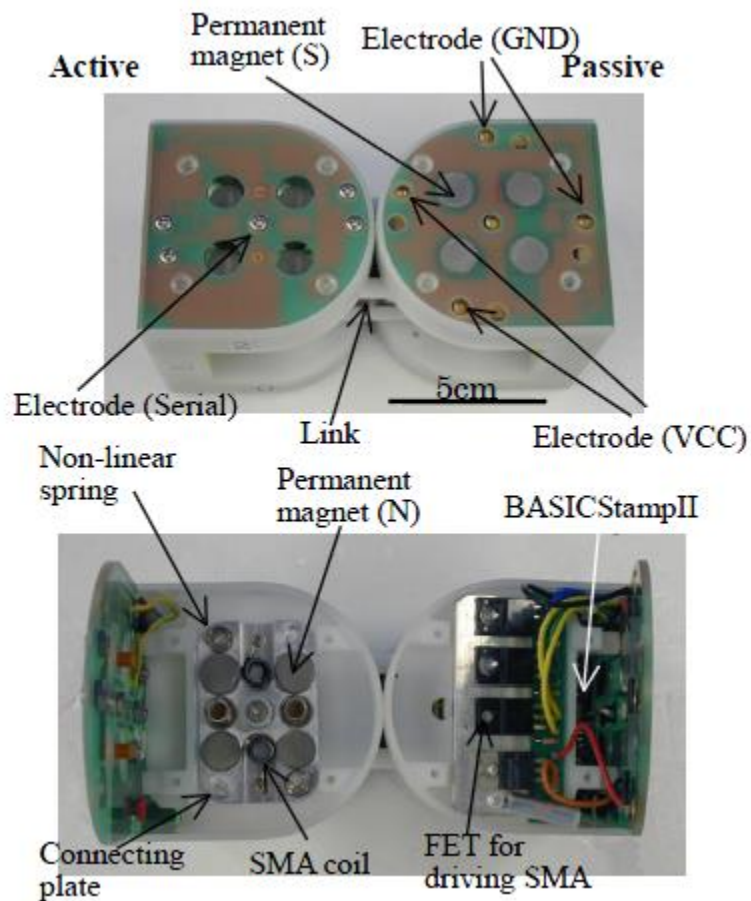
Figure 3: Photos of Appearance and Inner Structure of M-TRAN II [28]

7

Another interconnection method uses magnets instead of latch mechanisms. Figure 3 shows the appearance of the outer and inner structure of another kind of module robot, the M-TRAN II [28]. The active part includes the connecting mechanism. The connecting mechanism is composed of SMA coils and four permanent magnets (N poles on the surface), which are fixed on the connecting plate. The passive parts contain another four permanent magnets (S poles on the surface). The eight magnets contribute to the attachment between modular robots. Modular detachment is similar to PolyBot, achieved by heating SMA coils.

1.3.2   Soft Robots

Although soft robot technology is still immature, there has been an increasing interest in the investigation and exploration of this field. For example, a number of researchers have been studying the physical characteristic of these unconventional materials [29][30]. The newly developed soft materials, sensors and actuators were then integrated into various kinds of robots [31]. GoQBot [32], shown in Figure 4a, is a soft material robot capable of rapidly curling its body into a wheel-like structure for a ballistic rolling locomotion inspired by caterpillars. The robot has a composite body consisting of several mixtures of silicone rubbers and shape memory alloy which is used to control the body shapes. A Harvard University team created an octopus arm shown in Figure 4b driven by pneumatic actuators. The tentacle can complete multiple jobs with different embedded functionality installed on its tip [33]. The goal of the FILOSE robot [1], shown in Figure 4c, is to gain a better understanding of the principles underlying fish locomotion and sensing. It has a

8

continuous flexible body whose morphology and material characteristics are such that a minimal set of control parameters are sufficient to achieve various modes of locomotion.
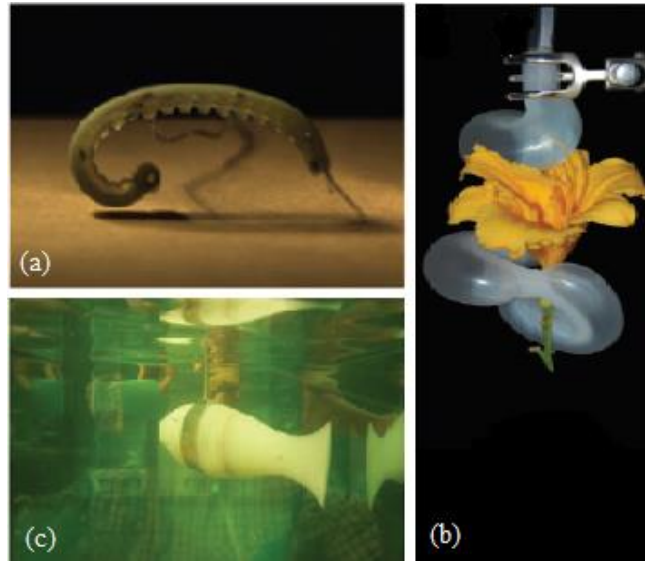
Figure 4: Example of Soft Robots. (a) GoQBot [32], (b) Octopus Arm [33], and (c) FILOSE [1]

F. Ilievski et al. created a soft body structure with embedded pneumatic networks (PneuNets) of channels [34], shown in Figure 5a. Using pneumatic systems supplying compressed air, the structure can be inflated like a balloon and form a concave shape as shown in Figure 5b.
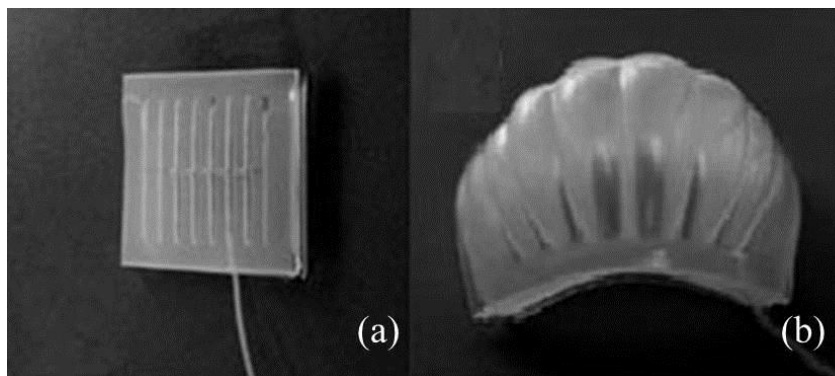
Figure 5: Soft Structure with PneuNets: (a) Original State and (b) Inflated State

1.3.3 Actuation and Control of Soft Robots

Unlike rigid robots, soft robots cannot be modeled as rigid links with rotational or sliding joints. For example, robot designs in which the entire robot body uses soft materials, like octopus arms or elephant trunks [35], are continuous and deformable which introduces additional complexity in actuation and control. There are many challenges on how to generate forces and torques within soft robots and how to plan target directed behaviors.

Hard robots have an actuator, typically an electric motor for every joint, and usually each actuator controls a single degree of freedom. Soft robot systems are under-actuated since there are more degrees of freedom than number of actuators. Some degrees of freedom may be influenced by the actuators, but many others are not controllable. To avoid using a lot of traditional hard actuators, the actuators of soft robots are typically integrated into and distributed throughout the structure. Through a long period of time studying of the outstanding capabilities of soft animals, researchers have developed soft robots based on electro-active polymer (EAP) [36] and pneumatic artificial muscle (PAM) [37] actuators.

Controlling the shape of a soft robot will be another challenge. Hard robots use high-resolution encoders to record the change in position. Then using forward kinematics, the shape and tip position of the robot can be precisely calculated if each joint position is known. Similarly, the inverse kinematics can be used to determine the necessary joint positions for a desired tip location. On the other hand, in soft robotics, for example, using a soft arm manipulator to grasp and handle objects, the actuators often apply a moment or a torque at the tip of the arm. The arm then wraps around the object

tightly to grasp it and the high-friction contact enables the arm to lift the object [33]. Unfortunately, the load of object and self-weight of the soft-robot can cause continuous deformations that may not be observable or controllable.

1.3.4 Modeling and Simulation of Soft Robots

Researchers have developed multiple of methods to model soft materials as well as soft robots. Some developed biomechanical models that predict the performance of soft robots by referencing animals. Gravagne et al. assume that each section of an elephant trunk manipulator bends into a circular arc with constant curvature and an inextensible backbone [38]. Similarly, Nakabo et al. used the constant curvature assumption to study the kinematics of a snake-like swimming robot [39]. Some modeled the dynamics of soft robots by approximating the dynamics of hyper-redundant hard systems with extremely large degrees of freedom. In this approach, the accuracy and computational cost are proportional to the number of degrees of freedom [40]. Boyer et al. used geometrically exact beam theory and the Newton-Euler technique to predict control torques of an eel-like robot as a function of expected internal deformations [41].

The high nonlinearity of both the material and geometry of the soft structural mechanics cause large deformations which makes modelling soft-body systems a challenging task. Simplified models of the complex physical characteristics of soft materials leads to unacceptable levels of inaccuracy and their inclusion makes modeling too computationally expensive to be of practical use. Developing fast and accurate models for soft robots requires further study.

1.4 Thesis Objectives

To enhance the robustness and versatility of modular robot for search and rescue operations, this thesis intersects the concept of modular robotic systems with soft-body materials. Towards an ultimate goal of developing a soft-body self-reconfigurable modular robots system, a soft-body interconnection mechanism will be designed and tested for use in self-reconfigurable modular robots in this project. The soft-body interconnection mechanism will be an expand-and-capture system actuated by using air to inflate and deflate soft-body chambers. Conceptually, when two modular robots are at a desirable distance, the soft-body interconnection mechanism of one robot will expand longitudinally to reach out to the other robot, expand radially to lock the modules together, and draw back to connect both modules.

The specific objectives of this project are as follows:

- To study the effects of structural parameters on the design of the extension and expansion actuators of a soft-body interconnection mechanism for self-reconfigurable modular robots.
- To determine the feasibility of using available research software for the 3D modeling and design of soft-body interconnection mechanisms and validate the simulation output with physical experimental results.
- To develop a method of evaluating extension and expansion soft-body actuator designs for use in an interconnection mechanism.
- To evaluate the functional response of the extension and expansion soft-body actuators to varying structural parameters via an empirical iterative study. The

empirical iterative study will utilize Initial designs of the extension and expansion soft-body actuators, incrementally modify the structural parameters, and evaluate the the functionality of the soft-body actuator designs based on the developed evaluation methodology.

- To generate pressure versus strain plots to aid in the design of soft-body based extension and expansion actuators. The generated data from the empirical iterative design study will be correlated and plotted with regards to effects of parameter modification on the extension or expansion of the soft-body actuator. The plots will provide a clear understanding on the shape changing trends of the actuators based on varying structural parameters under an increasing pressure. The plots will provide future designers with information to determine the required geometric values of the interconnect mechanisms for their task.

- To design and develop a modular robot for evaluating the soft-interconnection mechanism. The design and development of the modular robot includes the mechanical and electrical design and simple behavior programming enabling the modular robot to crawl.

- To design and develop a soft-body interconnection mechanism for a self-reconfigurable modular robotic system. The interconnection mechanism should mount to the developed modular robot. The soft-body interconnection mechanism will be evaluated to determine the maximum holding force and torque after the interconnection mechanism has engaged.

1.5   Thesis Organization

The remaining chapters are organized as follows. Chapter 2 defines the project and methodology. Chapter 3 details the design of the interconnection mechanism. The comparison of several different geometry shapes is presented. Chapter 4 presents the experimental results of the dimensional parameter adjustments. Chapter 5 introduces the design of the final interconnection mechanism. Chapter 6 shows the inflation behavior and connection behavior of the final interconnection mechanism. Chapter 7 discusses the system-level characterization of the soft-body mechanism and presents ideas of whole reconfigurable modular robot system implementation. Chapter 8 concludes the thesis.

Chapter 2

Soft-Body Modular Robot Interconnect

In this chapter, an initial hard shell robot design will be presented. Then, the project expands onto the methods of connecting the robot. The design considerations will be listed. Based on the design considerations, the conceptual interconnection methods will be presented and compared. Material selection, brief fabrication process and actuation method introduction will also be included in this chapter.

2.1 Hard Shell Modular Robot

A hard shell modular robot was rapid prototyped for this project. The mechanical design, electrical design and simple gait of the hard shell modular robot are presented. The final version of the interconnection mechanism will be created base on the size of the hard shell modular robot. Future work will aim develop a full soft-body modular robot.

15

2.1.1 Concept of Module Design

A hard shell modular robot module, shown in in Figure 6, is a two degrees of freedom robot which has a main body and two rotational blocks. Both blocks have identical shape, comprising of a half-cube and a half-cylinder. The two blocks can rotate independently about their axes by ±90 degrees.
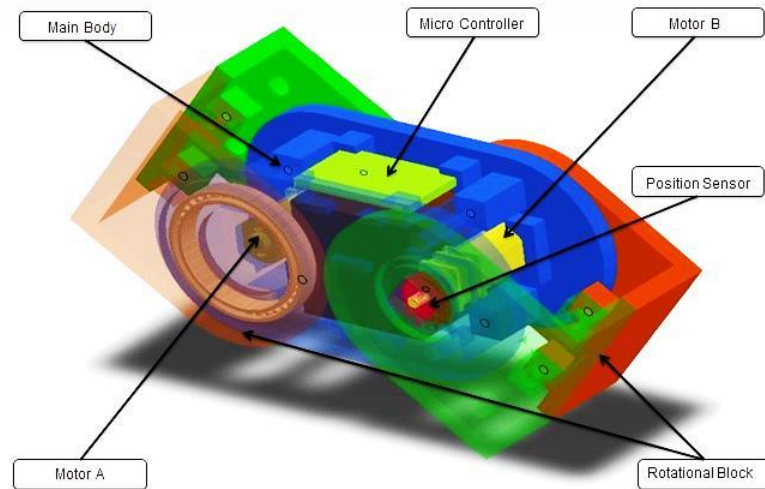
Figure 6: Design of the Hard Shell Robot

All the electrical components are housed within the main body, including the microcontroller, battery, motors and sensors. Rotational blocks are pure mechanical structures with no electrical component within them. Each rotational joint of the hard shell modular robot utilizes a rotational geared motor to drive the joint and a rotational potentiometer for angular position feedback.

2.1.2 Mechanical Design

The body of the hard shell modular robot comprises of six parts: two parts for the main body and the other four parts comprise the two rotational blocks. The structural

components of the hard shell modular robot was rapid prototyped from ABS plastic using the StrataSys Dimension SST 1200ES 3D Rapid Prototype Machine. The two parts that comprise the main body are mirrors of each other. A single side of the main body housing is shown in Figure 7. The housing contains extrusions for holding the microprocessor, battery, two motors and two sensors. The motors extrusions are rectangular and hold the motor in place by capturing the rectangular gear box attached to the motor. The small hole below the rectangle motor extrusion is a pass through for the rotational potentiometer wires. After assembling all the electrical components within the main body, the two parts that comprise the main body housing are fixed together using screws. The circular rails are used for attaching the rotational blocks. The rings have the same axis as the motors which guarantee that the rotational blocks will rotate about the circular rail.
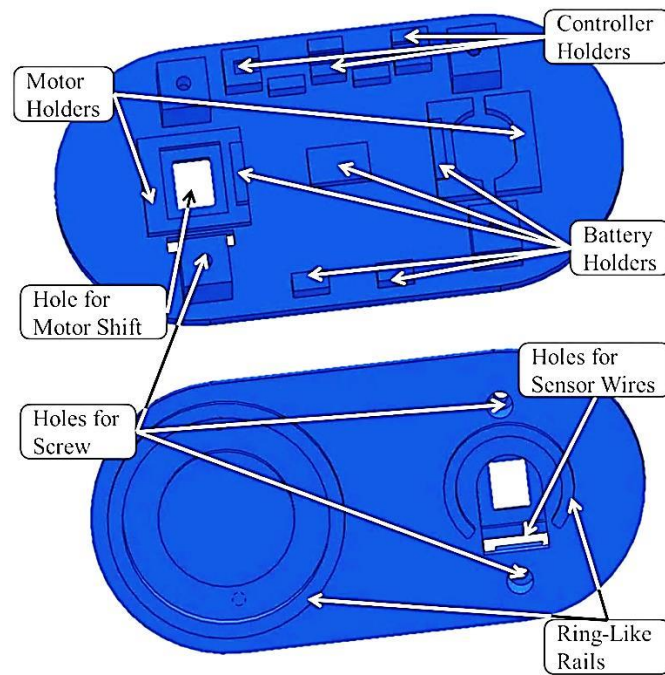
Figure 7: The Two Sides of the Part of Main Body

17

There are circular rails on the parts that comprise the rotational blocks which match the size of the rails on the main body. In the middle of the circular rails, there is a hole which captures the D-shaped shaft of the motors. Once the parts of rotational blocks are assembled to the main body, the two parts that comprise the rotational blocks are screwed to each other. Thus, the blocks will rotate along the circular rails and be driven directly by the motor shaft.

The hard shell modular robot is 118 mm in length, 46 mm in width, 46 mm in height, and 142g in weight. The thickness of the robot was kept at 5 mm to insure the strength and stability of the robot. The length was determined by the cross sectional area of the two motors plus the size of the battery. The width of the robot was determined by the body length of the motor. The height of the robot was determined by the size of battery and the controller.

2.1.3   Electrical Design

The electrical components of the robot include one microprocessor, one battery, two rotary sensors and two motors. An electrical schematic of the hard shell modular robot is shown in Figure 8.

The microprocessor is a Baby Orangutan B-328 Robot Controller from Atmel. Packing an ATmega 328p microcontroller and two motor drive channels in a 30.5 mm x 17.8 mm 24-pin broad, the controller can directly connect to the battery, sensors, and motors.
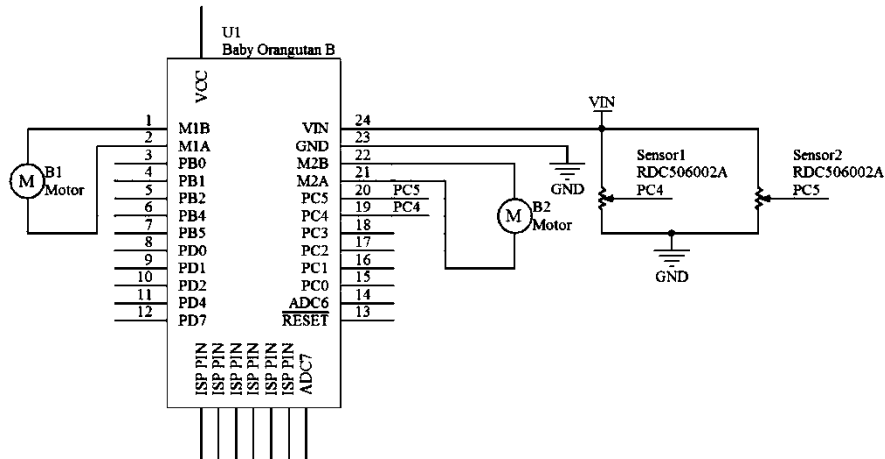
Figure 8: Electric Principle Diagram

The motors in the robot are low-current, brushed DC motor with a 100:1 metal gearbox. The motor provides 0.9 kg-cm torque and 120 RPM under 6V. The motor has a stall current of 360mA. It has a 9 mm long, 3 mm diameter D-shaped output shaft which directly attaches the rotational block of the robot.

The rotational potentiometers used in the robot are RDC506 Industrial Motion & Position Sensors from ALPS. The effective variable range is ±160 degrees. However, only ±90 degrees are used by the robot. The center of the sensor has a D-shaped hole which allows the motor shaft to go through it. Thus, the sensor can detect the rotation angle of the motor shaft easily and accurately.

Since the working voltage of the controller and sensors are similar, these devices are connected to a single battery. The motors are directly connected to the motor drivers on the microcontroller board. Motor A is connected to the controller via port M1A and M1B while motor B is connected to the controller via port M2A and M2B. Each motor and sensor forms a feedback loop. The outputs of the sensors are connected to the

19

microcontroller board via ports PC5 and PC4 because only PC0-5 can be used as both analog inputs and digital I/O lines. A position feedback controller has been implemented on the microcontroller to drive the rotational blocks to a desired configuration.

2.1.4 Control and Simple Gait

Currently, the hard shell modular robot is programmed with a crawling gait motion. The code was written in C using Atmel Studio under Windows. The code is programmed onto the microcontroller using Pololu's USB AVR Programmer, a programmer for AVR-based controllers. The programmer emulates an STK500 on a virtual serial port, making it compatible with standard AVR programming software. The Pololu USB AVR Programmer connects to a computer's USB port via a USB A to mini-USB B cable, and it connects to the target device via an included 6-pin ISP programming cable. The complete programming setup is shown in Figure 9.
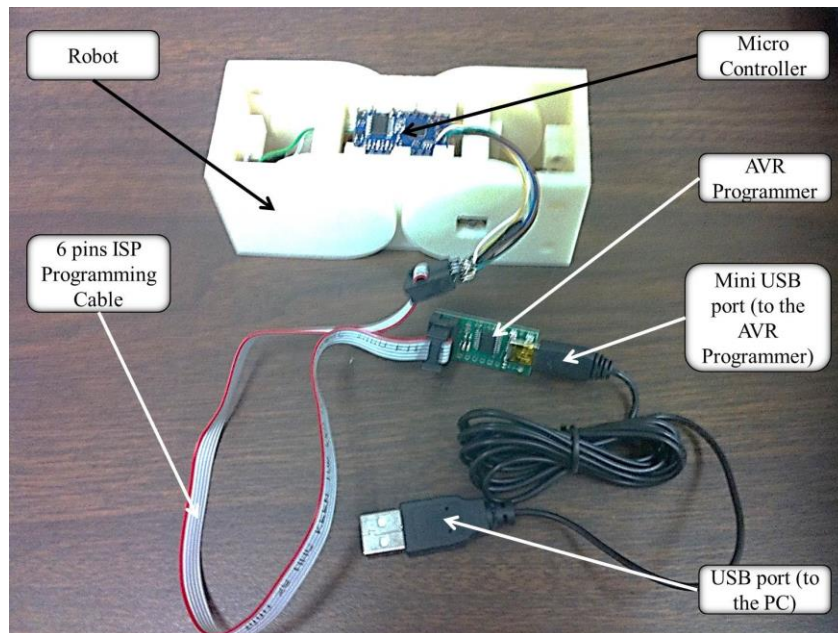
Figure 9: The Connection from PC to Robot

The flow chart for the embedded software to generate a crawling gait is shown in Figure 10. One complete cycle contains 4 steps: (1) motor A rotates a certain degree, (2) motor B rotates a certain degree, (3) motor A goes back to the initial position and (4) motor B goes back to the initial position.
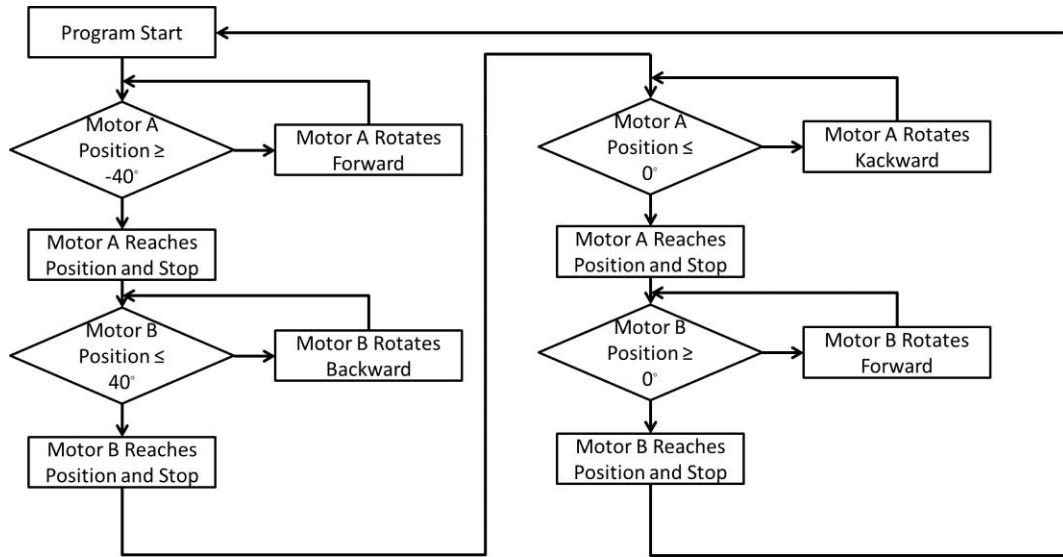
Figure 10: The flow chart of the embedded software to generate a crawling gait

During the crawling gait, both motor shafts are initially in the 0 degree position which is recognized by the sensor. Then, they rotate to -40 degrees respectively, and finally go back to the 0 degree position. The sensor monitors the rotation angle of the shaft and outputs an analog voltage signal to the controller. The sensor has a range of -160 deg to +160 deg, and output 0V to VCC (5V). The analog to digital convert (ADC) of the controller has two modes: either 8-bit or 10-bit. When the ADC is in 8-bit mode, conversion results will range from 0 to 255 for voltages ranging from 0 to 5 V. When the ADC is in 10-bit mode, conversion results will range from 0 to 1023 for voltages ranging from 0 to 5 V. The default mode setting, which is also the chosen setting in the code, is

10-bit mode. Hence, the initial position of the motor shaft is 0 degrees, which means the controller will read an input value of 511. The arbitrary rotation angle of -40 deg translates to an ADC input value 384. Figure 11 shows the robot performance in one cycle of the crawling gait.
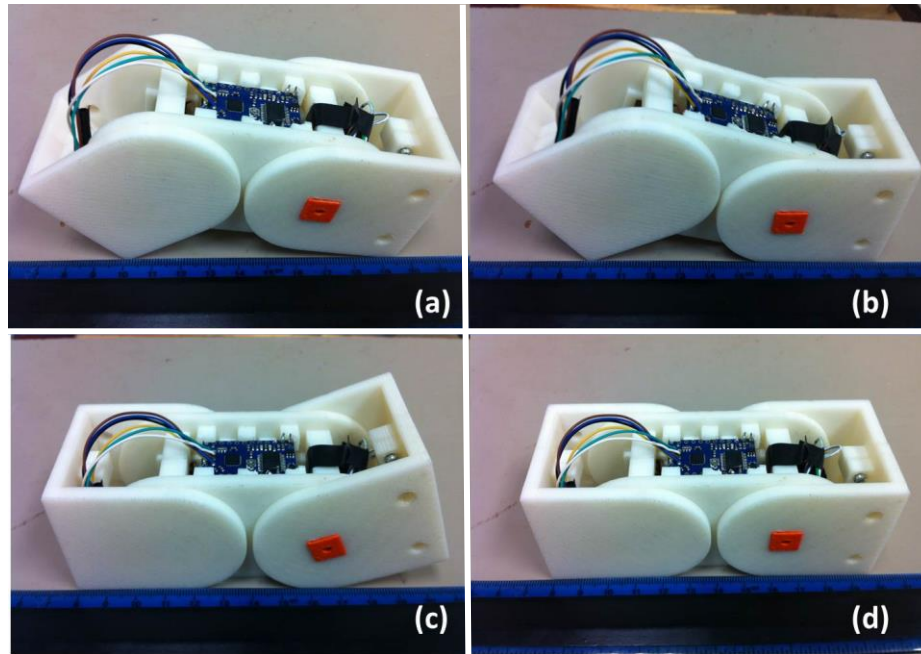
Figure 11 One Cycle of the Crawling Gait, (a) Motor A Rotates Clockwise for 40 Degree; (b) Motor B Rotates Counter-Clockwise for 40 Degree; (c) Motor A Rotates Counter-Clockwise for 40 Degree; (d) Motor B Rotates Clockwise for 40 Degree to Regain the Initial Shape

2.2 Interconnection Methods

There are two interconnection methods to connect the robot by taking advantage of the deformation of soft materials: the peripheral soft body method and the central soft body method
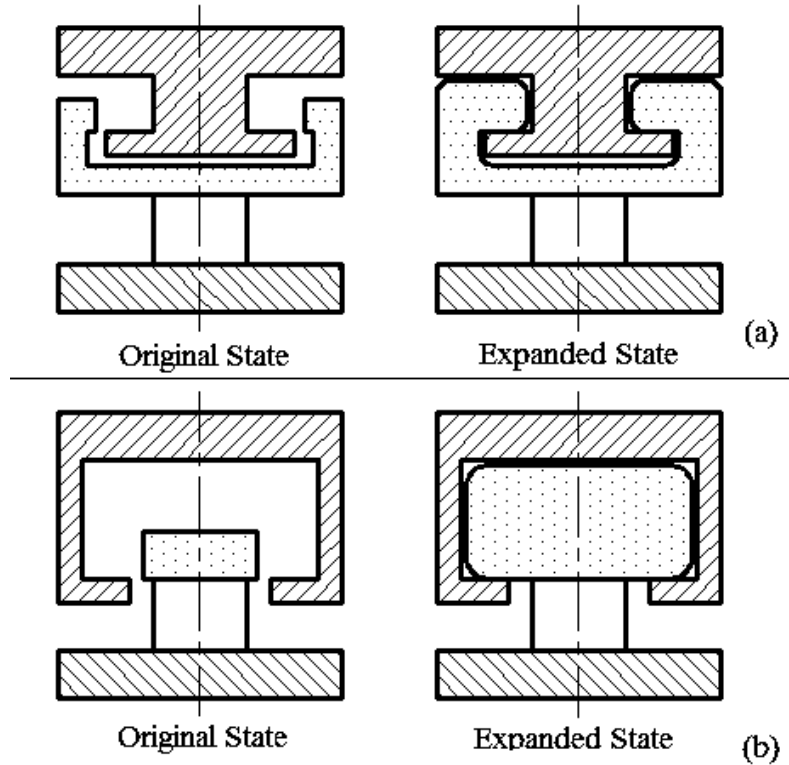
Figure 12: Two soft-body interconnection methods. (a) Peripheral Soft-Body Method and (b) Central Soft-Body Method

The peripheral soft-body method, shown in Figure 12a, contains hook-like soft mechanisms and a T-shape hard structure. The soft mechanisms are able to expend out to make close engagement with the T-shape structure. Figure 12b gives the idea of central soft-body method. In the central soft-body method, there is a soft-body bladder mechanism (part A in Figure 12b) and a C-shape shell. The bladder is able to inflate to fill the inside space of the C-shape shell.

2.3   Design Considerations

The interconnection mechanisms need to meet certain design demands. 1) Minimum overall scale: from a fabrication feasibility perspective, the smaller the overall scale the

23

better. The mechanism should be able to be equipped on a robot which a maximum dimension (length plus width plus height) of approximately 20 cm. 2) Maximum separation distance between modules: the mechanism should be able to reach out to another robot with a certain distance about 15 mm to 20 mm and drag it back. 3) Angular displacement tolerance: the mechanism should be able to connect two robots whose central axes are within a certain angular difference about a maximum of 5 degree. 4) Generate enough force: the soft mechanism needs to provide enough forces to pull another robot back as well as maintain connection during modular robot use and motion which is about 2 N.

Both soft-body interconnection methods provide locking functionality there by generating forces and realizing the connection. The close contact between the bladder surface and internal surface of the shell can provide extra friction. Furthermore, assuming the expansion amount of the tips of the soft hook are equal, it will have a poor angular displacement tolerance with short hooks since a portion of the hook will not be able to reach the correct position. The length of the soft hooks has to extend to improve the angular displacement tolerance, which means an increased overall scale. An example scenario of the peripheral interconnection method with an angular offset is shown in Figure 13a. On the other hand, the central soft body method provides a certain tolerance towards angular displacements. As long as the bladder is able to go inside of the shell, the connection can still be realized as shown in Figure 13b. In addition, the bladder shape is easier to be designed and the inflated shape is easier to be predicted which makes the central soft body method a better choice.

To fulfill the consideration of minimum overall scale and maximum permissible separation distance, a length-adjustable mechanism (area with no shadows in Figure 12b) should also be designed. The original length of the mechanism should not be too long to keep the overall scale small and it should have the capability to reach another robot within a certain distance when expanded. Because the soft bladder mechanism and the soft length-adjustable mechanism has their own functionalities and will be actuated asynchronously, it is infeasible to make the interconnection mechanism hermaphrodite, which means a single structure contains both soft mechanism and the C-shape shell. It will either lead to a huge interconnection surface or force the soft mechanism to be very small which is hard to fabricate. Therefore, the whole interconnection mechanism will have two parts: a deliver (male) port containing the soft structure and a receive (female) port which contains the C-shape shell.

(a)   (b)
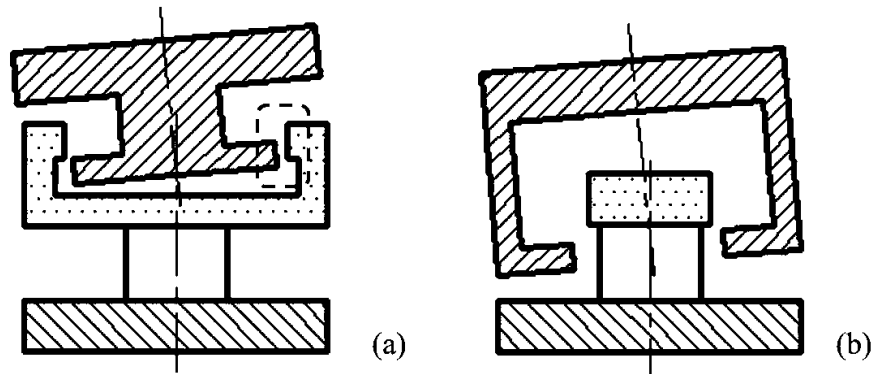
Figure 13: Angular Displacement Tolerance Performance of the Two Soft-Body Interconnection Methods. (a) Peripheral Soft Body Method and (b) Central Soft Body Method

2.4 A Conceptual 3D Model of the Soft Interconnection Mechanism

The finalized implementation of the soft-body interconnection mechanism is an extend-and-capture system as shown in Figure 14. The whole structure of the interconnection mechanism contains two parts: a male port and a female port. The male port contains a hard shell and the whole structure of the soft mechanism while the female port will be a rectangular shell with a cylindrical hole. Each modular robot will be equipped with at least one male port and one female port. During the reconfiguration process, the male port of robot A extends to reach out to the female port of robot B, expands to lock onto robot B, and finally retracts to draw robot B back.
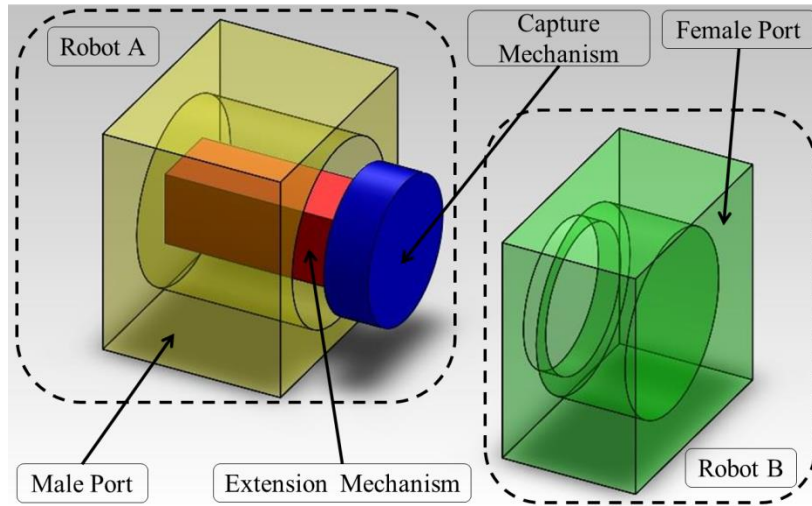
Figure 14: A Conceptual Design of the Soft-Body Interconnection Mechanism

The opening of the female port should be a little bigger than then size of the capture mechanism. This ensures the capture mechanism sent into the female port even if the axes of both robots are not perfectly much as shown in Figure 15.
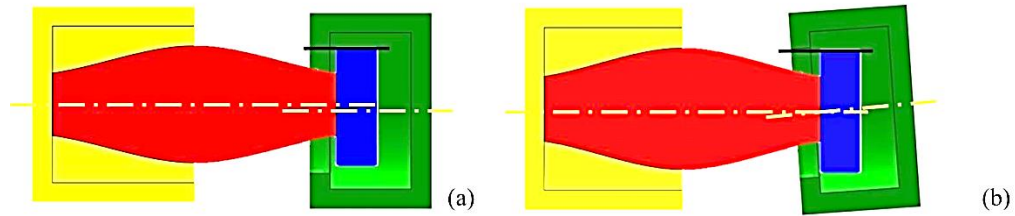
Figure 15: Alignment Issues. (a) Parallel Displacement; (b) Angular Displacement

Hence, the main emphasis of the soft mechanism is the male port. Since the soft bladder mechanism and the soft length-adjustable mechanism have their own functionalities and will be actuated asynchronously, the design of the male port is broken down into two separate sub-mechanisms: an extension mechanism which mainly deals with the elongation in the axial direction and a capture mechanism which radially expands evenly.

2.5   Soft-Body Interconnection Process

Figure 16 shows the complete reconfiguration function using the conceptual soft-body interconnection mechanism. Figure 16a is a 2D segmental view of Figure 14 as well as the initial positions of the two ports which are ready to engage in the interconnection process. In Figure 16a, the male port of robot A (colored red and blue) has a certain, but not too long, distance from the female port of robot B (colored yellow). Both the extension mechanism (red part) and capture mechanism (blue part) are in the original state.

In the first step, the extension mechanism begins to extend aiming to send the capture mechanism into the receiving port of robot B. Figure 16b shows the final state of

27

the first step in the process which allows the entire capture mechanism to get into the female port.

In the second step, the extension mechanism remains in its state. At the same time, the capture mechanism begins to expand until its body completely fills the void of the female port as shown in Figure 16c.
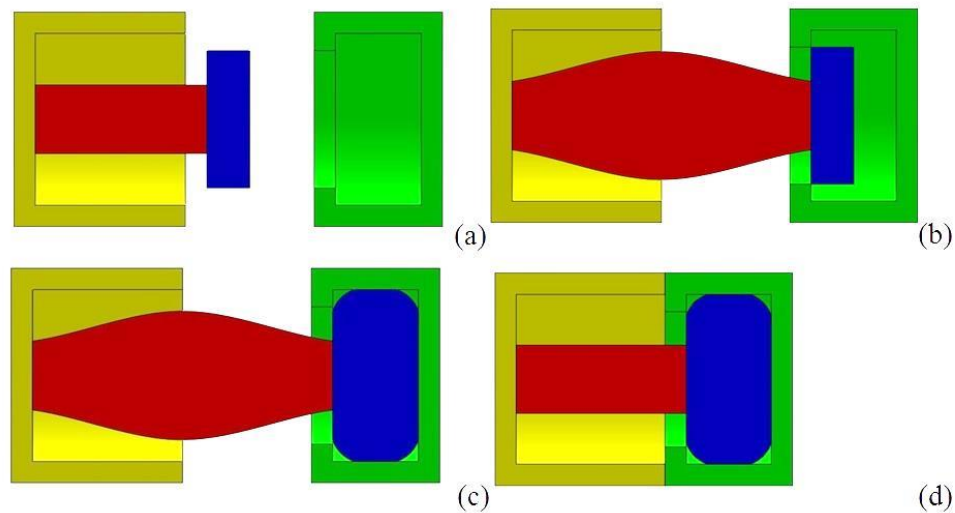
Figure 16: The Reconfiguration Process. (a) Initial State, (b) First Step: Extension, (c) Second Step: Capture, and (d) Final Step: Retraction

In the third step, the capture mechanism remains expanded and remains so as long as the two robots are connected. At the same time, extension mechanism is expected to gradually return to the original state. As the extension mechanism shrinks, robot B is forced to pull back to robot A due to the tight contact between capture mechanism and the female port. When the extension mechanism goes back to its initial state, the two robots will be strongly connected as shown in Figure 16d.

2.6   Soft-Body Materials

There are a wide range of soft materials that may be used for the soft-body interconnection mechanism. The soft material should be very soft and very extendable as well as maintaining certain amount of strength while extending. Many researches have been done for a wide variety of soft materials for different purposes [30][42][43][44] [45][46]. Among these, silicone, specifically the Ecoflex® series from Smooth-On, is widely utilized. The Ecoflex® rubbers are super soft silicones with an elongation rate up to 1000%. There are five kinds of products in the Ecoflex® series. Ecoflex® 0030 is chosen for the fabrication of the soft body interconnection mechanism. Ecoflex® 0030 has a 900% elongation rate and has a hardness of 30 in Shore00 Hardness level.

2.7   Soft-Body Actuation

Figure 17 provides a qualitative description regarding soft-body actuation. When the pneumatic actuator starts to push air into the soft-body actuators, the air will spread to all of the internal voids via an internal channel. Then, due to the rising internal pressure, the mechanisms will inflate and the volume of the soft-body actuator will increase. If the pressure is maintained at a certain value, the mechanisms will maintain a certain corresponding geometric shape. Once the air is evacuated, the mechanisms will return to their original shape.
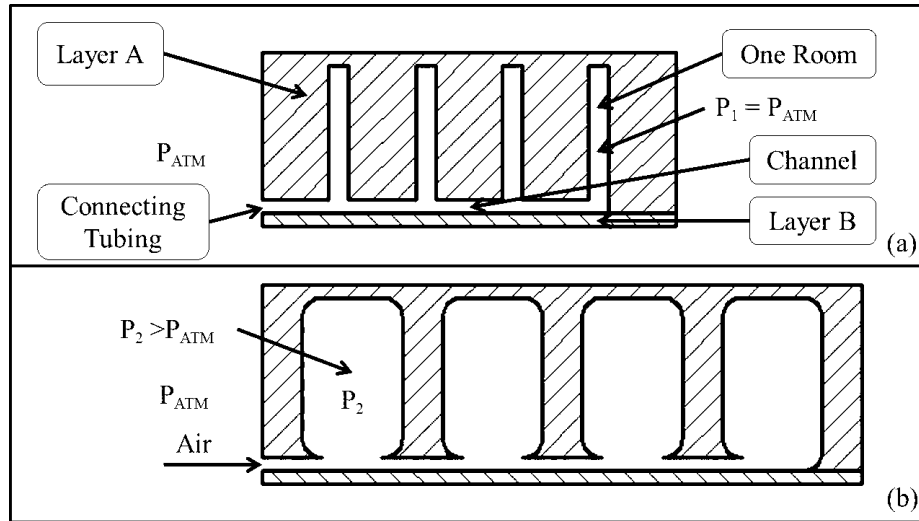
Figure 17: Qualitative Description about the Mechanisms, (a) Original State; (b) Inflated State

Different geometric designs lead to different inflation performances. For example, a complete symmetrical structure has an equalization expansion rate towards every surface when inflated which contributes to an elongation motion. However, if one surface is thicker than the others, the whole structure will bend towards the thicker surface when inflated.

2.8   Soft-Body Structure Fabrication Process

The initial state of Ecoflex® 0030 is two kinds of liquids in separate bottles. Depicted in Figure 18a, the rubbers are made by mixing two kinds of liquid in a 1:1 ratio by weight or volume, and cured at room temperature with negligible shrinkage. The cure time in room temperature (73°F/23°C) is four hours. An alternative way for curing is to use an oven at (180°F/80°C) with a cure time of one hour.

A molding process is used to build the external shape of the soft mechanisms and create the internal structure. The design of the mold is completed with SolidWorks®, a

computer aided drafting software. Then, the mold design is rapid prototyped using the Dimension SST 1200ES Rapid Prototype Machine. Once the molds are ready, the silicone liquid mixture, which has been thoroughly stirred, is poured into the molds and left to cure as shown in Figure 18b. After the soft parts have cured and removed from the molds, a gluing process is used to connect separated silicone components. Finally, a tube, which connects to the pneumatic actuator, is inserted and fixed to the soft mechanism.
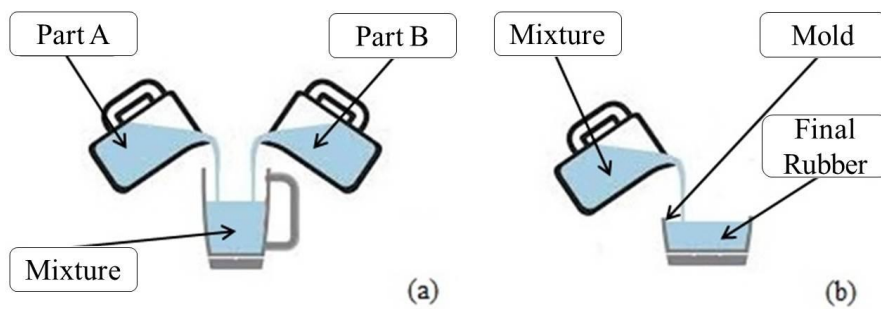
Figure 18: The Silicone Fabrication Process, (a) mixing and (b) Molding

To reduce the complexity of the molds, both the extension and the capture mechanisms are made using two separate layers that are glued together shown as layers A and B in Figure 17. The two layers are glued together using a thin, uncured layer of Ecoflex® 0030 as glue. After curing, the mechanisms will be perfectly sealed, leaving only one hole to insert the tubing. After the tubing is inserted, the tube protrusion location is covered with a silicone adhesive gel from General Electric® to ensure the whole mechanism is sealed. The other end of the tubing is connected to the pneumatic actuator.

Chapter 3

Design of a Soft-Body Interconnection Mechanism

This chapter discusses the simulation results for modeling a soft-body structure and details the procedures used in the empirical iterative study. The procedures for creating the varying iterative design samples for both the extension and capture mechanisms are provided. A discussion on the errors and issues encountered during the production of the samples is provided along with solutions and improvements for future implementations.

3.1 Simulation of a Soft-Body Structure

An initial simulation of a soft-body structure was attempted using Comsol Multiphysics®. If the simulation had been successful, it would have formed the foundation for developing multiple soft-body structures that provide the desired extension

and capture mechanism requirements and a means for optimizing them based on desired specifications. The following sections describe the process involved in simulating a soft-body structure, the results from the simulation, and the problems encountered.

3.1.1 A Constitutive Model for Rubber-Like Materials

There are many constitutive models for rubber-like material which may be used in simulation [47]. For the simulation, the Arruda and Boyce Model was used [33]. The elastic characteristics of rubbers can be expressed in terms of a strain energy function based on the strain invariants [48] as follow:

$$W = f(I_1, I_2, I_3)$$

where W is the strain energy density and I_1, I_2 and I_3 are the three invariant of the green deformation tensile.

The equation of Arruda and Boyce Model is [48]:

$$W = \mu \sum_{i=1}^{5} \frac{C_i}{N^i} (\bar{I}_1^i - 3^i)$$

with:

$$C_1 = \frac{1}{2}, C_2 = \frac{1}{20}, C_3 = \frac{11}{1050}, C_4 = \frac{19}{7000}, C_5 = \frac{519}{673750},$$

where μ is the initial shear modulus; N is a measure of the limiting network stretch.

In the simulation, the Arruda and Boyce Model was used to model the Ecoflex® 0030 silicone material with the following parameters which was previously studied by a researcher [33]:

$$\mu = 0.03 MPa, N = 15.21$$

3.1.2 Simulation Results

Figure 19a shows the geometric structure modeled within the simulation software. A two layer structures was designed with in the simulation software and given the elastic properties based on the soft material. The structure has a length 54 mm and a width of 22 mm. The upper layer has a thickness of 6 mm while the bottom layer has a thickness of 1.6 mm. Each pneumatic room has a thickness of 0.6 mm, a height of 4.4 mm and a width of 18.4 mm.

Comsol Multiphysics® has a built in library with hyper-elastic material models which includes the Arruda and Boyce Model. The surface at which the pneumatic tubing will be inserted (left end of Figure 19b, 17c and 17d) is set as a fixed constraint and all the inner surfaces (blue surfaces in Figure 19a) have applied pressure.

(a)

(b)

(c)

(d)
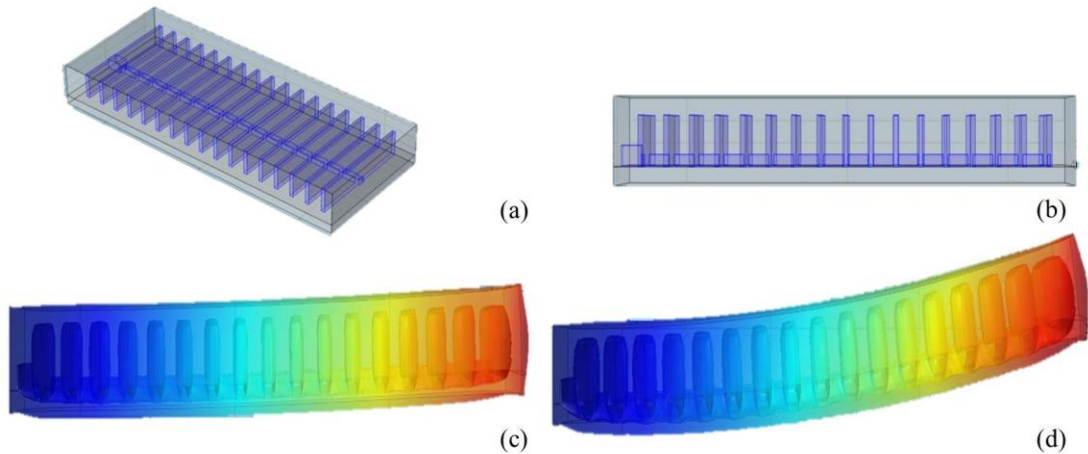
Figure 19: Multiple Views of the Simulation Model and Results. (a) Isometric View of the Initial Shape, (b) Front View of the Initial Shape, (c) Deformation of the Model under 2.5 psi, and (d) Deformation of the Model under 3.0 psi

Figure 19b shows the front view of the model. Figure 19c shows the deformation of the model with 2.5 psi while Figure 19d shows the deformation of the model with 3.0 psi. As can be seen, the results do no qualitatively correlate with Figure 5. Any higher pressures would destabilize the convergence of the simulation.

3.1.3   Experimental Validation of Simulation Results

To provide a basis for developing soft-body structures, an initial attempt at creating a soft-body actuator was completed using a published example [7] [34]. The structure and testing results of the example soft-body actuator are shown in Figure 20 which has the same geometric shape as the simulation modeling.

The structure has two layers. The upper layer contains pneumatic rooms (pneu-rooms) and is made using highly extensible elastomeric material, Ecoflex® 0030. The lower layer is a relatively complaint sheet using the same material. Figure 20a gives a 3D segmental vision of the structure. The geometric shape is the same as the model using in the simulation presented in the previous section. The structure has a length 54 mm and a width of 22 mm. The upper layer has a thickness of 6 mm while the bottom layer has a thickness of 1.6 mm. Each pneu-room has a thickness of 0.6 mm, a height of 4.4 mm and a width of 18.4 mm. Once the soft-body actuator structure has been assembled, a soft tube (Chemical-Resistant Clear PVC Tubing, McMaster-Carr) is inserted into a hub located at one side of the actuator. This tube fed through all of the pneu-rooms through a center channel. The channel is 0.5 mm in height. Figure 20c and 19d show the deformation of the structure under 2.5psi and 3psi, respectively. Figure 5 shows the result

of previous published results. Comparing Figure 20c and Figure 20d to Figure 5, the results are similar.
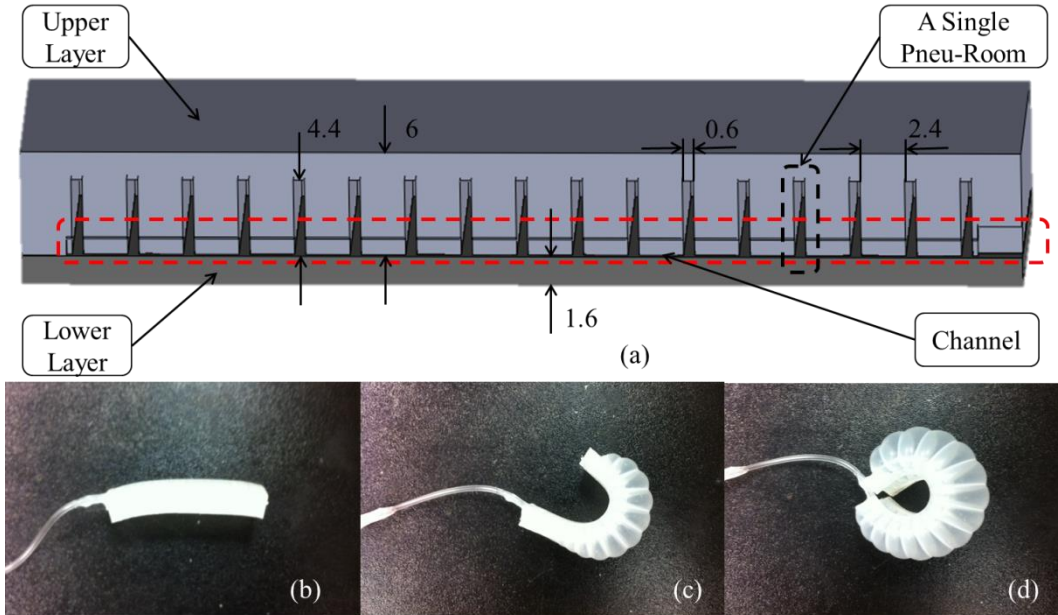
Figure 20: Soft Structure, (a) 3D Model; (b) Original State; (c) Deformation under 2.5psi; (d) Deformation under 3.0psi

3.1.4 Discussion on the Simulation and Experimental Results

Although many researchers have successfully modeled soft materials and soft-body systems using non-linear FEM, most of the simulations focused on 2D representations of the design while the simulation attempts presented here focused on 3D representations. 3D modeling is far more complicated than 2D modeling. Modifying the material parameters, loading conditions, or boundary conditions greatly affects the final outcome.

Figure 20c and Figure 19c show the deformation of the same soft structure for both the real physical test and the simulation result with 2.5 psi while Figure 20d and Figure 19d show the deformation of the structure with 3.0 psi. The difference between the

simulation results and physical results are substantial. Hence, the simulation cannot be used to determine the final structural outcome of the soft-body structure with internal pneumatic pressure in this project. Since the simulated model cannot be used in the design process, an empirical iterative method is utilized to correlate parameter modifications to evaluated outcomes.

3.2   Design of Capture Mechanisms

The design of the interconnection mechanism is broken down into two mechanisms: the extension and capture mechanisms. The extension mechanism is capable of significantly changing its dimension along the axial direction while the capture mechanism significantly changes its dimension along the radial direction. To realize these functions, these mechanisms should be able to expand by inflating air and then shrink to their original size by deflating.
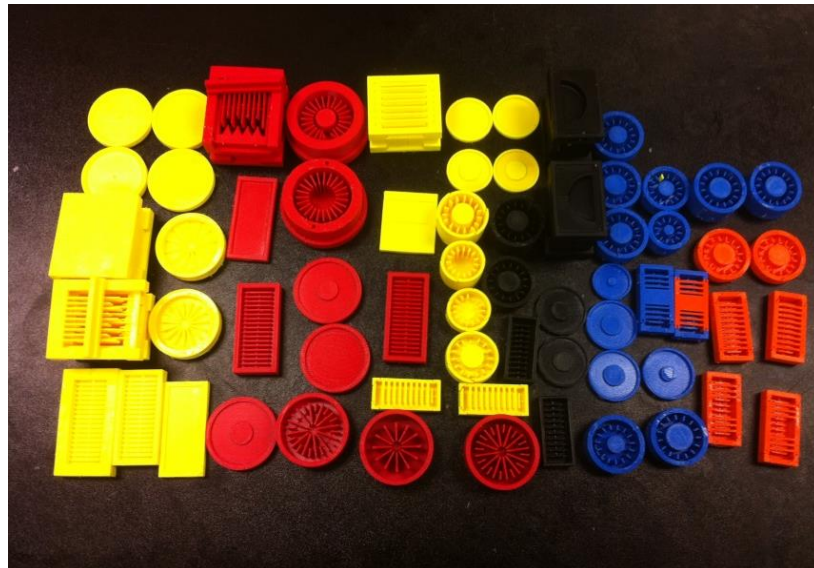
Figure 21: Molds Used in the Projects

As previously discussed, the Ecoflex® 0030 silicone material is a two part system that requires mixing and a mold to form it into the desired shape. The molds are designed in SolidWorks® and fabricated using the Stratsys Dimension SST 1200ES Rapid Prototype Machine. Figure 21 shows most of the molds fabricated during the empirical study. To easily withdraw the cured silicone from the molds as well as create internal geometries, a two piece mold was utilized with each forming half of the final structure. Both halves of the final structure are glued together using the same Ecoflex® 0030 silicone mix and left to cure.

The following sections discuss the design and iterative process of developing the capture mechanism. The empirical iterative concept is to create multiple versions of the structure with modified structural parameter and evaluate the performance of the design. Based on the outcomes, a new set of designs are generated and evaluated. After multiple iterations, the data is processed and placed into a form readily usable for design.

3.2.1   Capture Mechanism V1

The initial design for the capture mechanism was based on the example soft-body actuator. The example soft-body actuator was designed to curl when inflated. The height of the example soft-body actuator was 7.6 mm and expanded to become more than 15 mm under 3.0psi pressure. The capture mechanism needs to radially expand evenly. Hence, to remove the curling aspect but retain the expansion, the initial design of the capture mechanism is circular instead of linear with the pneu-rooms in a circular pattern about the center axis. The design is expected to radially expand more than 200% with limited expansion in the axial direction.

The first version of capture mechanism utilized a cylindrical shape. The pneu-rooms inside the blocs form a radial pattern shape about the center. At the bottom of the upper layer, there is a disk shape hollow which connects all of the pneu-rooms. The lower layer is a sheet with a hole in the center. Tubing is inserted through the hole, connecting to the disk channel and feeding air to all the pneu-rooms.

Figure 22a and Figure 22b show two kinds of capture mechanism V1 created using different molds. Both of the mechanisms share the same geometric shape: both upper layer and lower layer are 40 mm in diameter, the upper layer is 5.5 mm in height, the lower layer is 2 mm, the pneu-rooms are 4 mm in height and 11 mm in length, and the disk channel is 1 mm in height. The only difference is in the shape of pneu-rooms. Figure 22a has 12 thin rectangular shape pneu-rooms which were created using mold V1a while Figure 22b has 15 wedge-shape pneu-rooms which were created using mold V1b. Since the segmental views of two capture mechanisms are similar, Figure 22c provides only a 3D segmental view of the capture mechanism created using mold V1b.
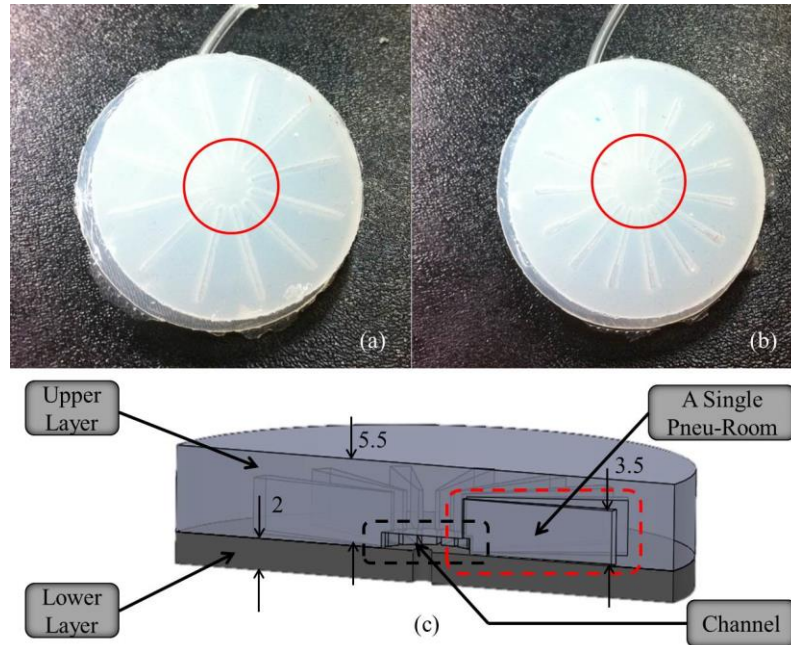
Figure 22: First Version of Capture Mechanism, (a) Capture Mechanism Created by Mold V1a; (b) Capture Mechanism Created by Mold V1b; (c) 3D Image for Capture Mechanism Created by Mold V1b

Both capture mechanism V1 samples were evaluated. Unfortunately, the samples did not achieve the expected design goals. The samples barely expanded along the radial direction when inflated. At 2.5 psi, the diameter expanded to 41 mm. At 3 psi, the diameter expanded to 43 mm. Figure 23 shows the inflated shape of the sample created using mold V1a. The inflation outcome of the mechanism created using mold V1b is similar.

From the experimental results, it was concluded that the head of each and every pneu-room was too close to the center which weakened the center support and made it easier to inflate at the center compared to the rest of sample structure. The upper surface was greatly inflated while the bottom surface barely inflated. The thickness from pneu-

rooms surface to the upper surface is 0.5 mm thinner than the lower layer, which indicates that the design is highly thickness-sensitive. Also, with a great expansion at the center and weaker supports, the tips of the wedge shaped pneu-rooms (the red cycles in Figure 22) easily tore away from the bottom layer rendering the samples useless after a few inflation cycles.

Figure 23: Shape of the Inflated Mechanism

3.2.2   Capture Mechanism V2

The main objectives for the second version of the capture mechanisms are as follow. First, the thickness shown in Figure 24a, which includes 1) the pneu-rooms surface to the cylindrical surface, 2) the pneu-rooms surface to the top surface of the part and 3) the height of the lower part, are designed to be same. The height of upper layer should increase and the height of pneu-rooms should increase correspondingly. Finally, the width of pneu-rooms should be reduced to keep the pneu-rooms away from the center as shown in Figure 24b. These modifications hold two promises: 1) reduce the height inflation amount as well as increase redial inflation amount and 2) make the center less likely to be tear.
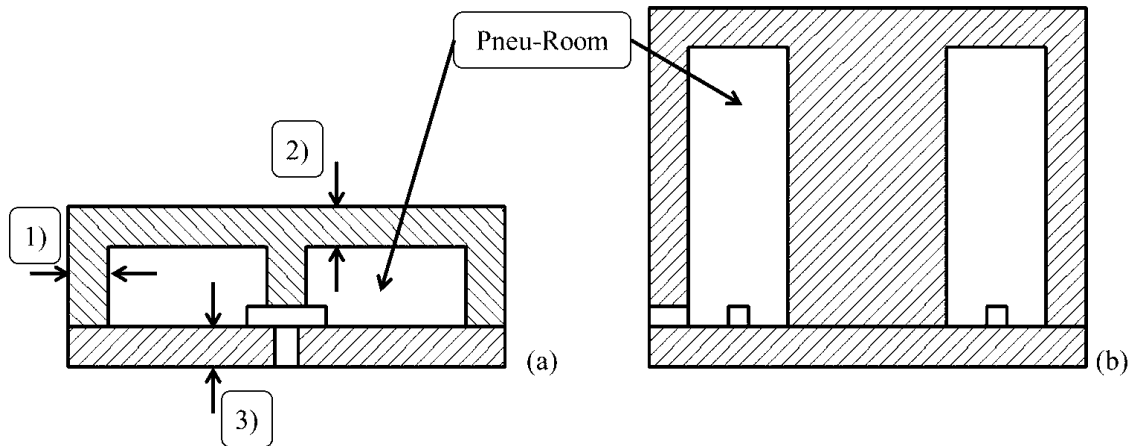
Figure 24: The External Sizes and Pneu-Rooms Sizes of Two Versions of Capture Mechanisms, (a) Capture Mechanism V1; (b) Capture Mechanism V2

Based on above conclusions, the second version of the capture mechanism was created. The height of the upper part of the capture mechanism V2 was increased to 20 mm, while the lower part was reduced to 1.5 mm. There are 23 pneu-rooms within the mechanism and each pneu-room is 0.6 mm wide and 18.5 mm high. The length of the pneu-rooms was reduced to 7.5 mm to prevent the material between the pneu-rooms from forming a wedge shape, hence, making it stronger. A ring shape channel located in the bottom of the upper layer, which connects all the pneu-rooms, has replaced the previously used disk shape channel. Figure 25 provides a 3D model of the upper part.
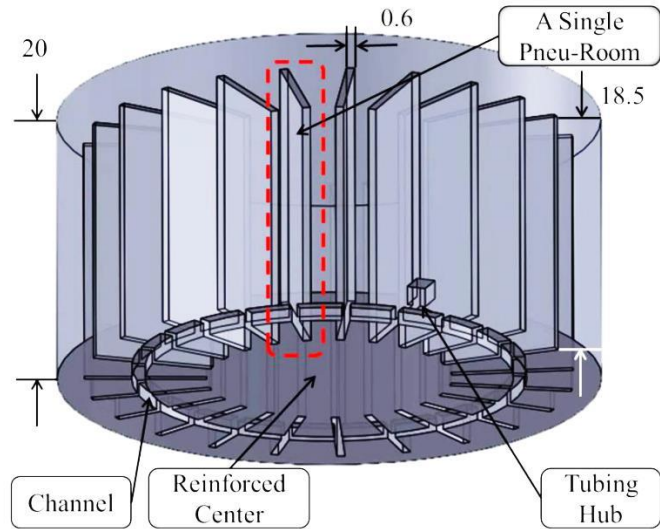
Figure 25: 3D Upper Part of Second Version of Capture Mechanism

With the new modification, the capture mechanism was capable of successfully expanding along the radial direction. At 2psi, the maximum diameter was 53 mm with a minimum diameter of 47 mm. At 2.5psi the maximum diameter and minimum diameter were 79 mm and 61 mm, respectively. Figure 26a shows the original shape of the block while Figure 26b shows the shape change at 2.5psi. This result indicates that increases in the height of the capture mechanism will enhance the radial deformation and that decreasing the length will strengthen the center of the capture mechanism.

Looking at Figure 26, the design still had some obvious disadvantages. The center part is over reinforced. The solid center not only prevents the whole mechanism from expanding out, but also uses a lot of extra silicone material. For these reason, the center may need to be hollow. The total scale is too big. It requires a lot of material to construct and a lot of air to operate. Hence, the overall dimension needs to be decreased.
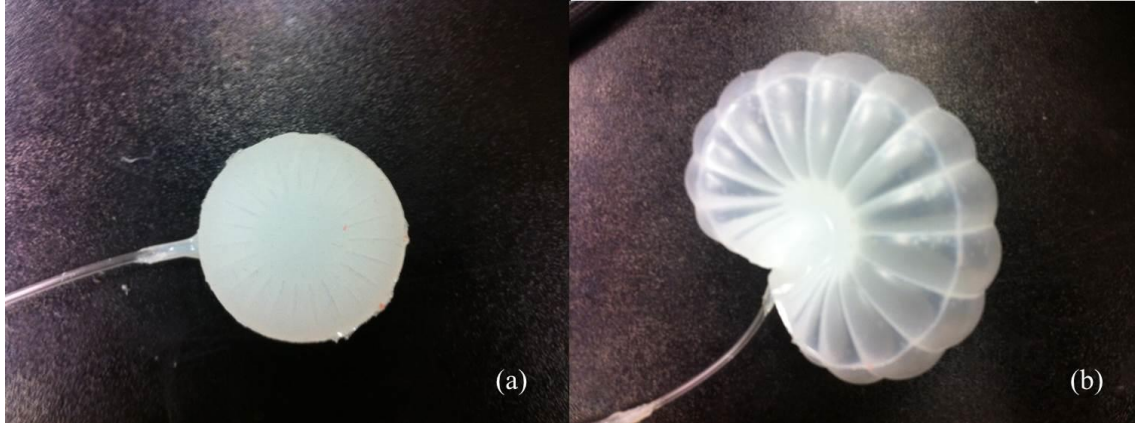
Figure 26: Capture Mechanism V2, (a) Original State; (b) Inflated State

In addition, the fabrication process became more intricate. Figure 27a and Figure 27b show the V2a and V2b molds which were used to make the capture mechanism V2 samples. Figure 27a shows some single piece molds. After the material cured in the mold it was extremely difficult to remove the molds even with the mold release sprayed in advance. Figure 27b shows the two-piece molds which allowed the molds to be removed after the silicone rubber had cured but still required significant effort. To simplify the mold release process, the molds should be made from multiple parts and assembled together.
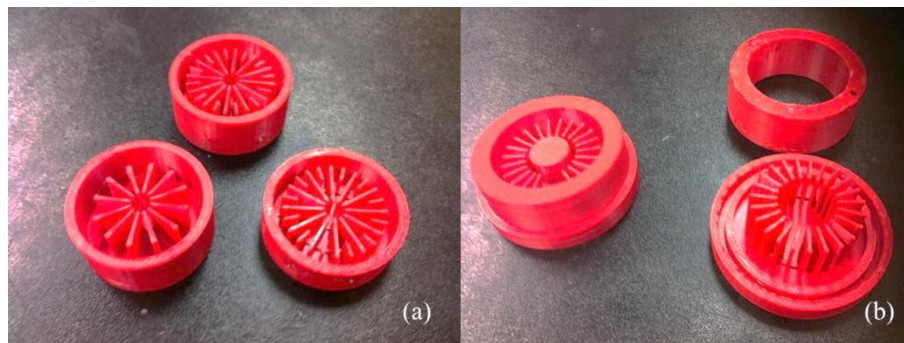
Figure 27: Molds for Capture Mechanism V2, (a) Mold V2a; (b) Mold V2b

3.2.3 Capture Mechanism V3

Figure 28 shows two different designs for the third version of capture mechanism. The design to the left is smaller in scale compared to the sample on the right. The left sample has a diameter of 25 mm, a height of 11.5 mm (10 mm of upper layer plus 1.5 mm of lower layer), and a thickness of 1.5 mm. The sample on the right utilizes a hollow center with a 15 mm diameter. The sample to the right has a total diameter of 30 mm and has the same height and thickness as the left sample. Both designs have 15 thin rectangular shape pneu-rooms with the same width of 0.6 mm but the length has been further reduced to 3.5 mm.

Figure 28: Third Version of Capture Mechanism

Figure 29 shows the experimental deformation of the samples at 3psi of pressure. This performance is still similar to the capture mechanism V2 design when inflated. From Figure 29a, the expansion along the radial direction is limited by the solid center. With a hollow center, the result seems to be good. The diameter of the part is doubled and the expansion along the axial direction is limited.
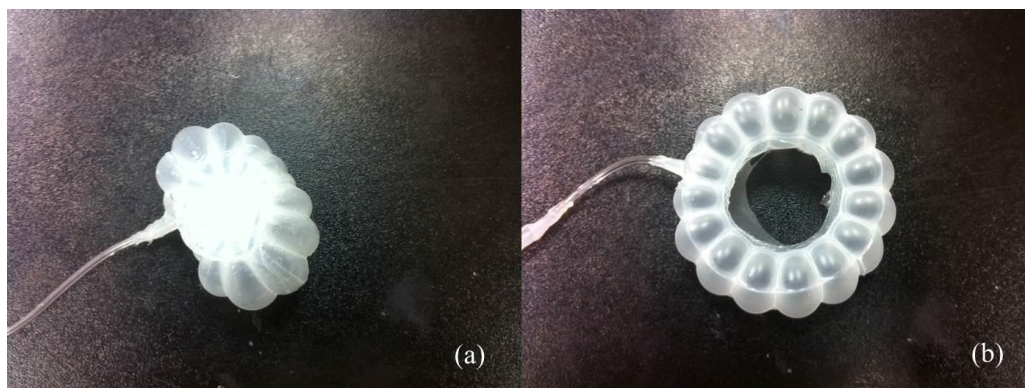
Figure 29: Inflated State of Two Mechanisms, (a) Mechanism with Solid Center; (b) Mechanism with Hollow Center

Although the samples exhibited the desired behavior, there is still a problem with the mold. The mold V3a (for third version of capture mechanisms) for the upper layer contains three pieces as shown in Figure 30. This design makes the mold easier to assemble and disassemble. Some parts of the mold (red dash cycles in Figure 30) lead to major leaking problems, while some other parts of the mold (blue solid cycles in Figure 30) are easily broken.
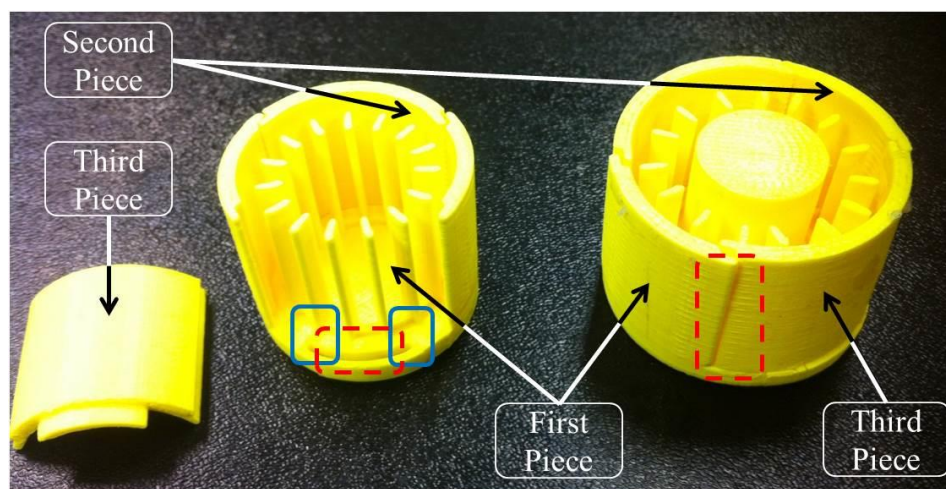
Figure 30: Molds V3a for Capture Mechanism

To avoid the problem mentioned above, the mold V3b was fabricated. The mold for the upper layer still contains three pieces. The main component of the three pieces is shown in Figure 31. The base and the wall of the mold are 3 mm thick to provide strength. The solid cylindrical part (light blue part) in the middle creates a 15 mm diameter hollow center. The ring shape hump (black part) at the bottom creates the channel which connects all the pneu-rooms. The small rectangular part (dark grey part) at the bottom creates a hub for inserting the tubing. There are 15 thin rectangular parts in a circular array to form the 15 pneu-rooms which are 3.5 mm in length, 0.6 mm in width, and 8.5 mm in height. The blue part shows the walls and flanges of the mold. The wall, which is 10 mm in height, is separated into four symmetrical parts. Two of them are integrated to the main part as shown in Figure 31. They are two 40-degree arcs facing each other. The flanges are 1 mm in thickness and 2 mm in height which helps fix the position of the other two parts of the upper layer mold and contributes to a good seal. The other two parts of the wall are two other pieces of the upper layer mold which are shown in Figure 32. They have three grooves with a width of 1.3 mm and a depth of 2.2 mm which fit the flanges on the main piece. Figure 33 shows the lower layer mold. The structure is simple and creates a sheet of silicone with a depth of 1.5 mm and a hollow center with a diameter of 15 mm.
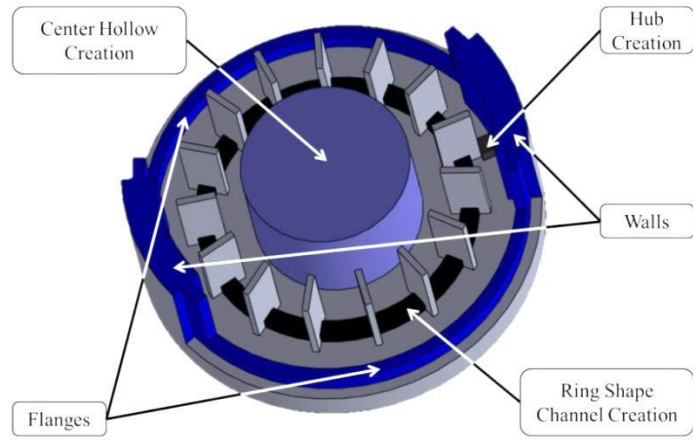
Figure 31: Main Piece of Mold V3b
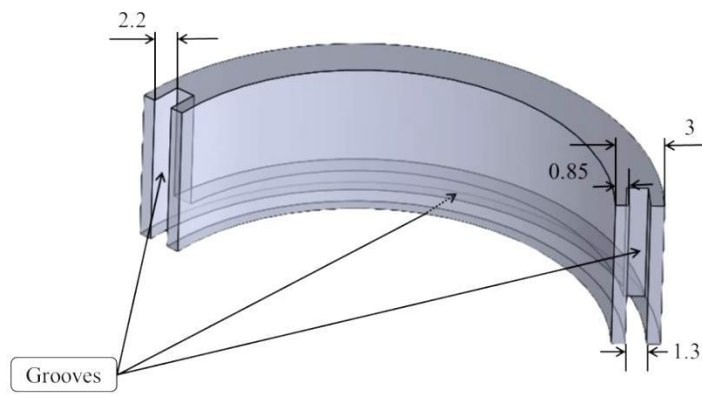
Figure 32: Other Two Pieces of Mold V3b

Figure 33: Lower Layer Mold of Mold V3b

The new mold design generates a capture mechanism of 30 mm in diameter and 11.5 mm in height. The thickness of the material between the pneu-rooms and the top surface of the cylinder is 1.5 mm as is the distance between the bottom of the pneu-rooms and the lower surface in relation to the diagram shown in Figure 24. The thickness of the pneu-rooms surface to the hollow center is 2.5 mm. This design forces the whole mechanism to expand radially when inflated. Figure 34a shows the original shape of the capture mechanism made using mold V3b. Figure 34b shows the total deformation of the mechanism at 3 psi. The average diameter at 3 psi is 60 mm which is 200% more than the original shape.
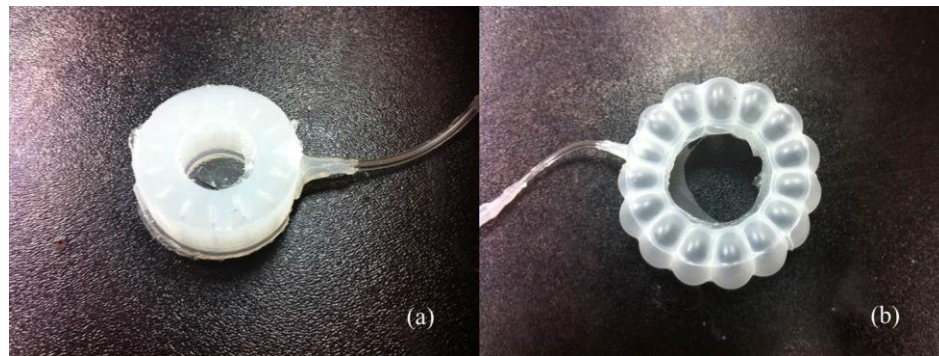
Figure 34: A Good Result with Capture Mechanism V3; (a) Original State; (b) Inflated State

3.3 Design of Extension Mechanism

The inspiration for the first version of the extension mechanism comes from the concertina-type hinge near the top of a bendable straw. The design of extension mechanism should achieve an equal, but limited, radial expansion when inflated and the inflation of each pneu-room should contribute to a large elongation in the axial direction. The shape of the extension mechanism is cylindrical which means each and every 2D segmental shape along the axial direction is circular. Plus, the pneu-rooms are thin disk

shapes and linearly patterned along the axial direction. The walls in-between the pneu-rooms constrain the expansion along the radial direction

3.3.1 Extension Mechanism V1

The extension mechanism does not have an upper or lower layer, but it still contains two parts. Each part makes up half of the mechanism and has the same structure.
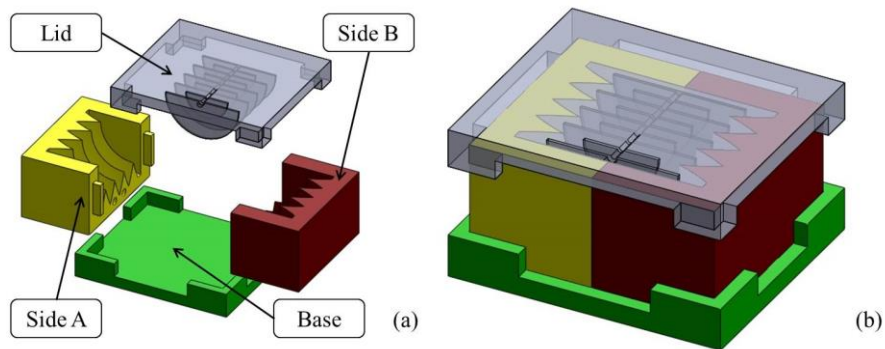
Figure 35: 3D Mold V1 for First Version of Extension Mechanism, (a) Exploded View; (b) Assembly View

Figure 35 shows a series of the molds which were used to fabricate the first version of the extension mechanism. The mold contains five pieces. The yellow piece (Side A) and brown piece (Side B) together form half of the extension mechanism. The green piece is the base piece that firmly holds the side pieces in place. The light grey piece is the lid which has two functions: one is to provide a better seal and another is to create the pneu-rooms inside the body. Figure 36 shows the assembled and disassembled mold.
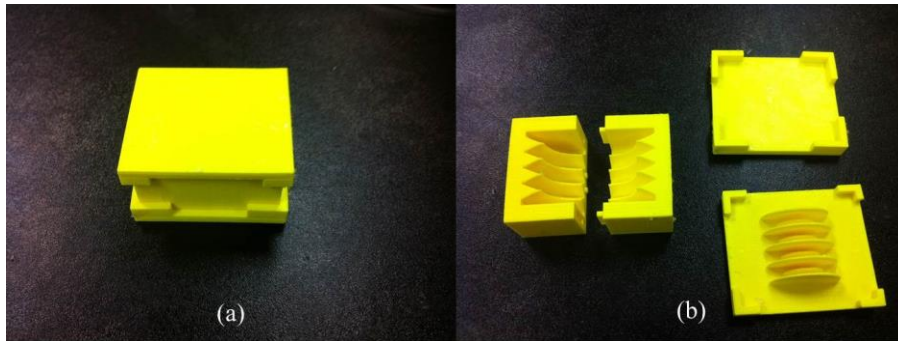
Figure 36: Mold V1 for Extension Mechanism V1, (a) Assembled Mold; (b) Separated Mold Pieces

Figure 37a, Figure 37b and Figure 37c give the isometric view, left view and front view, respectively, of the 3D model of the extension mechanism V1. The maximum diameter of the mechanism is 40 mm, and the minimum is 25 mm. The length is 30 mm. The mechanism has 9 thin disk shaped pneu-rooms with 5 large pneu-rooms and 4 small ones. The pneu-rooms have a thickness of 0.6 mm. The larger pneu-rooms have a diameter of 28 mm while the small ones have a diameter of 19 mm. The thinnest distance between the big pneu-rooms to the body surface is 2.5 mm and the thinnest distance between the small pneu-rooms to the body surface is 3 mm. The small hole located on one side of the body is for inserting the pneumatic tube. A 1 mm round channel goes through the middle of the body connecting all of the pneu-rooms. The geometric dimensions were arbitrarily chosen. The maximum diameter of 40 mm is the same as the diameter of first version of the capture mechanism.
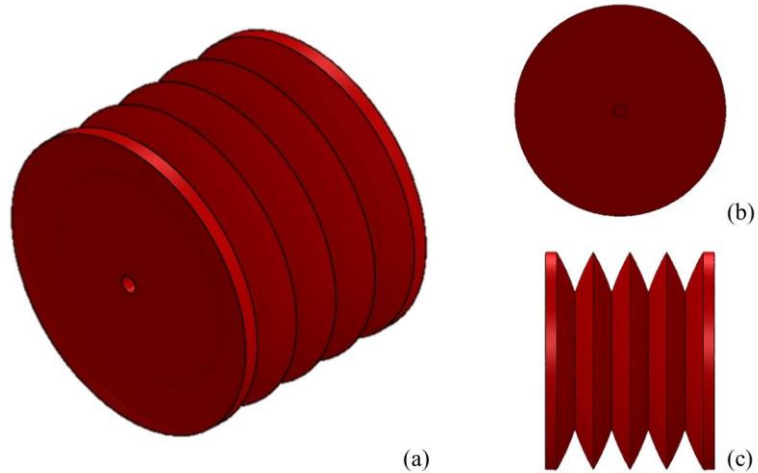
Figure 37: A 3D Model of the Extension Mechanism V1

Besides the unacceptable inflation shape of the extension mechanism V1, this design still has certain problems. There are bubbles in the initial silicone mixture. Generally, any bubbles within the mixture would rise to the top surface and diffuse into the air. However, the solid design of the lid prevents the bubbles from escaping the mold. Therefore, the bubbles accumulate at the top surface of the mechanism and cause imperfections in the mechanism as it cures. Examples of the imperfections are shown in Figure 38a. In addition, the bellows features within the green box did not contribute to any useful expansion which can be deleted. Figure 38b shows the 2D segmental sketch of the extension mechanism V1.
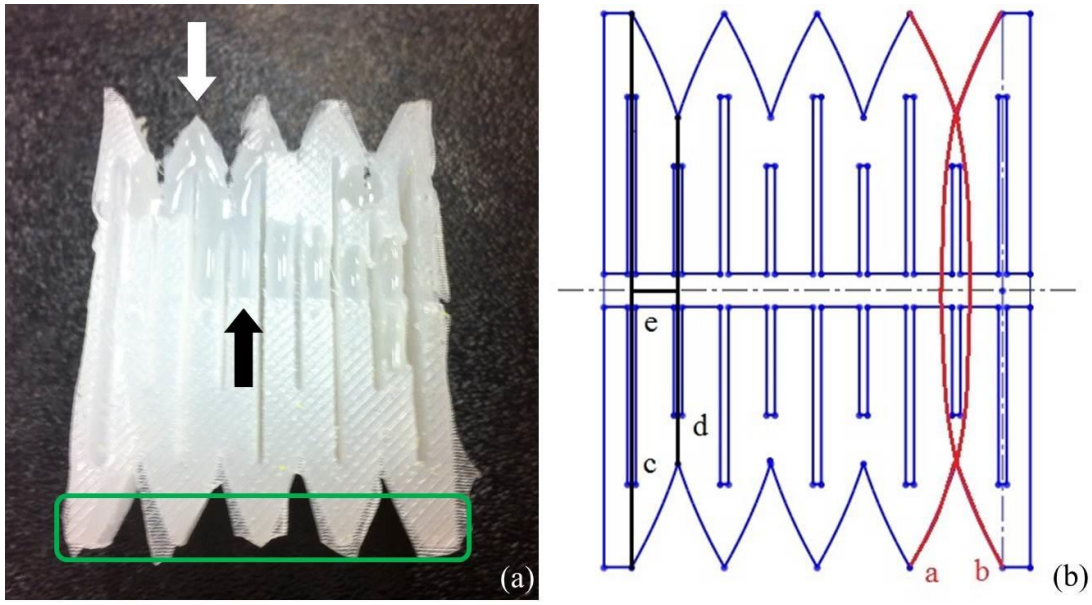
Figure 38: A Half of Extension Mechanism V1 Created by the Mold V1d, (a) Real Piece; (b) 2D Sketch

Because of the complicated geometric shapes, the distance between the large pneu-rooms and the surface of the mechanism is at least 0.5 mm less than the distance between the small pneu-rooms to the surface of the mechanism. The unequal thicknesses lead to an unequal inflation performance. During the inflation, the large pneu-rooms are the major contributors to the overall deformation of the mechanism. The small pneu-rooms hardly deformed.

3.3.2 Extension Mechanism V2

For the second iteration of the extension mechanism, the redundant features and the small pneu-rooms were removed. Figure 39 gives a 3D model for a series of V2a molds which create the second version of extension mechanism. The body dimensions have also been modified. The maximum diameter is 32 mm, the minimum diameter is 29 mm and the total length is 34 mm. The pneu-rooms are still 0.6 mm wide but are 30 mm in diameter.

The minimum thickness is 2 mm. In Figure 39, the light blue piece is a brush. The overflow material which exceeds the top surface of the brown and yellow pieces is brushed to the opening of the lid.
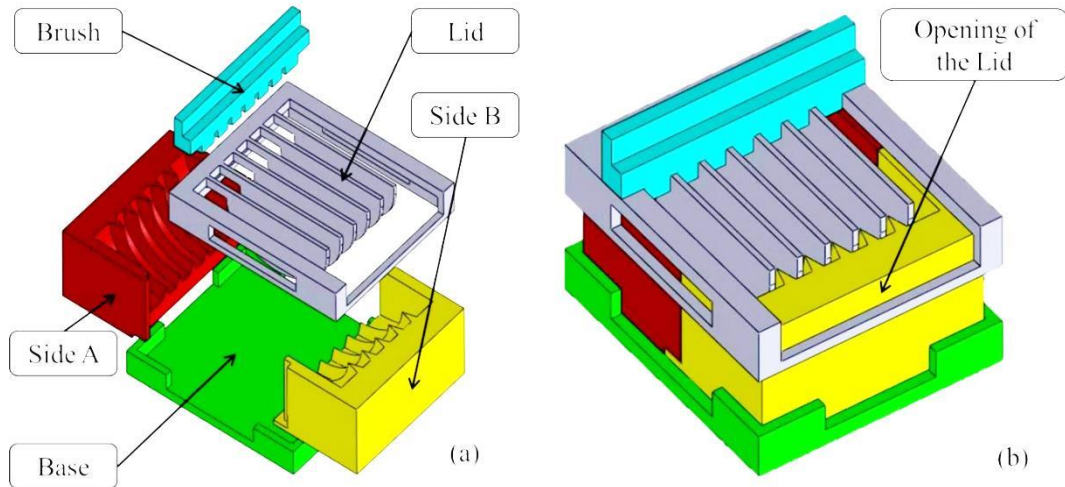
Figure 39: 3D Model for Mold V2a for Creating Second Version Extension Mechanism, (a) Exploded View; (b) Assembly View

Figure 40 shows a cross-sectional sketch of the extension mechanism V2. The arcs are now 52 mm in radius instead the previous 40 mm. The lines a, b and c, shown in Figure 40, form a right triangle where b represents the radius of arcs and c represents the maximum radius of the mechanism. The length of the green line e is the distance between c and d. The edges of the bellows have been trimmed down.

Even with the new open top design to release any trapped air, the final product still contained imperfections. There are a lot of "glitches" by the edges of the pneu-rooms as shown in Figure 41. Just like the hollows in the first version, these glitches affect the glue process.
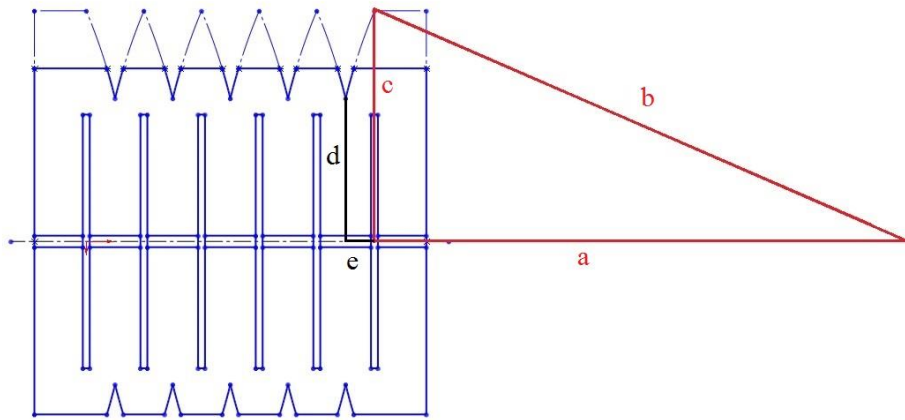
Figure 40: 2D Sketch of Extension Mechanism V2
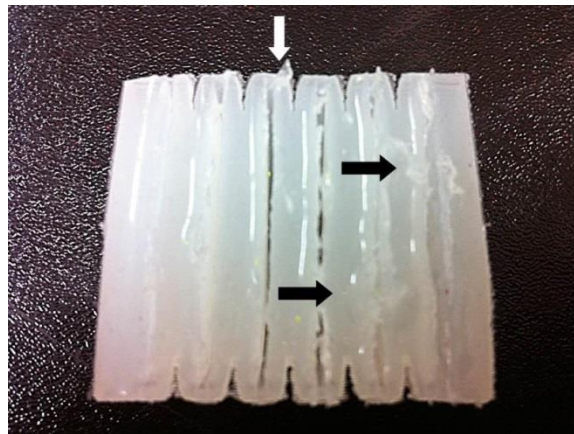
Figure 41: Half Extension Mechanism V2

To improve the quality of the silicone sample, the V2b mold was designed. The major change is the assembling of the mold. From Figure 42, the mold now "stands up." The brown and yellow pieces are still for holding the liquid materials and create body shape of the extension mechanism. The grey piece is no longer a lid and it now an L shaped piece. Together with the brown and yellow pieces, these three pieces form a container to hold the material. The opening at the top can release the bubbles. The green

and blue pieces hold the three pieces together for improved sealing. Figure 43 shows the fabricated mold assembled and disassembled.
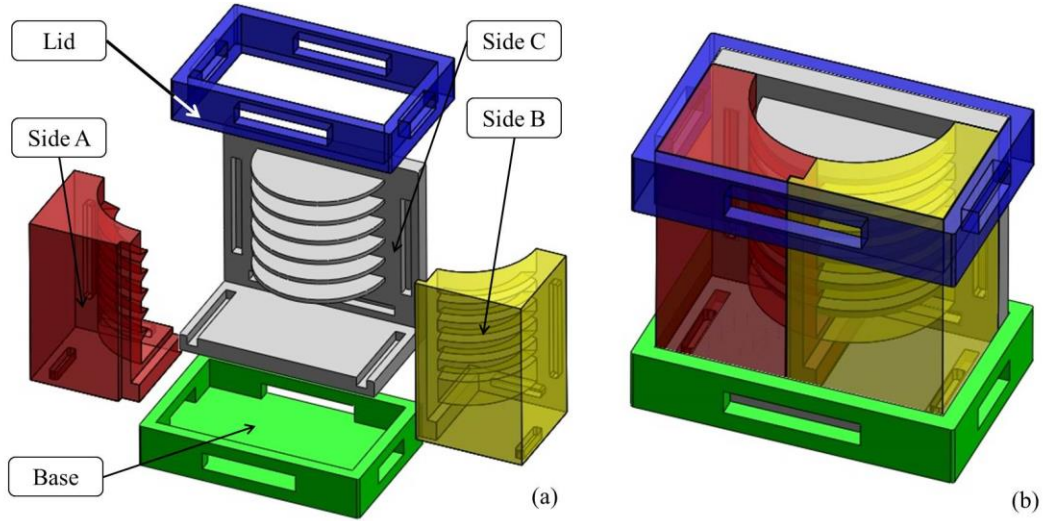
Figure 42: 3D Model of Mold V2b for Extension Mechanism V2, (a) Exploded View; (b) Assembly View
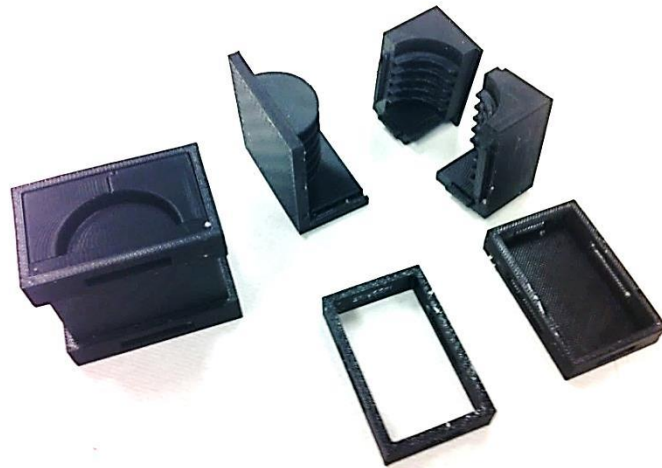
Figure 43: Real Parts Mold V2b for Second Version Extension Mechanism

Figure 44 shows the extension mechanism V2 sample produced with the new mold. The surface is flatter and more consistent, providing a better gluing surface. Figure

45a shows the original shape of a whole second version extension mechanism while Figure 45b show its inflated state at a pressure of 3psi. The length at 3psi is 118 mm which is 347% of the original length, but the distribution is not even. Also, the maximum diameter of the mechanism when inflated is 62 mm which is nearly 200% of original value.
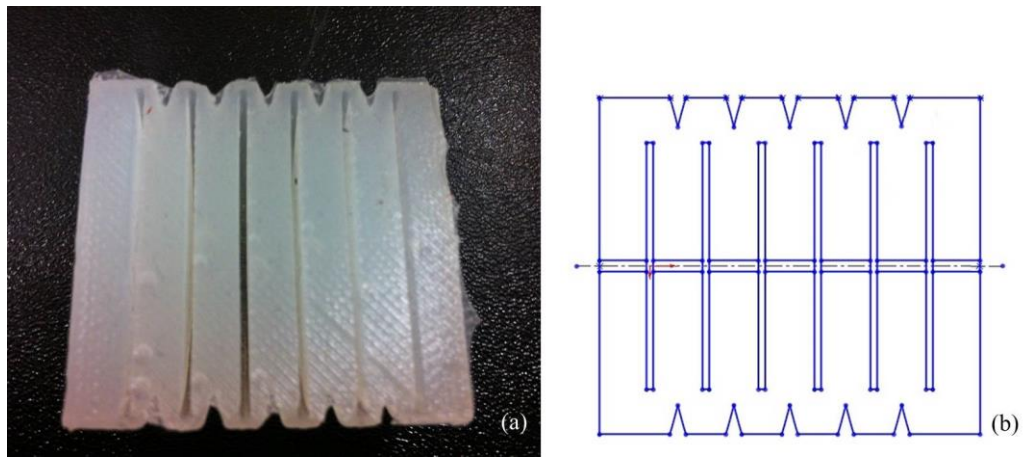
Figure 44: Half Optimized Second Version Extension Mechanism, (a) Real Piece; (b) 2D Sketch
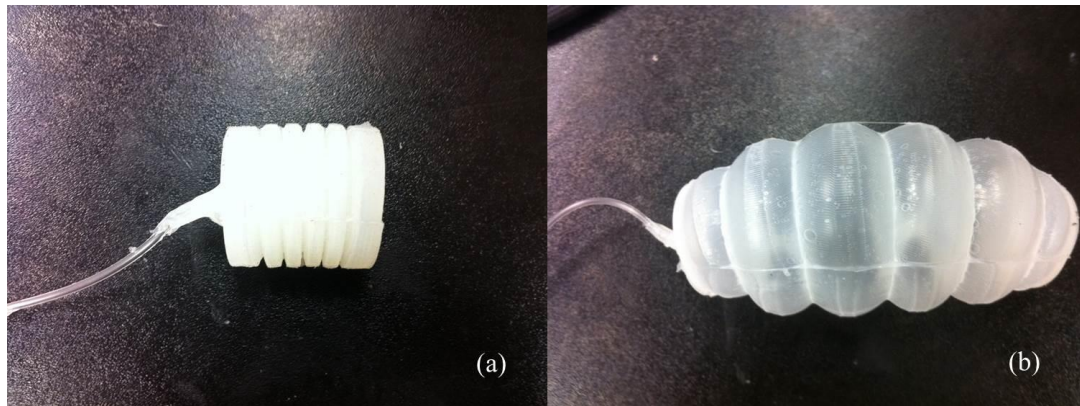
Figure 45: Extension Mechanism V2, (a) Original State; (b) Inflated State

3.3.3 Extension Mechanism V3

The third version of the extension mechanism design utilized a tubular form with ridges instead of previous cylindrical form with bellows. Figure 46 shows the 3D model of the mold for the extension mechanism V3. The mold contains 13 pieces. The blue piece creates the channels and pneu-rooms. The two red pieces and one yellow piece are the walls of the mold. There are hubs and supports on the two red wall pieces to capture the blue piece. These pieces are designed for simplifying the process of removing the sample after it has cured. The remaining nine pieces (green pieces) form the ridges on the surface of the extension mechanism.
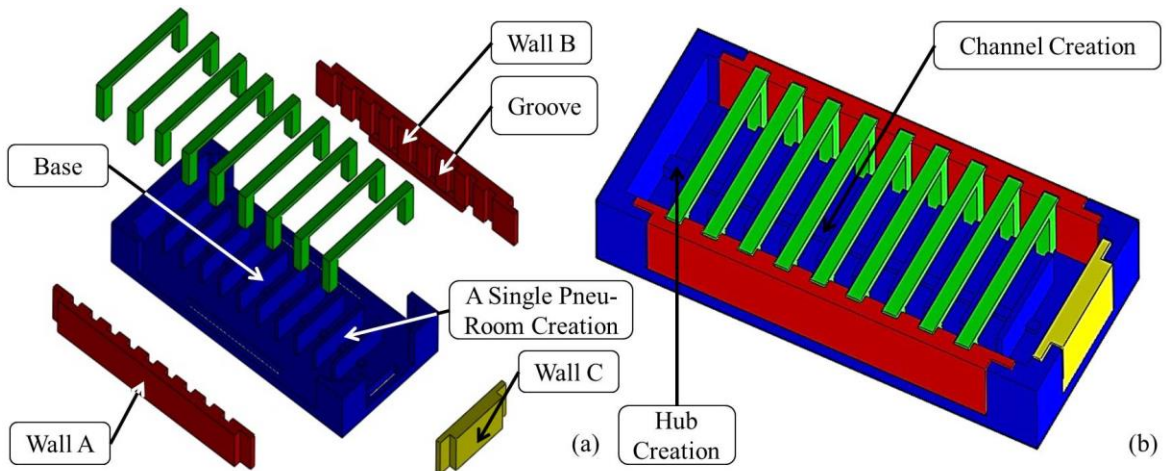
Figure 46: 3D Mold V3a for Extension Mechanism V3, (a) Exploded View; (b) Assembly View

Figure 47a shows the original shape of the extension mechanism V3. The dimension of the mechanism is 40 mm by 16 mm by 16 mm. There are 10 thin rectangular shaped pneu-rooms within the mechanism with dimensions of 0.6 mm by 10 mm by 10 mm. The channel is in the center of the part and is 1 mm by 1 mm. Each ridge is 16 mm by 16 mm with the nine troughs being 1 mm shorter than the ridges. This

mechanism performance well when it is inflated as shown in Figure 47b. The length at 3 psi is 80 mm which is 200% of the original length. The distribution is much better compared to the pervious cylindrical version. The maximum diameter of the mechanism when inflated is 30 mm which is 187% of original value. However, like the mold V3a for capture mechanism V3, the mold V3a for the extension mechanism V3 shares two similar problems. First, the mold does not seal properly. Figure 48 gives shows both a disassembled and assembled mold for the extension mechanism V3. The red circle in Figure 48 indicates the location which leaks during the fabrication process. Second, the pieces that form the ridges are 1 mm in thickness, which are extremely weak and may easily be broken. The feature indicated by the green circle can also be easily broken.
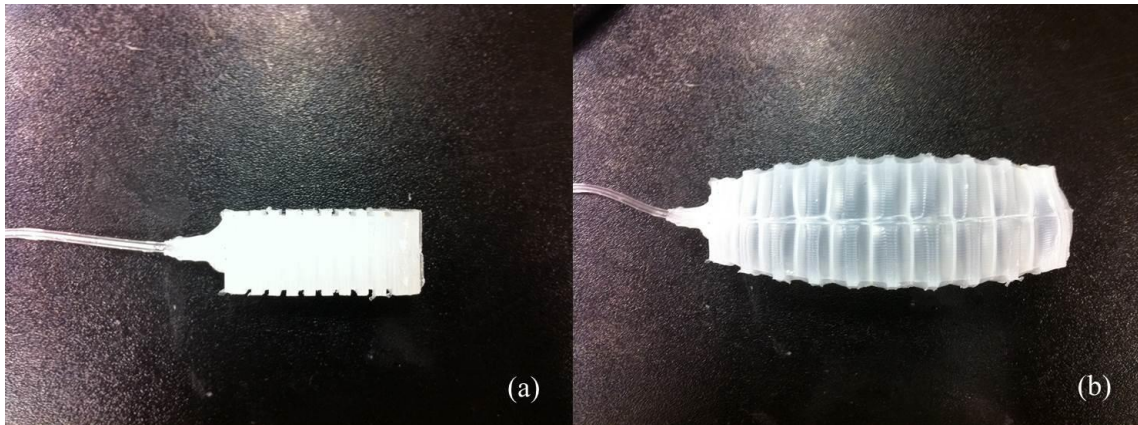
Figure 47: Extension Mechanism V3, (a) Original State; (b) Inflated State

To correct the leaking and weak aspects of the mold, a new mold V3b was developed. Figure 49 shows the modified design of the red pieces and green pieces in mold V3a (Figure 46). These pieces are now a single piece which increases strength, and simplifies assembly and sample removal. This design follows the idea of the mold V3a for the capture mechanism. There are flanges on the main piece, shown in Figure 50, to

locate and fix other pieces as well as provides a better seal. The bottom flanges are 1 mm in height and the wall-side flanges are 2 mm in height. All of the flanges are 1 mm wide. There are grooves on the wall pieces as well. The grooves are 1.4 mm wide which simplifies the assembly process.
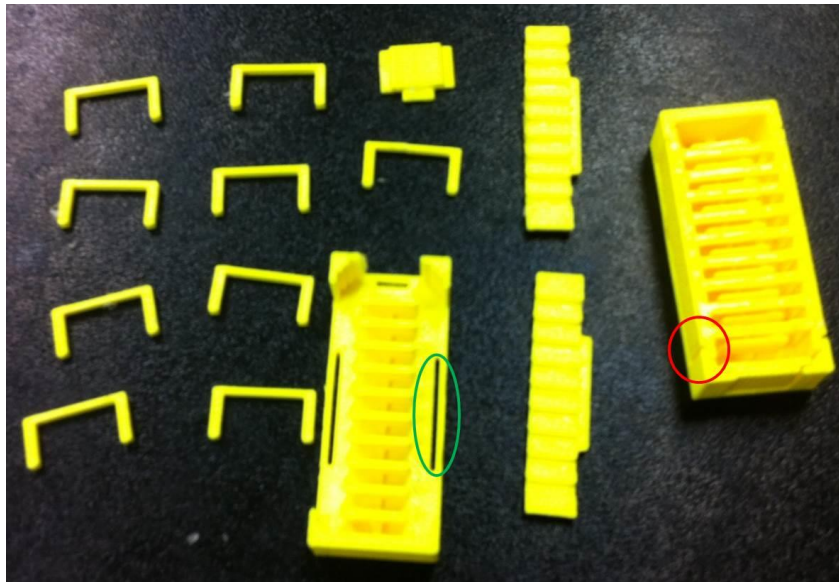
Figure 48: Mold V3a for Extension Mechanism V3
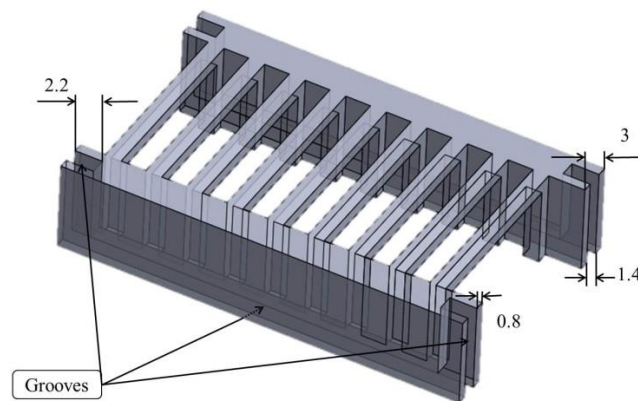
Figure 49: A Modified Piece of Mold V3b Integrated all Small Pieces in Mold V3a
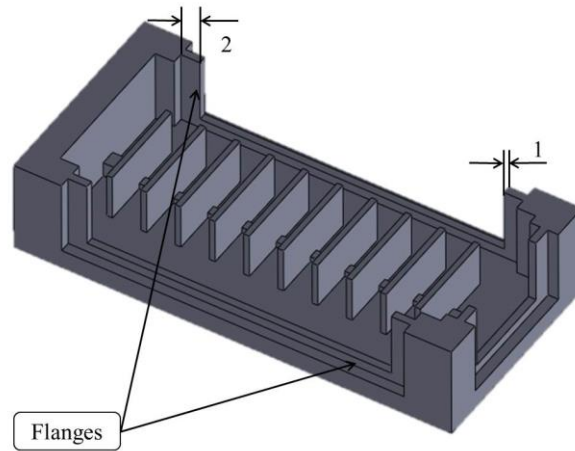
Figure 50: Main Piece of Mold V3b for Extension Mechanism V3

3.4 Precautions in the Fabrication Process

The fabrication process of the mechanisms can be complicated and tricky. There are two kinds of problems which can ruin the final outcome: post-fabrication problems such as the mechanism being inflated with too much pressure and imperfections in the mechanism. This section will provide some common fabrication problems and their resolution.

3.4.1 Glue Process in Fabricating Capture Mechanisms

The gluing process is the most difficult process. In this process, a thin but evenly spread glue layer of silicone material is applied above the lower layer. Then, the upper layer is removed from the mold and placed on top of the glue layer. After the glue layer has cured, the upper layer and lower layer form a single mechanism. The majority of failures during the fabrication process are caused by the gluing process.

61

If the glue layer is too thin to spread over the entire top surface of the lower layer, it will lead to a an improper seal as shown in Figure 51. If the glue layer is too thick, it will fill into the ring-shape channel and after curing, the channel will disappear. The left bottom mechanism of Figure 52 is a good quality mechanism whose channel can be seen clearly. The channel of the right bottom mechanism is totally gone and all the pneu-rooms are separated with no inflation channel. The channel of the top mechanism has been half jammed.
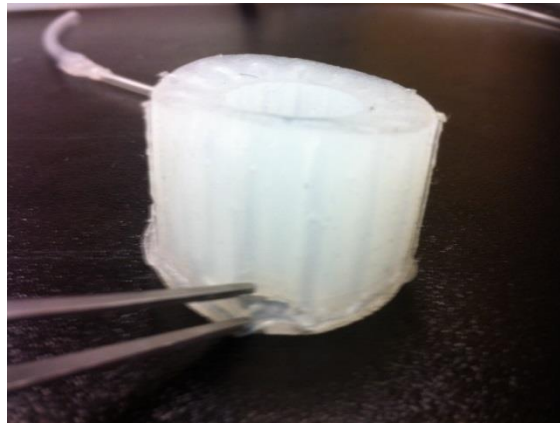
Figure 51: Fail to Glue Together

The following lists the gluing procedures for obtaining the best sample. After applying a glue layer, wait for 1 minute to let the material spread all over the surface. Then, scrape off the redundant material to keep the thickness of the layer around 0.2 mm. After waiting for another 15 minutes, the material should become stickier and more viscous. Finally, put the upper layer onto the glue layer. The waiting time should not be too long since the viscosity quickly increases. If the viscosity becomes too high, the gluing process may still fail.
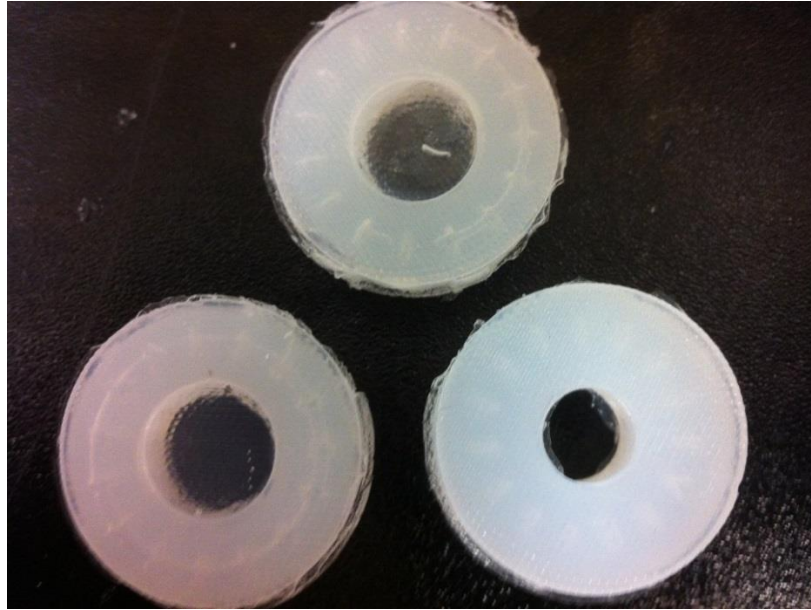
Figure 52: How Gluing Process Affects the Channels

3.4.2   Burst in Inflation of the Capture Mechanisms

There are two factors which may cause mechanisms to burst while in use: 1) too high of an inflation pressure or 2) poor mechanism quality e.g. improper glue or residual bubbles within the structure.
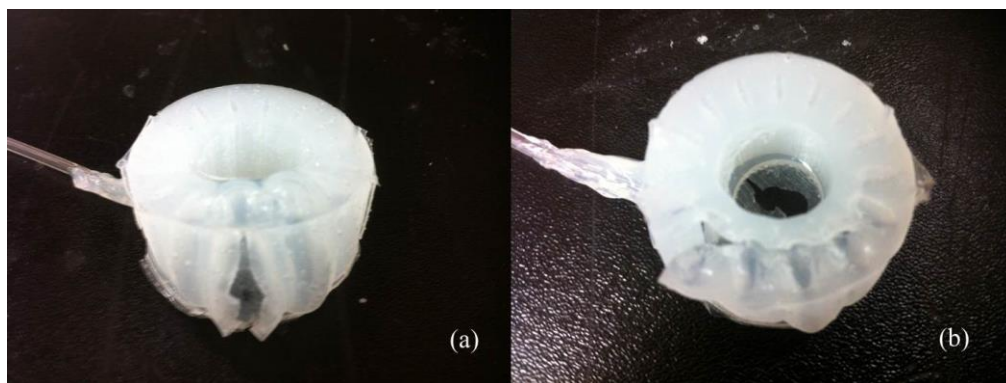
Figure 53: Surface Burst, (a) Cylindrical Surface Burst; (a) Top Surface Burst

Figure 53a and Figure 53b shows an external surface burst. Figure 54a shows an internal structural burst of a mechanism when not inflated, and Figure 54b shows the deformation of the same mechanism with a low inflation pressure. As can be seen, the distribution of air is not evenly spread to each pneu-room after a wall between two pneu-rooms has burst. Any burst, no matter where, leads to a completely destroyed mechanism that cannot be used again.
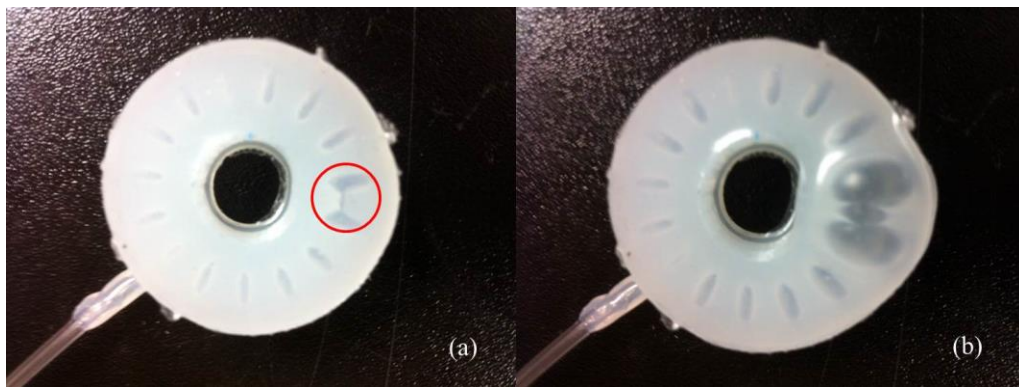
Figure 54: Internal Structural Burst, (a) Original State; (b) Inflated State

3.4.3   Problems in Fabricating Extension Mechanisms

As with the capture mechanism fabrication process, the gluing process is the most difficult process when fabricating the extension mechanism. Unlike the gluing process in the fabrication of the capture mechanisms, which applies glue onto the flat surface of lower layer, for the extension mechanisms, the glue is applied to the middle of the mechanism as shown in Figure 55. There are channel and pneu-rooms which make the surface full of grooves. If a thick glue layer is applied, the extra material may flow into the inflation channel and pneu-rooms which can cause the two walls to stick together or

the bottom of the pneu-rooms to be full of the silicon materials and reduce the size of pneu-rooms. A lack of glue would cause a trend of internal bursts as shown in Figure 56.
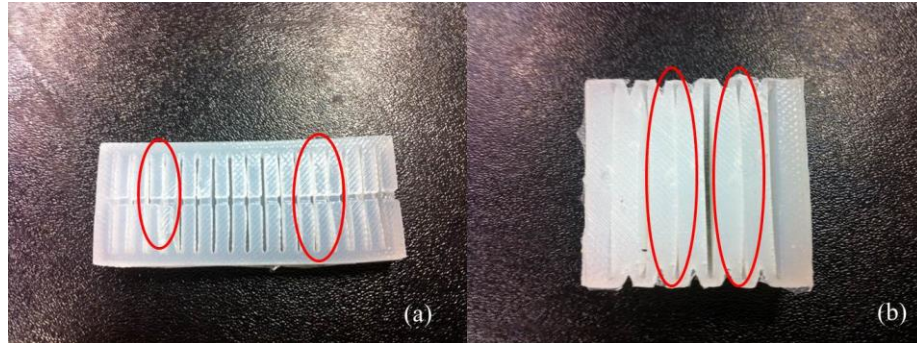
Figure 55: The glue Surfaces, (a) Mechanism V3; (b) Mechanism V2

Another result is the size of the mechanism would affect the fabrication process. Since the material is viscous and extremely soft, if the mechanism has a big size, the walls between pneu-rooms are correspondingly long. It is hard to keep the long walls straight, as the walls tend to stick together as red cycle shown in Figure 55.

Figure 56: An Internal Structure Burst

Chapter 4

Empirical Study on Soft-Body Interconnect Mechanism Designs

The third versions of capture and extension mechanisms performed well when inflated. However, the value of the geometric parameters such as height, diameter and thickness for the mechanisms were arbitrarily chosen. There may exist a more optimal selection of parameters for designing extension and capture mechanisms for soft-body interconnection mechanisms. An empirical study was completed to generate diagrams that correlate parameter selection with desired performance outcomes. Future designers of soft-body interconnection mechanisms may utilize the diagrams as design tools.

The following sections detail the methodology and hardware setup for evaluating the performance of the soft-body extension and capture mechanisms, and present the

results of the empirical study. The study generated multiple samples of soft-body extension and capture mechanisms, each with varying changes in the structural parameters. The effect of the parameter change was evaluated and presented in a series of pressure versus strain diagrams. The diagrams were used to design a final version of the soft-body interconnect mechanism.

4.1   Evaluation Methodology and Hardware Setup

The evaluation of the soft-body extension and capture mechanisms correlates the physical deformation of the mechanism with the inflation pressure. Generally, this process would require incrementally changing the inflation pressure and manually measuring the deformation. However, this process would be rather tedious when dealing with more than a few samples.

An evaluation setup was created to help simplify data gathering and sample measurements. Figure 57 depicts the block diagram of the evaluation setup. The sample being evaluated is connected to an air pump which provides incremental inflation pressures. To measure the pressure, a Y-junction was added to the inflation line with the second channel going into a pressure transducer to measure the inflation pressure. The pressure transducer is connected to LabVIEW which converts the reading and displays it. A camera was used to measure the inflation deformation of the sample. A ruler was placed within the field of view of the camera to provide a pixel to mm reference.

During the evaluation process, the pressure is manually increased by 0.1 psi. At each interval, a snapshot is taken to record the shape of the sample and the pressure is recorded.
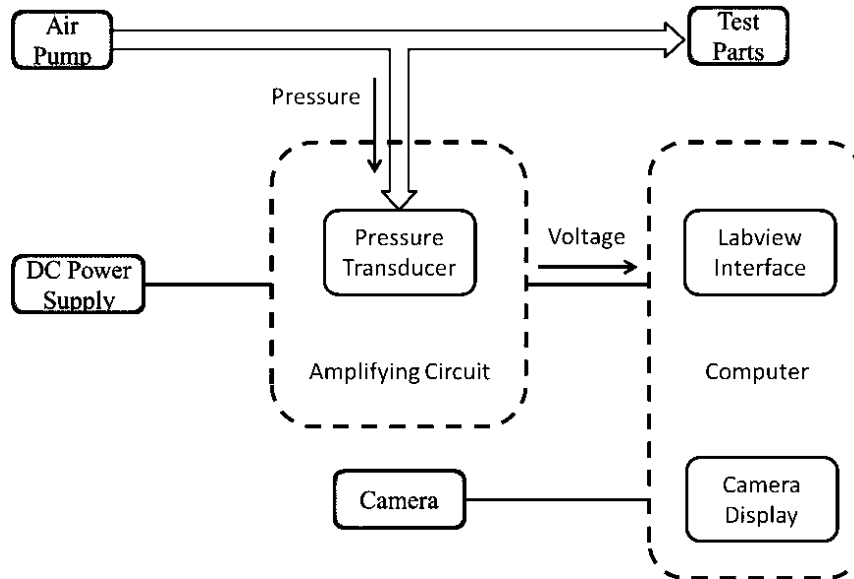
Figure 57: A Block Diagram of the Soft-Body Evaluation Setup

4.1.1   Hardware Setup

Figure 58 shows the physical image of the hardware setup. An air pump, an amplifying circuit with a pressure transducer implemented on a bread board, a data acquisition (DAQ) board, a camera and a power supply which provide power to both pressure transducer and the amplifying circuit are used in this experiment.
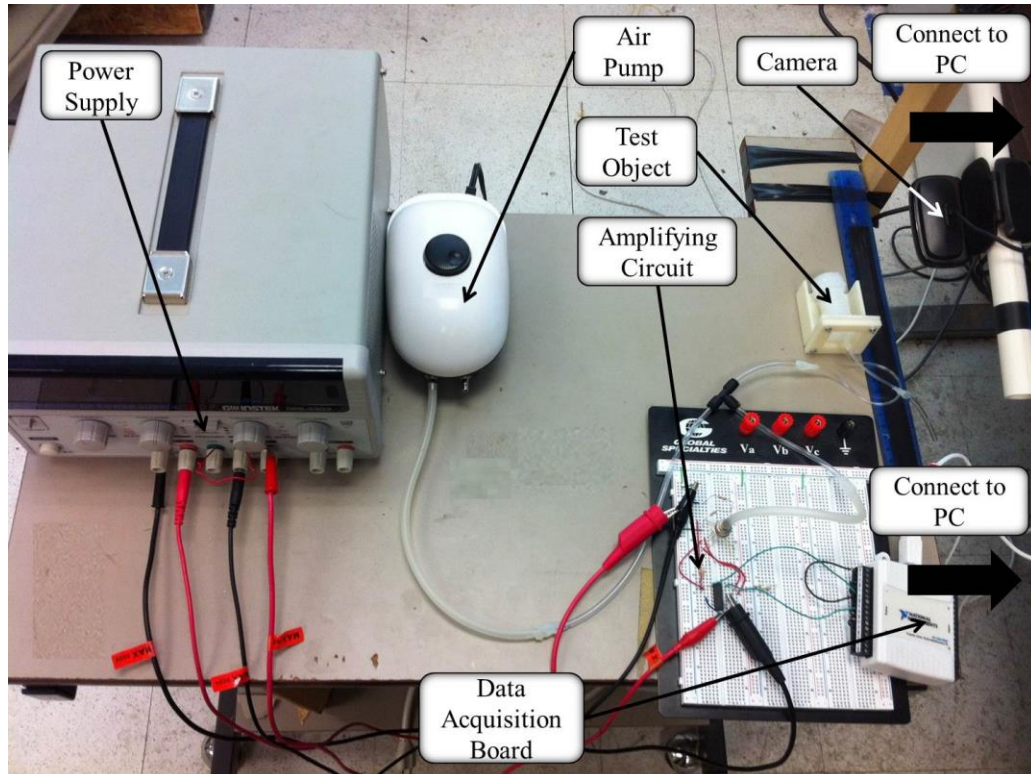
Figure 58: Hardware Setup

The core equipment among all hardware is pressure transducer. The pressure transducer is a temperature compensated, piezoresistive silicon pressure sensor packaged in a TO-8 configuration. The transducer detects pressure and outputs a corresponding voltage signal. The pressure range of the sensor is 0 to 5 psi and with an output range of 0 to 100 mV. To obtain higher resolution, an amplifying circuit was built. Figure 59 shows the schematic of the circuit.
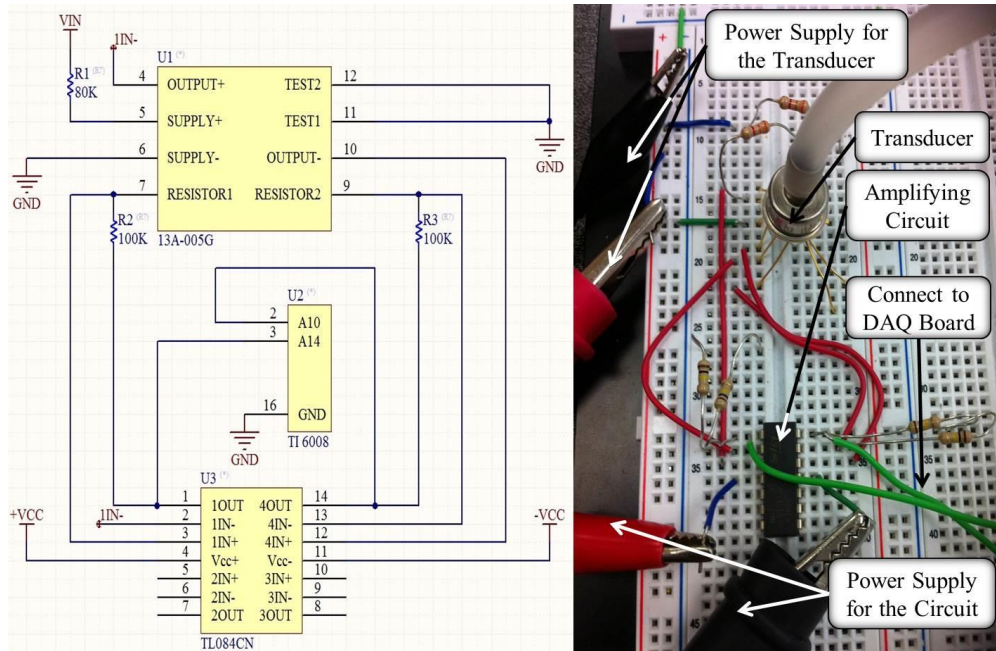
Figure 59: Amplifying Circuit, (a) Schematic; (b) Real Circuit Built on a Bread Board

The DC power supply provides power to both the amplifier circuit and pressure transducer. The voltage signal will be collected by a DAQ board (USB-6008 from National Instruments) then displayed on computer through Labview interface. The required operating voltage of amplifier is -12V to +12V and the required operating current is 1.5mA.

There will be an air pump providing air. The air goes through tubing and a tee pipe fitting to the pressure transducer as well as the test part (capture mechanism and extension mechanism). The pressure range of air pump is 1.4psi to 3.0psi. The corresponding voltage range is 1.055V to 2.475V after amplified. The pressure transducer provides a highly linear relationship of pressure versus voltage.

4.1.2 Evaluation Methodology

Using the captured images of the sample, the deformation of the sample is acquired with the following steps:

- Determine how many pixels of the diameter, height or length of a certain test part.
- Determine how many pixels of one millimeter.
- Calculate the actual dimension.

The formula of calculation for the dimension is following:

$$y = \frac{1}{\rho}\frac{\bar{x}}{a}$$

where y is the actual dimension in millimeter, $\bar{x}$ is the average value of multiple measures in number of pixels, a is the numbers of pixel of one millimeter and ρ is a compensation factor.
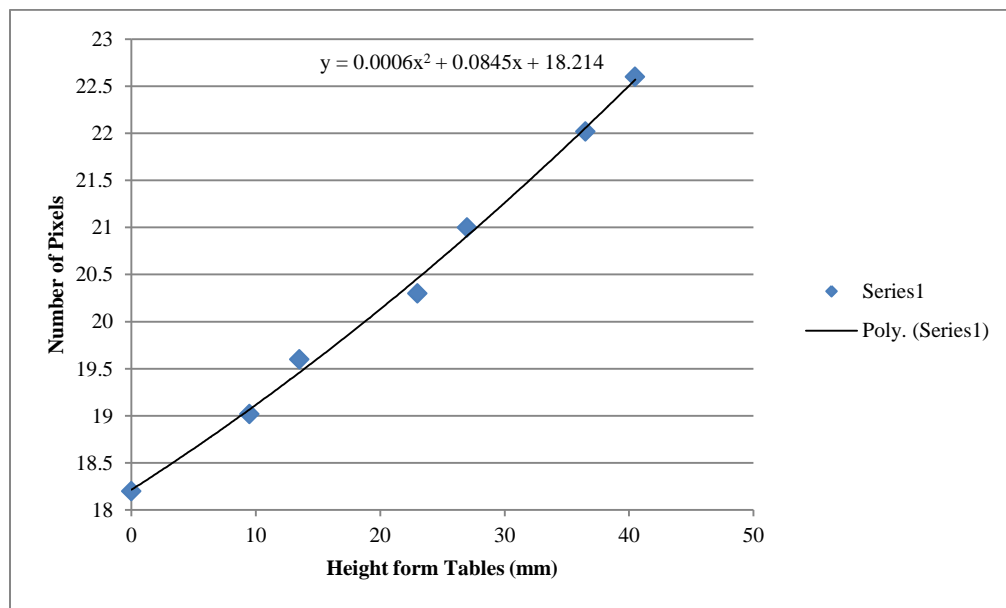
Figure 60: Pixel Changing of One millimeter in Different Height

The reason of introducing a compensation factor into the formula is as follows. The camera is fixed above the table and the test sample and ruler are placed on the table. As the sample is inflated, the sample expands and the top of the sample displaces towards the camera. Due to the characteristics of the camera lens, the closer anything gets to the camera lens, the bigger it will display on the photo. Hence, a series of snapshots of the ruler at different heights were taken. The data was plotted providing the pixels per millimeter versus height as shown in Figure 60.

4.2 Empirical Study Results for the Capture Mechanism

This section provides detailed empirical data of the shape changing trend of the capture mechanism when inflated. The final capture mechanism design (V3), from the iterative design process, has a cylindrical shape with a cylindrical hollow center. The dimensions of the capture mechanism are as follows: the diameter of the cylinder shape is 30 mm, the height is 11.5 mm (including the 10 mm for the upper layer and 1.5 mm for the lower layer) and an overall thickness of 1.5 mm which is the distance from the pneu-rooms edges to all of the surfaces of the mechanism except to the hollow center. To insure that the pneu-rooms will be inflated radially outwards, the thickness of pneu-rooms to hollow center is 1 mm thicker than the other thickness.

The deformation occurs towards both radially and axially, thus, the diameter and height will be adjusted to see if they have an impact on the deformation performance. As mentioned in Section 3.3.1, the material is highly thickness-sensitive when inflated. Therefore, the thickness will be included in the parameters adjustment. The height of the pneu-rooms will change correspondingly since the thickness and height of the mechanism

will also varying accordingly. During the iterative design phase, the number of pneu-rooms was varied (12, 15 and 23) along with the length (11 mm, 7.5 mm and 3.5mm). During the iterative design phase, it was found that the number of pneu-rooms and their length did not drastically affect the deformation performance which can be seen in Figure 22, Figure 26 and Figure 29.

The empirical study for the capture mechanism was focused on varying the diameter, height and thickness of the capture mechanism. For the diameter samples, the base design has a height of 11.5 mm and a thickness of 1.5mm. Three diameters were tested: 22 mm, 26 mm and 30 mm (default). For the height samples, the base design had a diameter of 30 mm and a thickness of 1.5 mm. Five heights were tested: 9 mm, 11.5 mm (default), 14 mm, 17.5 mm and 19 mm. For the thickness test, the base design had a height of 11.5mm and a total diameter of 30 mm. Four thicknesses were tested: 1 mm, 1.5 mm (default), 2 mm and 2.5 mm.

4.2.1 Varying Diameter

The diameters tested in this experiment, shown in Figure 61, were 22 mm, 26 mm and 30 mm (default). Figure 62 shows the diameter changing (radial direction deformation) between 1.4 psi to 3.0 psi. Figure 63 shows the height changing (axial direction deformation) between 1.4 psi to 3.0 psi.
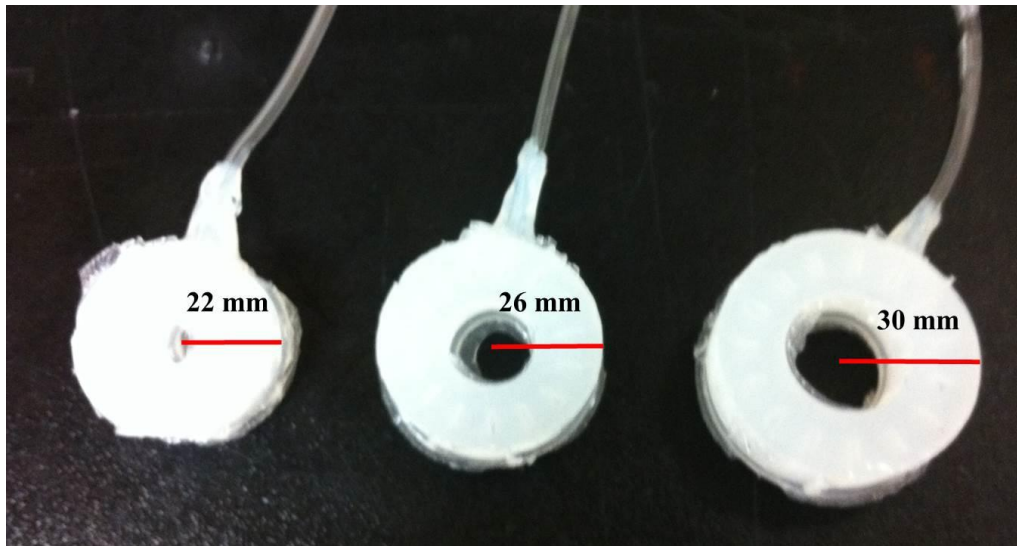
Figure 61: Three Breeds Varying in Diameters
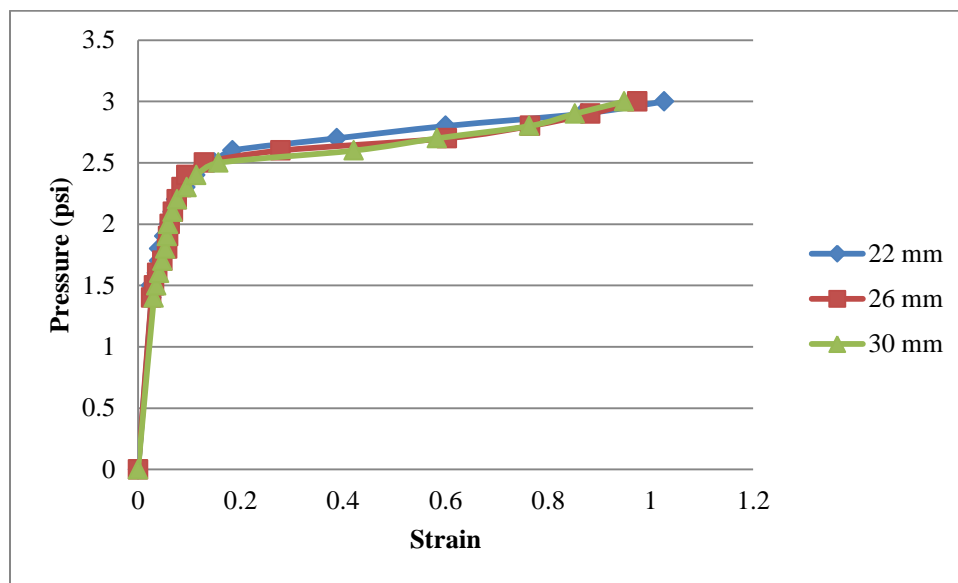
Figure 62: Radial Direction Strain for Diameter Values Adjustment Experiment
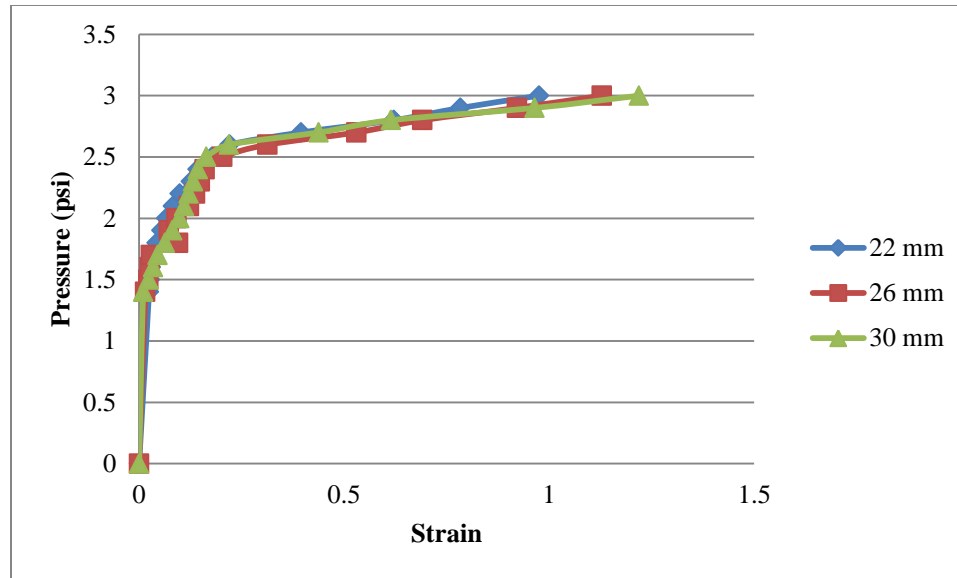
Figure 63: Axial Direction Strain for Diameter Values Adjustment Experiment

As can be seen in Figure 62, the pressure versus strain curves in the radial direction are similar, which indicates a direct correlation between the diameter and radial expansion.

Table 1: Data of Diameter Values Adjustment Experiment in the Final State (3psi)

	22 mm	26 mm	30 mm
Diameter (mm)	44.6	51.3	58.5
Height (mm)	22.8	24.7	25.5
Deformation Rate in Radial Direction (%)	202.7	197.4	194.8
Deformation Rate in Axial Direction (%)	197.5	212.8	221.9

The capture mechanisms with a smaller diameter have a slightly higher deformation rate as indicated in Table 1. However, the difference between the 30 mm to 22 mm diameters is approximately 7.1% or 4% relative to the largest deformation percentage. Similar to the radial deformation, the axial deformation indicates a direct correlation between diameter and axial deformation with a difference of approximately 1 mm.

4.2.2   Varying Height

For the height test, five different heights were evaluated: 9 mm, 11.5 mm (default), 14 mm, 16.5 mm and 19 mm. All five samples are shown in Figure 64.
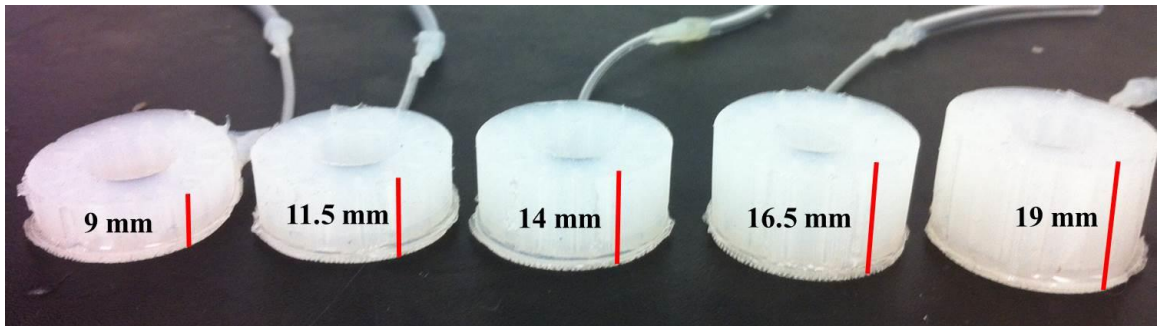
Figure 64: The five samples varying in height

Figure 65 shows the diameter changing (radial direction deformation) between 1.4 psi to 3.0 psi. Figure 66 shows the height changing (axial direction deformation) between 1.4 psi to 3.0 psi.
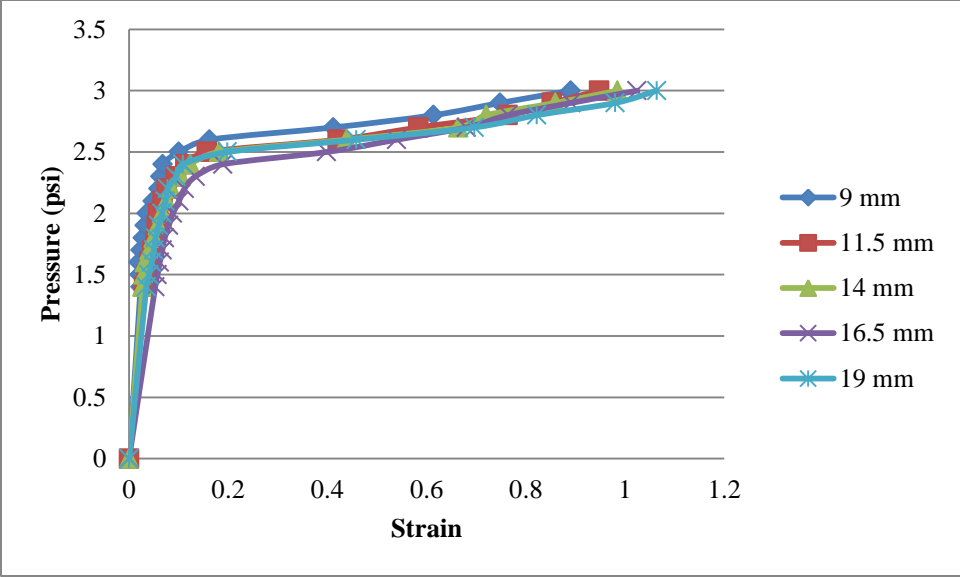
Figure 65: Radial Direction Strain for Height Values Adjustment Experiment

Varying height values does not help mechanisms performing differently in height deformation. The curvatures are almost the same of all five samples, which can be seen in Figure 66.
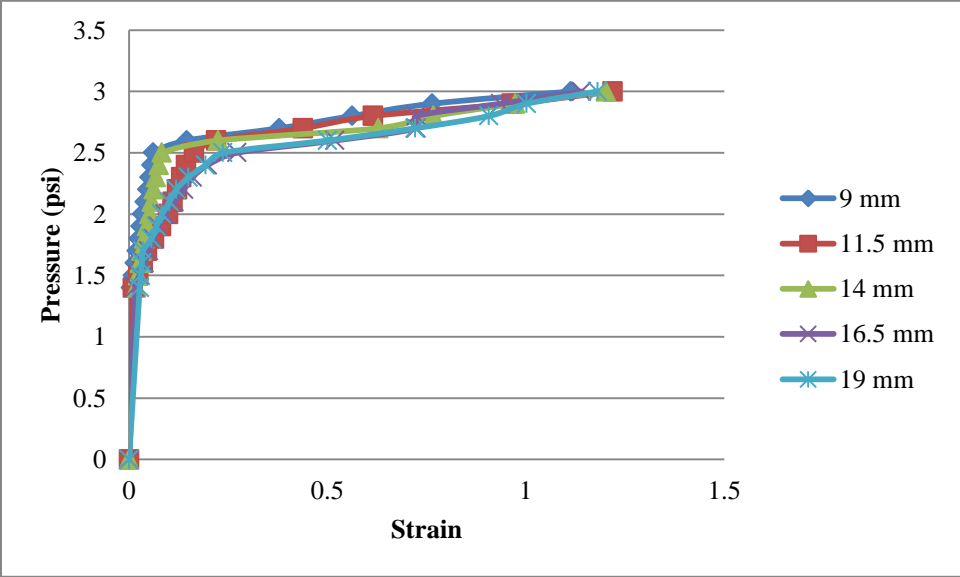
Figure 66: Axial Direction Strain for Height Values Adjustment Experiment

The initial height differences also have an insignificant influence on the radial direction deformation. The taller the sample, the larger the deformation rate it will have along the radial direction, which can be seen in Table 2.

Table 2: Data of Height Values Adjustment Experiment in the Final State (3psi)

	9 mm	11.5 mm	14 mm	16.5 mm	19 mm
Diameter (mm)	56.8	58.5	59.6	60.8	61.9
Height (mm)	19.2	25.5	30.7	35.3	41.4
Deformation Rate in Radial Direction (%)	189.0	194.8	198.5	202.5	206.4
Deformation Rate in Height Direction (%)	211.4	221.9	220.2	214.1	218.1

4.2.3   Varying Thickness

The thickness test had 4 samples with varying thickness: 1 mm, 1.5 mm (default), 2 mm and 2.5 mm. The distance between pneu-rooms to the hollow center is always 1 mm greater than the values above making it 2 mm, 2.5 mm (default), 3 mm and 3.5 mm, respectively. In this experiment, a syringe is applied to supply extra pressure. The upper limit of pressure in this experiment is 3.5 psi. Though the thickness difference cannot be clearly witnessed by appearance of the design, the four samples are shown in Figure 67.
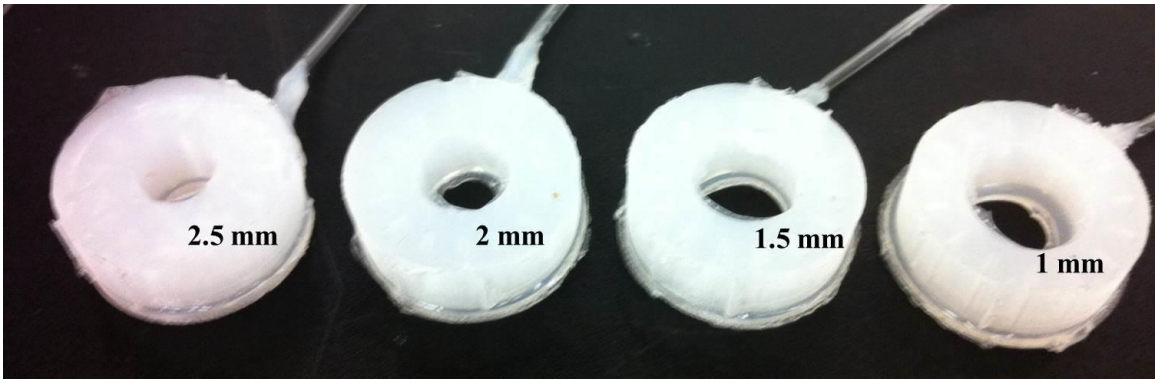
Figure 67: Four Breeds Varying in Thickness

Figure 68 shows the diameter changing (radial direction deformation) between 1.4 psi to 3.5 psi in which the solid green and purple line shows the mechanisms operated by air pump and the dashed green and purple line shows the mechanisms operated by syringe. Figure 69 shows the height changing (axial direction deformation) between 1.4 psi to 3.5 psi in which the meaning of solid lines and dashed lines are the same of Figure 68.
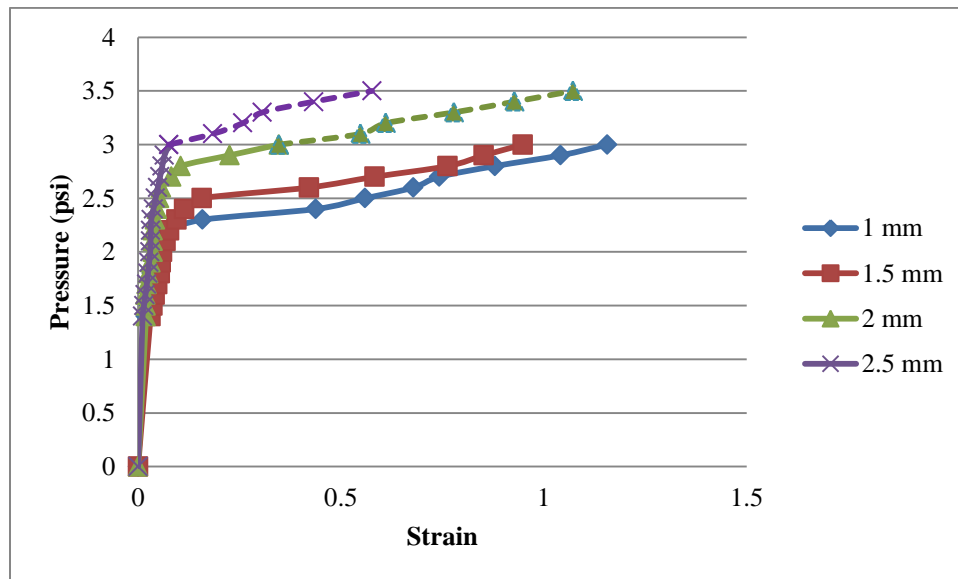
Figure 68: Radial Direction Deformation for Thickness Values Adjustment Experiment
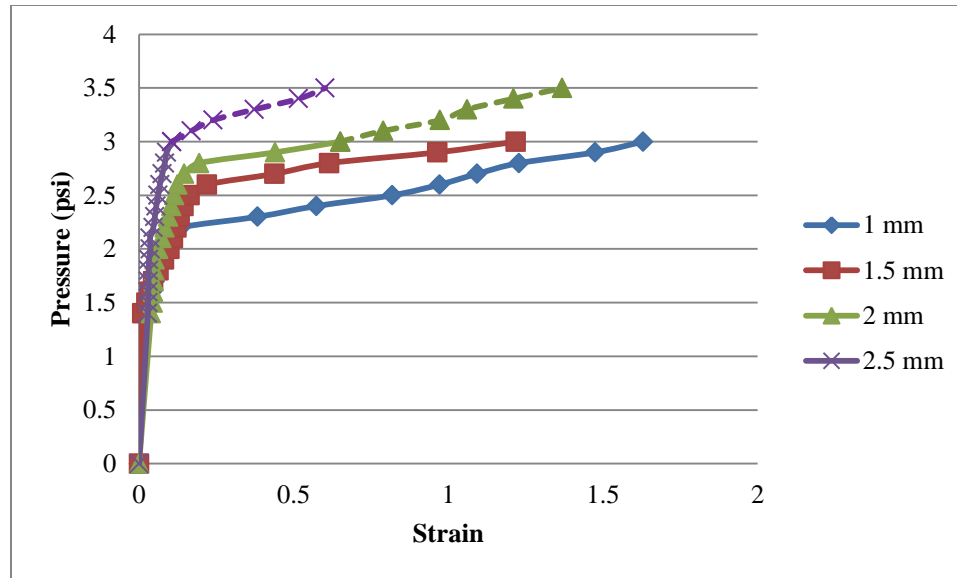
Figure 69: Axial Direction Deformation for Thickness Values Adjustment Experiment

The thickness adjustment has great effects on both diameter and height deformation. As can be seen in Figure 68 and Figure 69, two pictures are similar despite the difference in strain values. The sample with 1 mm thickness has a greatest strain, compared to others, under same pressure. However, at the same time, this sample is weakest due to its thin walls. There are multiple measures of each sample used in the experiment, and the pieces with 1 mm thickness start to burst at 2.8 psi. Therefore, 3.0psi is the upper limit of this sample with 1 mm in thickness. The default design performance good as well, the majority of them burst under the pressure of 3.1 psi to 3.5 psi. The sample with 2 mm in thickness does not fully extend in 3psi which just has a deformation rate of 135% which can be seen in Table 3. It provides a similar performance under 3.5psi as sample of 1 mm in thickness did under 3.0psi. Some the pieces of this samples used in the experiment burst at 3.5psi. Therefore the sample with 2 mm in thickness is better to inflate no more than 3.5psi. The sample with a thickness of 2.5 mm does not fully extend in 3.0psi and even does not fully extend in 3.5psi. Its deformation rate is

80

158% at 3.5 psi. In this experiment, it shows that the thinner sample provides better performance, but thinner samples are weaker.

Table 3: Data of Thickness Values Adjustment Experiment in the States of 3psi and 3.5psi

	1 mm	1.5 mm	2 mm		2.5 mm	
			3.0 psi	3.5 psi	3.0 psi	3.5 psi
Diameter (mm)	64.6	58.4	40.4	62.2	32.3	27.3
Height (mm)	29.0	26.3	19.9	28.5	13.9	20.1
Deformation Rate in Radial Direction (%)	215.6	195.6	134.7	207.0	108.3	157.6
Deformation Rate in Height Direction (%)	262.9	221.8	165.1	236.8	110.6	160.2

The Pressure-Strain Relationship of each design of third version of capture mechanism can be simplified to two linear parts. There is a threshold in the relationship. If the pressure is lower than the threshold, the mechanism expands in a small amount every time when added gradient pressure (0.1psi). However, the mechanism expands obviously after the pressure higher than the threshold. The experiments show that threshold and strength of the mechanism depends greatly on a small change of thickness, for example, the threshold of a capture mechanism in thickness of 1 mm is 2.2psi and of a capture mechanism in thickness of 2.5 mm is 3psi. The diameter and height change also have influence on these two characteristic of mechanism but is not that obvious. For

example, the threshold of a capture mechanism in height of 9 mm is 2.4psi while the threshold of a capture mechanism in height of 19 mm is 2.6psi.

4.3 Empirical Study Results for the Extension Mechanism

This section provides detailed empirical data of the shape changing trend of the extension mechanism when inflated. There are five samples of third version of extension mechanism will be tested. Figure 70a shows the original state of the initial design and Figure 70b to Figure 70e are four samples which have tiny differences being applied. All five samples are 40 mm in length and the maximum height and width are 16 mm while the minimum height and width are 14 mm. There are 10 thin rectangular shape pneu-rooms in it and the dimension is 0.6 mm x 10 mm x 10 mm. the channel is in the center of the part and the segmental dimension is 1 mm x 1 mm.
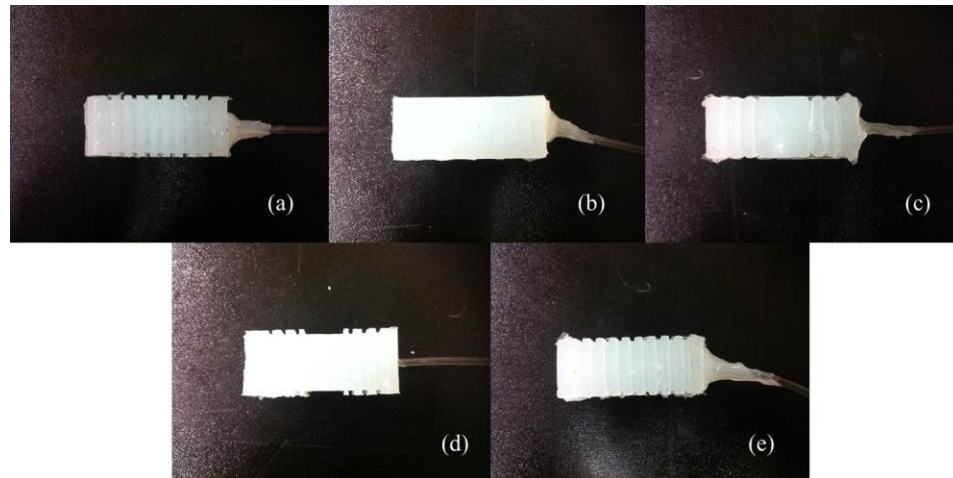
Figure 70: Five Breeds of Third Version of Extension Mechanisms

The sample of Figure 70a is called a "full texture" design which has 9 troughs on the surfaces. The sample of Figure 70b is called a "no texture" design which has all flat surfaces. The sample of Figure 70c is called a "reinforced center" design which canceled

the three middle troughs. The sample of Figure 70d is called a "reduced center" design which, on the contrary to "reinforced center" design, has a giant trough in the center of the surfaces while all the 7 troughs still are 1 mm in depth. The sample of Figure 70e looks the same as "full texture" design, but the width of four middle pneu-rooms is 7 mm which is 3 mm shorter than the original design. All the samples are aiming at two goals: Trying to extend as long as possible as well as making equal distribution of each pneu-room when inflated.
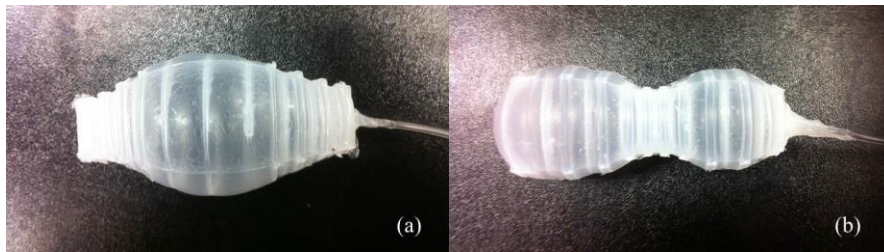
Figure 71: Two Kinds of Bad Inflation Shapes

Figure 71a shows the inflated state of a reduced center design which is similar to a spindle shape. The center expands too much along the direction perpendicular to the axial direction while two ends expand much less. Figure 71b shows the inflated state of a reduced pneu-room size design, the center is barely inflated. These two designs extend less than other three do and have poor distribution, so neither of them will be applied into experiment.
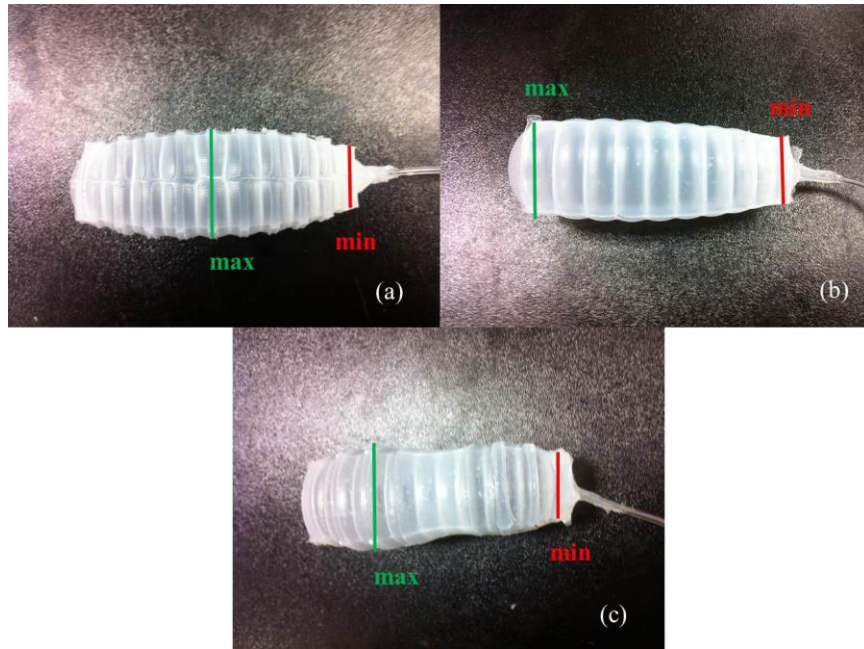
Figure 72: Inflated States of Remaining Three Designs

Figure 72a to Figure 72c provide the inflation state of "full texture" design, "no texture" design and "reinforced center" design. As can be seen, all mechanism has a constraint end (right end). The surface of constraint end is applied with silicone adhesive materials to fix the connection between mechanisms and tubing as well as provide a good sealing ability. The silicone adhesive materials prevent this end from expanding when inflated which causes inevitable uneven distribution. Thus, the minimum deformation of width/height is all occur in the right end (red lines in Figure 72). The "full texture" design inflate most in the middle while "no texture" design most in the free end (green lines in Figure 72). The "reinforced center" design provides a best result and the detailed date is following.

Figure 73 shows the length changing (axial direction deformation) between 1.4psi to 2.3psi. Figure 74 shows maximum height/width versus pressure (1.4psi to 2.3psi)

relationship while Figure 75 shows maximum height/width versus pressure (1.4psi to 2.3psi) relationship.
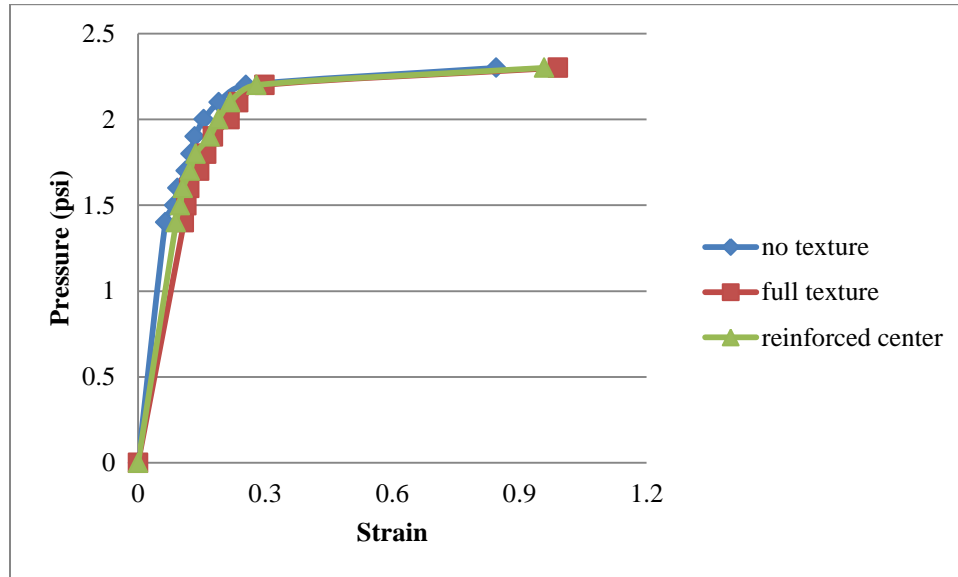
Figure 73: Length Changing of Three Designs of the Extension Mechanism
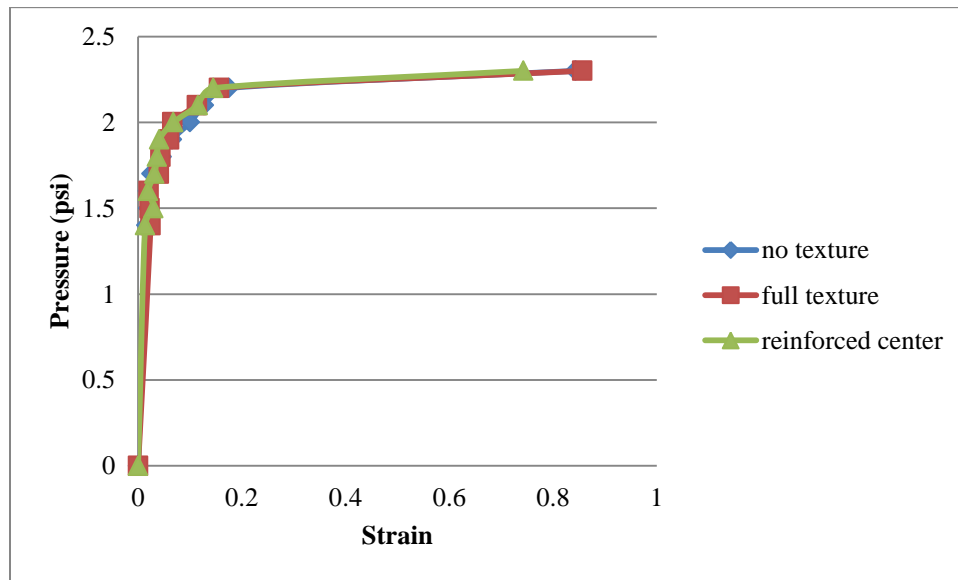
Figure 74: Maximum Height/Width of Three Designs of the Extension Mechanism

85
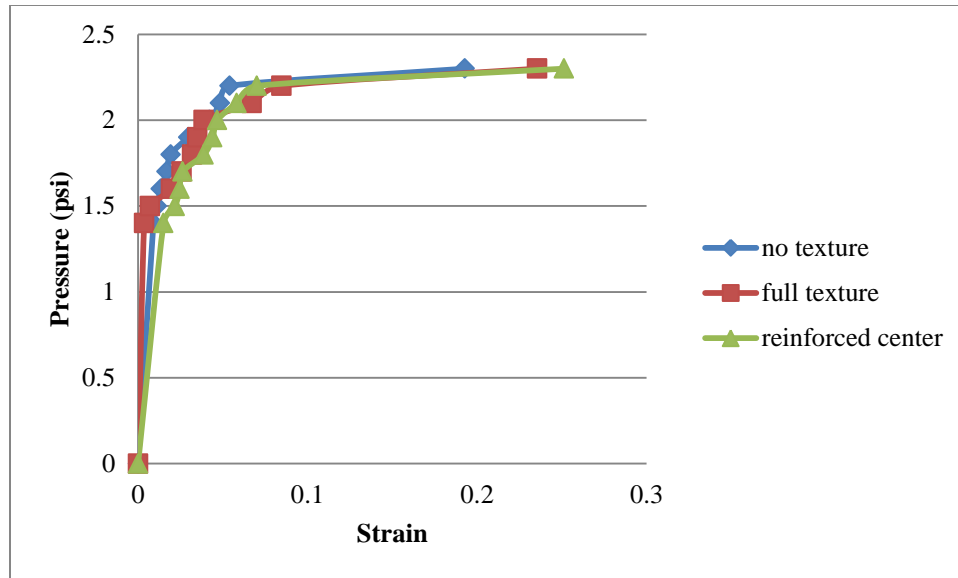
Figure 75: Minimum Height/Width of Three Designs of the Extension Mechanism

The samples with texture can extend longer than "no texture" design. The "full texture" design extends a little more than "no texture" design along the irrelevant direction. "Reinforced center" design not only can extend the similar length as "full texture" design, but also greatly reduced the expansion along the direction perpendicular to the axial direction due to flat ridged center.

Table 4: Data of Inflation Experiment of Third Version of the Extension Mechanisms at 2.3 psi

	full texture	no texture	reinforced center
Length (mm)	79.7	73.8	78.3
Max Height/Width	29.7	29.5	27.9
Min Height/Width	19.7	19.0	20.0

In addition, "reinforced center" design has an evenest distribution which can be clearly seen from and Table 4: it has a smallest value of maximum height/width and a biggest value of minimum height/width. So the "reinforced center" design will be used into the whole interconnection mechanism design.

Chapter 5

Final Interconnection Mechanism Design

In this chapter, a whole design of interconnection mechanism will be carried out and tested. The interconnection mechanism will be equipped onto the modular robot introduced in Section 2.1 to see if it works. The size of the mechanism is constraint by the size of hard version robot. The dimensional design of interconnection mechanism will be followed of the works presented in Chapter 4.

The mold design of the soft mechanism will be presented as well. In addition, in order to assembling the separate capture mechanism and extension mechanism design together as one complete soft mechanism, some essential shape modification for both mechanisms will be presented.

5.1 Design of the Male Port

A male port contains an exterior hard housing, soft capture mechanism and extension mechanism.

5.1.1 Dimensional Design of Capture Mechanism

The much inflated shape of capture mechanism touches the inner surfaces of the female block, the more friction it can generate. Since the height and diameter does not affect the shape of inflation, and the inflated shape under certain pressure can be predicted, the overall initial shape can be decided on the size of the robot. Then, the shape of female block can be decided correspondingly.

Since the rotational block has a sectional area of 46 mm x 46 mm and the hard shell of male port also has a certain thickness, the maximum diameter of capture mechanism in inflation state cannot exceed 46 mm. According to Figure 63 and Table 1, the deformation rate of capture mechanism along radial direction is nearly 200% at 3.0 psi. There are certain chance for the mechanisms to burst if pressure beyond 3.0psi. So the capture mechanism will be operated at a pressure of 2.8psi for the concern of safety and the deformation rate is expected to be a bit lower than 200%.

In conclusion, the initial diameter of the capture mechanism will be 24 mm and the diameter when inflated is expected to be 40-42 mm. The average height deformation rate of capture mechanism is 216.4% at 3.0 psi according to Table 2. The shape changing along the axial direction is not expected to be too large. So the initial height of capture mechanism is chose to be 10 mm and height when inflated is expected to be 21-22 mm.

As can be seen in Figure 68, capture mechanisms with thickness greater than 1.5 mm are not preforming so good when inflated, which is they need much higher pressure to inflate significantly. The capture mechanism with 1 mm in thickness provides an excellent deformation rate along radial direction of 215.7% shown in Table 3, but it is so weak and easy to be burst under 3.0psi or a higher pressure. So the thickness are determined to be 1.3 mm to acquire a good deformation performance and at the same time, to prevent the mechanism from breaking easily.

Other data of size are followed the dimension of third version capture mechanism. The distance of pneu-rooms to the hollow center is 1 mm greater than thickness, which is 2.3 mm. The size of pneu-room is 3.5 mm x 0.6 mm x 7.4 mm.

5.1.2 Dimensional Design of Extension Mechanism

The dimensional design of extension mechanisms are almost following the design of third version extension mechanism. This extension mechanism uses "reinforced center" design, the maximum height and width are 16 mm x 16 mm and the minimum height and width (6 troughs) are 14 mm x 14 mm. the 10 pneu-rooms share a dimension of 0.6 mm x 10 mm x 10 mm. The only difference is the length, which is 39 mm instead of 40 mm in third version extension mechanism design.

5.1.3 Modification of Capture Mechanism Design

The modification here is to make two mechanisms easy to assemble together rather than make for a better inflation performance.

The only modification applied to the capture mechanism is to change the position of hub. Hub is used to fit the position of tubing. Figure 76a shows a third version capture mechanism and its tubing. The tubing is inserted and glued to the mechanism from the outside cylindrical surface. Figure 76b shows the latest design, which shows the tubing is inserted to mechanism from in inside hollow surface.
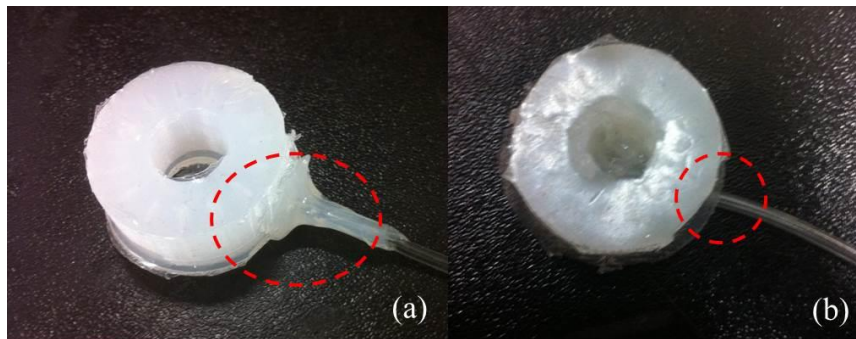
Figure 76: Capture Mechanisms with Tubing, (a) Tubing Connection Location in the Capture Mechanism V3; (b) Tubing Connection Location in the Final Capture Mechanism

The reason for applying this change is when the capture mechanism inflates, the outside surface is supposed to be closely and fully contact with inner surface of the female port. Thus, there is no room for tubing and the glue.

5.1.4 Modification of Extension Mechanism Design

Although the overall dimension of the mechanism is not changed, there are some modifications applied. There are a cylindrical hollow of 2.4 mm in diameter applied in the center of the mechanism. The tubing of capture mechanism, whose outer diameter is 2 mm, will get through from this hole. Figure 77 shows a 3D modeling sectional view of a extension mechanism. The highlighted edges using red dashed line draw the outline of a single pneu-room.

This modification makes the extension mechanism hard to fabricate. Instead of gluing two half third version extension mechanism together, the new extension mechanism has three pieces which need to be glue twice to make a whole body. Two pieces of new extension mechanism are similar to the two pieces of third version extension mechanism which can be seen from their molds: Figure 78a shows the seventh beta version molds for making third version extension mechanism while Figure 78b show the seventh version molds for making the new extension mechanism. They are almost the same except the half cylindrical ridges in the bottom of the seventh version molds which exactly contributes to the fabrication of the hollow center.
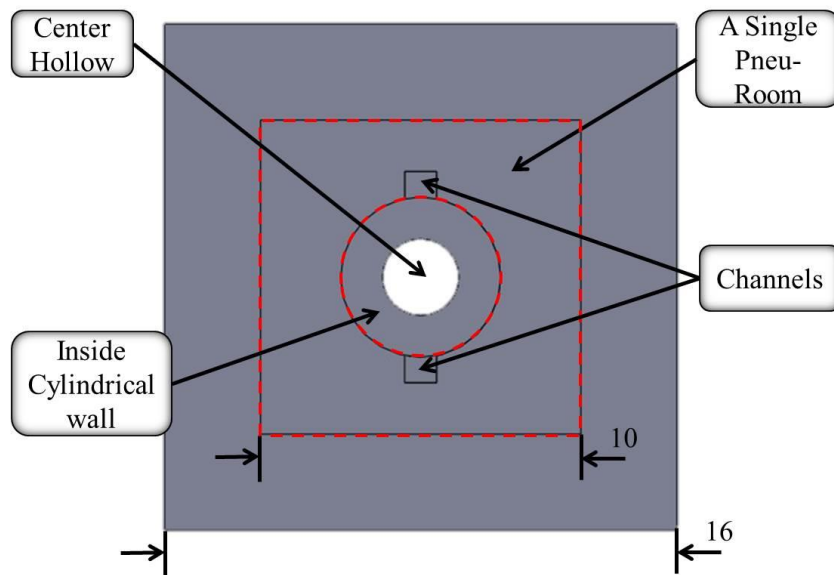
Figure 77: 3D Model Sectional View of a Extension Mechanism
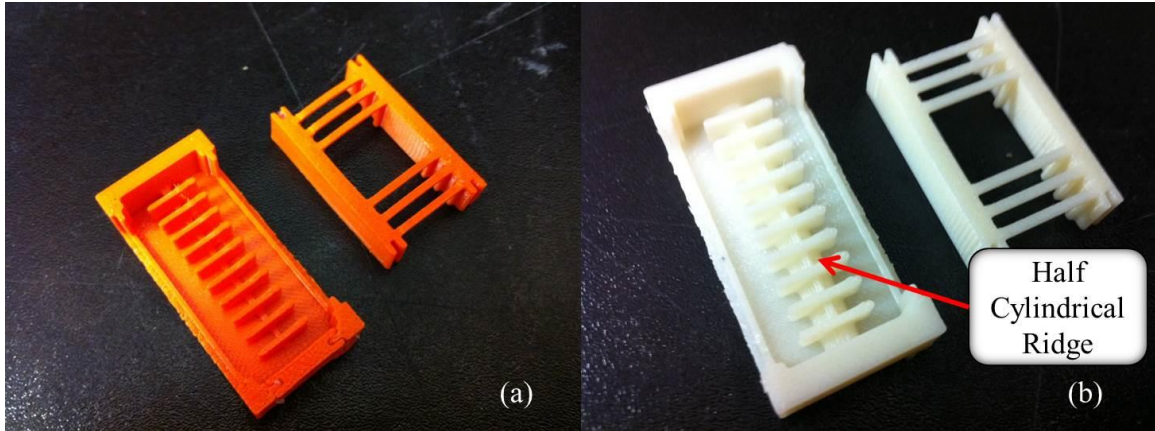
Figure 78: Molds for Extension Mechanisms, (a) Mold V3b; (b) Mold for Final Extension Mechanism

The third piece is a ring-shaped cylindrical part. This part, which acts as an inside surface of the new extension mechanism, together with other surfaces insure every pneu-room sealed. This cylindrical piece has a length of 39 mm, the inner diameter is 2.4 mm and outer diameter is 5 mm. Figure 79 shows a 3D modeling of the mold making cylindrical piece.
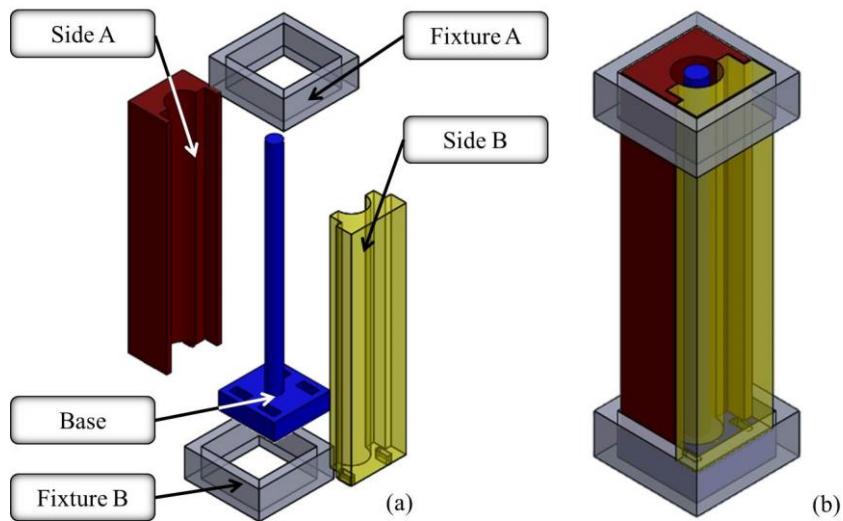
Figure 79: 3D Model for Mold of Making Ring-Shaped Wall, (a) Exploded View; (b) Assembly View

5.1.5 Exterior Hard Housing

The hard shell is a rectangular shell with a thickness of 2.5 mm. The height and width are 46 mm x 46 mm which fit for the size of hard version modular robot. The length is 51 mm which is long enough to hold two soft mechanisms inside. The bottom of the shell has four #2x56 screw holes for assembly to the robot. Figure 80 shows the 3D model of the shell.
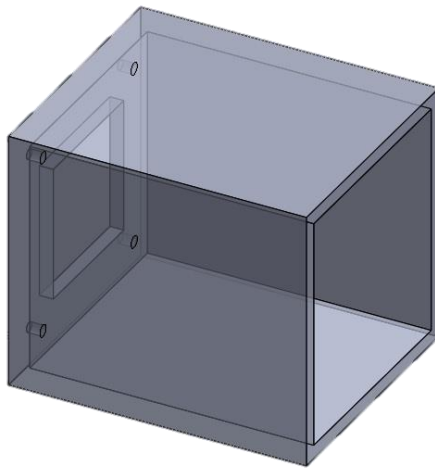
Figure 80: 3D Model of the Male Port Shell

5.2 Male Port Assembly

Figure 81a shows a front view of a whole structure of soft mechanism and Figure 81b gives a trimetric view. The red part is extension mechanism (Figure 81d) and the blue part is capture mechanism (Figure 81f). At one end of the extension mechanism, there is a 2 mm thick soft rectangular sheet (the grey part in Figure 81a and Figure 81c gives an actual image of the sheet). The size of the sheet is 46 mm x 46 mm which is same size as the robot.

94
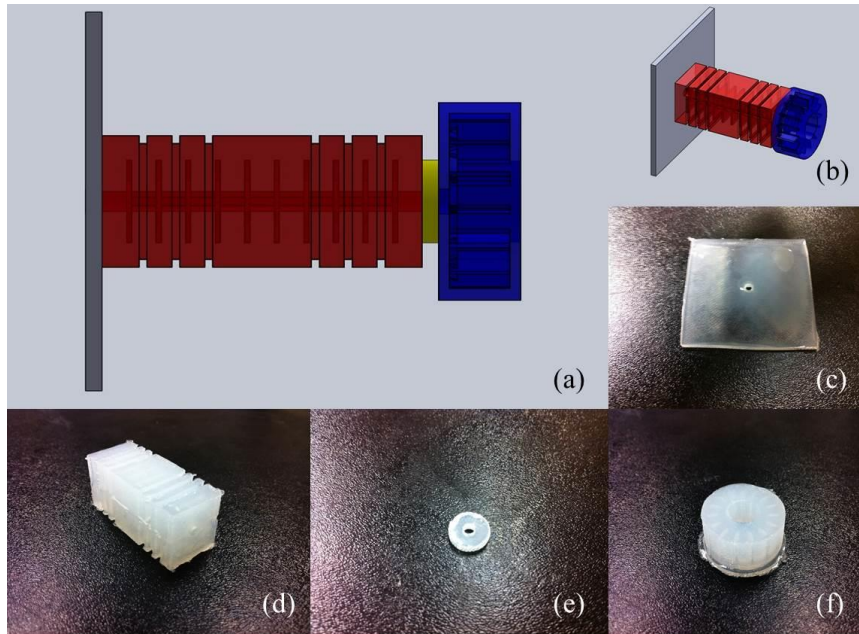
Figure 81: A Whole Soft Mechanism, (a) Front View of 3D Soft Interconnection Mechanism Model; (b) Trimetric View of 3D Soft Interconnection Mechanism Model; (c) Flat Sheet; (d) Extension Mechanism; (e) Connection Ring; (f) Capture Mechanism

During the assembly process, the rotational block of the robot and the male port will clamp the sheet tightly to fix the position of the soft mechanism. The yellow part in Figure 81a is a 2 mm thick disk shape soft piece. The actual image is shown in Figure 81e. The piece is 10 mm in diameter and has a 2.4 mm hole in the center. This piece connects two mechanisms together instead of gluing two pieces together directly. If the two mechanisms glued directly, the glue layer will largely prevent the bottom of the capture mechanism expand along the radial direction when inflated. The yellow piece successfully connect two bocks together while keeps two mechanism in good shape when they are inflated separately.

Figure 82a shows the mechanism before assembling. The male port (in the right) will be assembled onto a rotational block of the robot (in the left). At the same time the

soft mechanism (in the middle) will be assembled into the male port except the rectangular sheet. The sheet will be put in the middle of the rotational block and the male port. Four half inch #2x56 screws and nuts will be used to assemble. Figure 82b gives the image of the mechanism after assembled. In order to give a clear view, a board is used to substitute the rotational block, and a half shell male block is applied to give a vision of the soft mechanism inside the port.
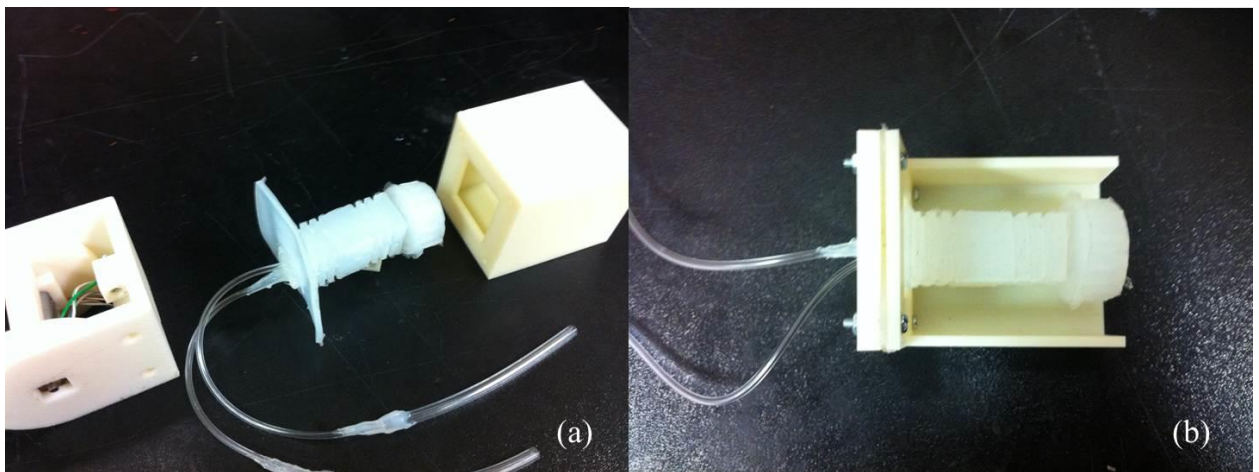
Figure 82: Male Port, (a) Before Assembly; (b) After Assembly

5.3 Female Port

The female port is also a shell. The shell has an external rectangular shape and an inner cylindrical chamber as well as a lip at the opening. Figure 83a shows an isometric view of a female port. The height and width are 46 mm x 46 mm which are the same of a male port. The total length is 26 mm which includes the thickness of lip and bottom (both are 2.5 mm) and the length of cylindrical inner chamber which is 21 mm.
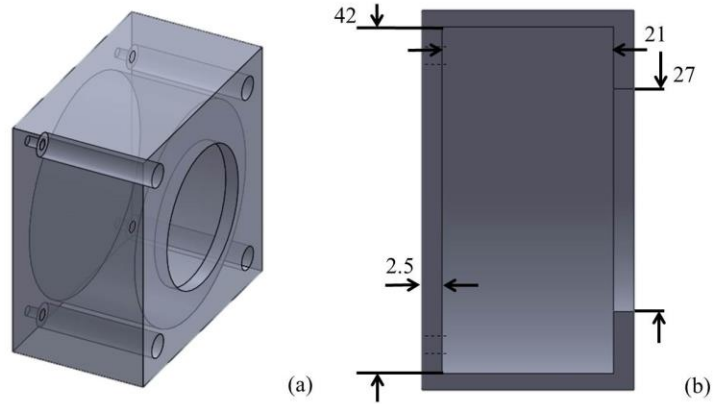
Figure 83: 3D Model of a Female Port

Figure 83b shows the sectional view of a female port which is designed and presented as a C shape. The inner cylindrical chamber is 42 mm in diameter and 21 mm in height which is for fit the inflated capture mechanism. The function of lip is to lock the inflated capture mechanism and make sure that the inflated capture mechanism will not disconnect to the female port in any case. There is a circular opening in the center of the lip which is 27 mm in diameter. The size of the opening is a bit larger than a capture mechanism in its original shape. This open enables extension mechanism to bring the un-inflated capture mechanism inside the inner cylindrical chamber of the female port.

Chapter 6

Experimental Results

This section presents results from two types of experiments. Section 6.1 presents the holistic deformation evaluation of the soft-body interconnection mechanism when inflated under certain pressure ranges. Section 6.2 presents the experimental validation of the design through the successful interconnection of two modular robots.

6.1 Deformation Performance

The test is separated to two parts. Firstly, the extension mechanism will be inflated while the capture mechanisms remains in its original shape. The pressure range is 0 psi to 2.8 psi and the interval is 0.1 psi (most of the extension mechanisms burst when the pressure exceeds 2.8 psi). Secondly, the capture mechanism will be tested at a pressure range of 0 psi to 3.0 psi with an interval of 0.1 psi. The results of the deformation evaluation for the

capture mechanism are provided in Figure 84, Figure 85 and Table 5. The results of the

deformation evaluation for the extension mechanism are provided in Figure 86, Figure 87

and Table 6.
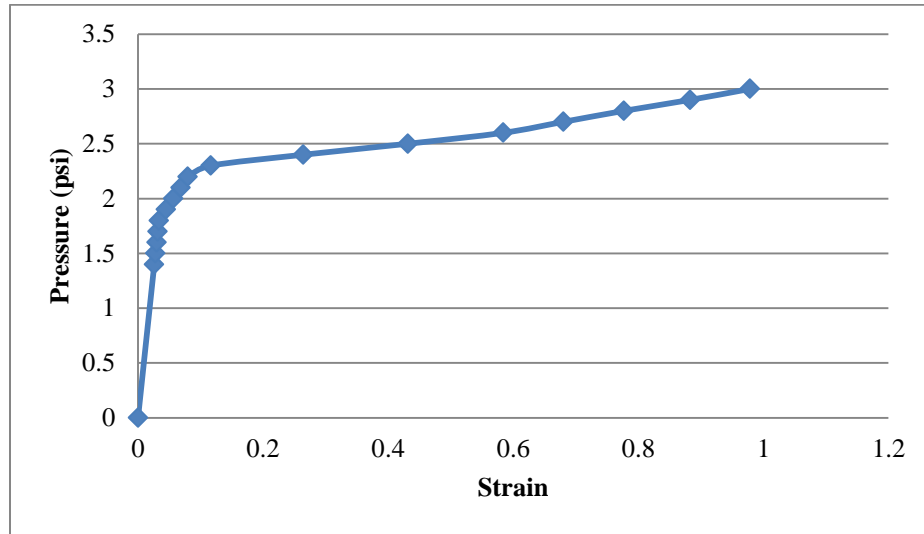
Figure 84: Radial Direction Strain Tests for Capture Mechanisms
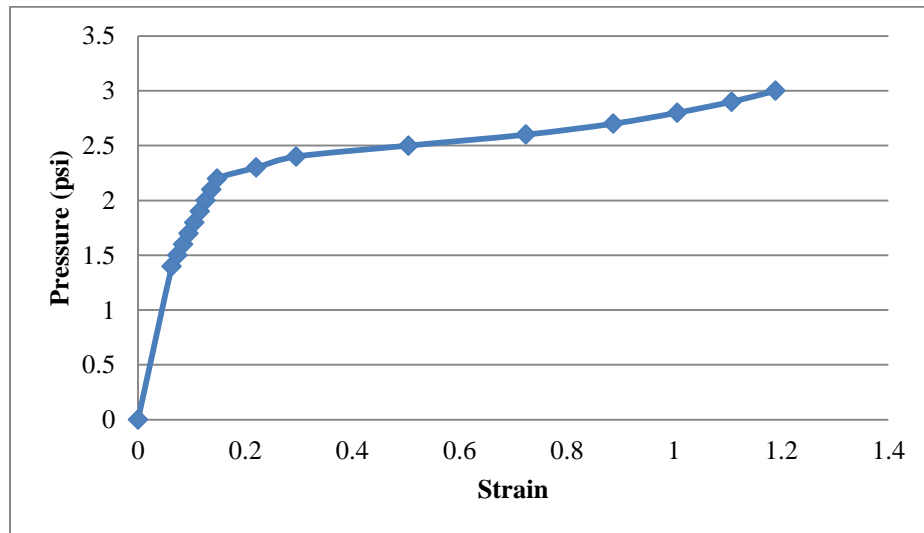
Figure 85: Axial Direction Strain Tests for Capture Mechanisms

Figure 84 and Figure 85 show the pressure versus strain diagrams for radial and

height deformations for the capture mechanism. As expected, the results match the

pressure versus strain diagrams from the empirical study. Table 5 provides more detailed data of the results. The capture mechanism is able to expand up to 197% of its original dimension at 3.0 psi along the radial direction and 222% along the axial direction. Since the capture mechanism has a high possibility bursting at pressures higher than 3.0 psi, the working pressure is chosen to be 2.8psi. At 2.8 psi, capture mechanism is able to expand to 42.64 mm.

Table 5: Data of the Capture Mechanisms Inflation Tests

	Radial Deformation		Height Deformation	
	3.0 psi	2.8 psi	3.0 psi	2.8 psi
Deformation (mm)	47.49	42.64	22.15	20.29
Deformation Rate	197%	177%	222%	203%

Figure 86 and Figure 87 show the pressure versus strain diagrams for the length and height/width deformations of the extension mechanism. The amount of inflation is not as large as predicted. Since pressure beyond 2.8psi will greatly cause the mechanism to burst, the deformation at 2.8psi is taken as the maximum deformation of the extension mechanism. Table 6 provides more detailed data of the results. The deformation rate of at the maximum deformation is 190% which is a little smaller than the deformation rate of the "reinforced center" design extension mechanism. The deformation rate of the "reinforced center" design extension mechanism at 2.3 psi was 201%. The major difference in elongation versus pressure of the newly designed extension mechanism

compared to the "reinforced center" design is due to a shape modification. The newly designed extension mechanism contains an inner cylinder to provide clearance for the inflation tube of the capture mechanism. Having the inner cylinder greatly enhances the strength of the structure which constricts the expansion of the inflated structure.
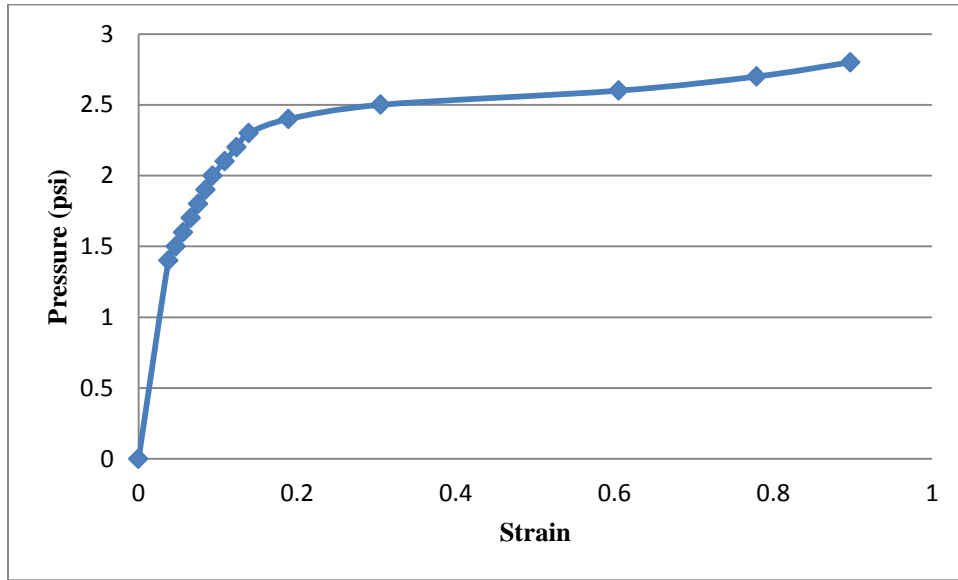
Figure 86: Length Strain of the Extension Mechanisms
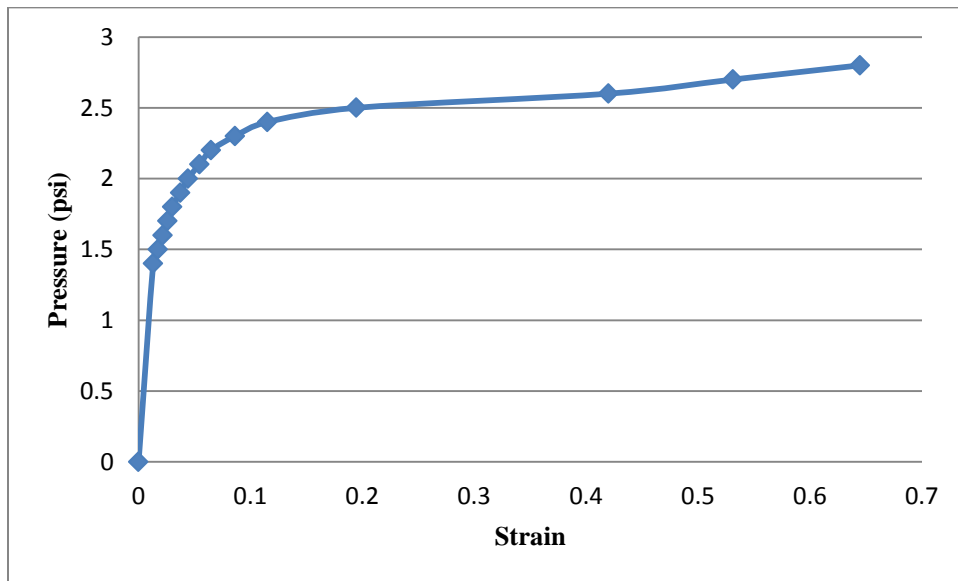
Figure 87: Height/Width Strain of the Extension Mechanisms

101

Table 6: Data of the Extension Mechanisms Inflation Tests

	Length Deformation		Max Height/Width Deformation	
	2.8psi	2.7psi	2.8psi	2.7psi
Deformation (mm)	74.06	69.85	26.43	24.21
Deformation Rate	190%	179%	165%	151%

6.2 Interconnection Validation

To validate the design functionality of the soft-body interconnection mechanism, the design was fabricated and installed onto two hard-shell modular robots. Figure 88a shows the initial state of the experiment.

In order to show the deformation of the soft mechanism, the hard-shell of both the male port and female port are moved apart. A ruler was used as a distance reference. The edge of male port opening is at 14 mm and marked using black tape. The edge of female port opening is at 15.5 mm and also marked with black tape.

Figure 88a shows the initial state of the system with both robots a given distance apart. The first step of the interconnection procedure, as defined in Section 2.1, is to inflate the extension mechanism to insert the capture mechanism into the female port of the mating modular robot. Figure 88b shows the extension mechanism inflated to 2.8 psi with the capture mechanism successfully inserted into the female port of the mating modular robot. The second step is to maintain the elongation of the extension mechanism while inflating the capture mechanism. Figure 88c shows the fully inflated capture

mechanism within the female port of the mating modular robot. Note that part of the capture mechanism extends past the edge of the female port since the female port has been cut in half for visual purposes. With the capture mechanism inflated and securing the modular robot, the extension mechanism is deflated to bring the two modular robots into contact as shown in Figure 88d. The soft-body interconnection mechanism was successfully able to cross a 15 mm gap, securely capture a modular robot, and retract to mate the two modular robots together.
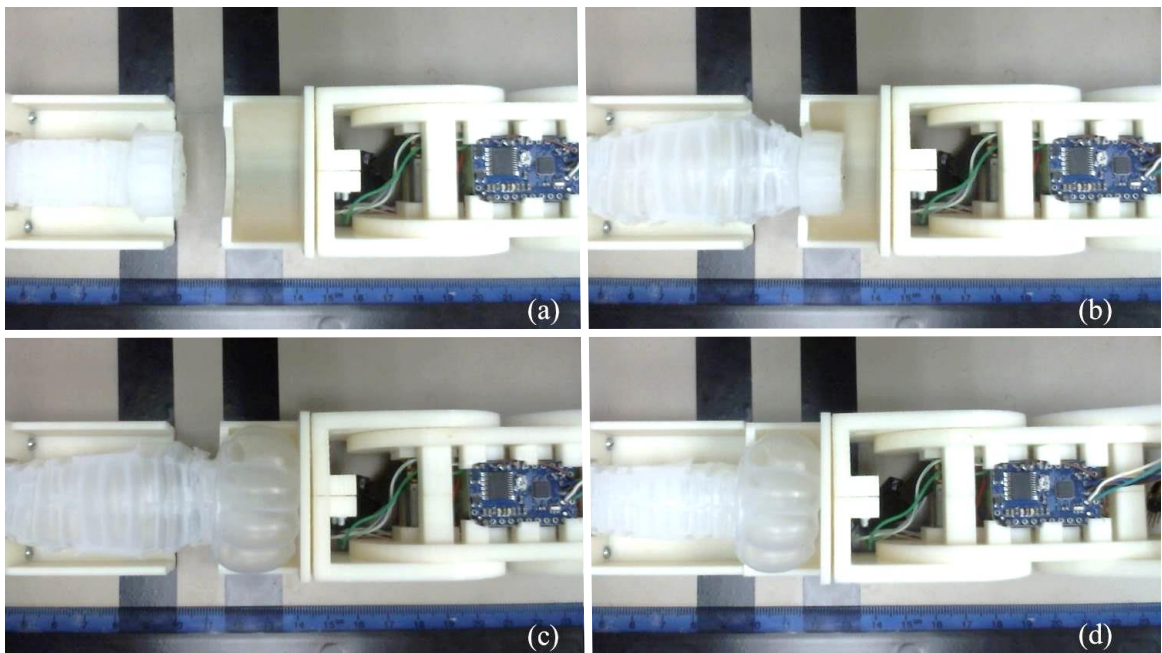
Figure 88: Experiment for Connecting Functionality of the Interconnection Mechanism (a) Initial State; (b) Extension Step; (c) Expansion Step: Capture; (d) Final Step: Retraction

6.3   System Level Testing

In this section, three experiments are executed to evaluate the system level performance of the final soft-body interconnection mechanism. The soft-body interconnection needs to be able to maintain connection when, at least, a force equivalent to the weight of one

modular robot attached is attempting to break the connection. The first experiment determines the pull-out force of the capture mechanism. The second experiment determines the maximum permissible shear force of the capture mechanism. The third experiment determines the maximum holding force and required vacuum for the extension mechanism.

After the capture block inflated to capture a female port, a tensile test and a bending test will be applied to see how much force a capture mechanism can hold. Furthermore, after the extension mechanism deflated to drag the female port back, a tensile test will be applied to see how much force an extension mechanism can hold and a vacuum test will be applied to see how much negative pressure an extension mechanism needs to keep the female port and male port connecting tightly under certain force.

These experiments are applied to see the strength of the soft-body interconnect mechanism as well as to find out whether the soft-body interconnect mechanism can successfully maintain connection under a series of normal tensile forces and shear forces.

6.3.1 Tensile Test for Capture Mechanism

In this experiment, the capture mechanism will be fixed onto a roof and will be inflated in different operated pressure to capture a female port. Under each operating pressure, a series of tensile force will be applied by hanging different weight onto female port. The setup sketch is shown in Figure 89.
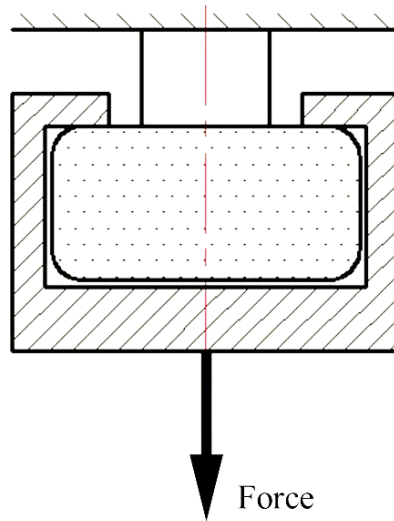
Figure 89: Tensile Test for Capture Mechanism

Since the capture mechanism was not fully inflated under 2.5 psi to 2.7 psi which can be seen in Figure 84, the tensile force it can hold under these pressure is limited. As can be seen in Table 7, the holding force became greater when the inner pressure reached 2.8 psi and higher which indicates: 1) the higher pressure leads to larger friction due to the closer contact between the capture mechanism surface and the inner chamber of the female port, which will help the capture mechanism to hold more forces; 2) the maximum inflation shape of the capture mechanism is limited by the fixed shape of the inner chamber, which means even the inner pressure of the capture mechanism is higher than 3 psi, it is still safe and can generate extra friction.

Figure 90 shows the real capture mechanism performance subjected to 5 N force under 2.8 psi. As can be seen, a portion of the capture mechanism started to squeeze out from the opening of the female port due to the large tensile force.

Table 7: Affordable Tensile Force for Capture Mechanism under Certain Force

Pressure (psi)	2.5	2.6	2.7	2.8	2.9	3.0	3.1	3.2	3.3
Tensile Strength (N)	1.5	2	3.5	4.5	9	10	10	10	10
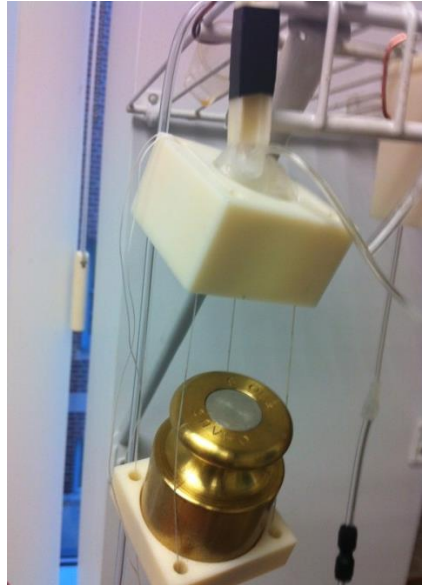
Figure 90: The Capture Mechanism Subjected to 5 N Force under 2.8 psi

6.3.2 Bending Test for Capture Mechanism

In this experiment, the capture mechanism will be fixed onto a wall and will be inflated in different operated pressure to capture a female port. Under each operating pressure, a series of shear force will be applied by hanging different weight onto female port. The setup sketch is shown in Figure 91.
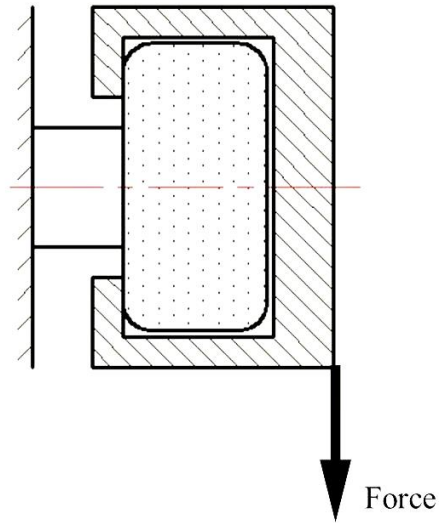
Figure 91: Bending Test for Capture Mechanism

As can be seen in Table 8, the capture mechanism can hold more 5 N weight of the shear forces when it was fully inflated. During the experiment, the capture mechanism started to become dysfunctional when subjected to shear force higher than 5 N. The weakest part is the cured adhesive gel at the tube protrusion location of the capture block, which started to tear of from the capture block and cause a leaking problem.

Table 8: Affordable Shear Force for Capture Mechanism under Certain Force

Pressure (psi)	2.5	2.6	2.7	2.8	2.9	3.0
Shear Strength (g)	2.5	3.5	5	5	5	5

6.3.3 Holding and Vacuum Test for Extension Mechanism

In this experiment, the soft-body mechanism will be fixed onto a roof and the capture mechanism will be inflated to 3psi to capture a female port. The extension mechanism will be deflated to 0psi to maintain a tight connection between the male and female port. Then, the weights attached on the female port will be increased gradually to see how much force the soft-body mechanism can hold. In the main time, a vacuum test will be applied using syringes to see how much negative pressure an extension mechanism needs to keep the female port and male port connecting tightly under each weight interval. The setup sketch is shown in Figure 92.
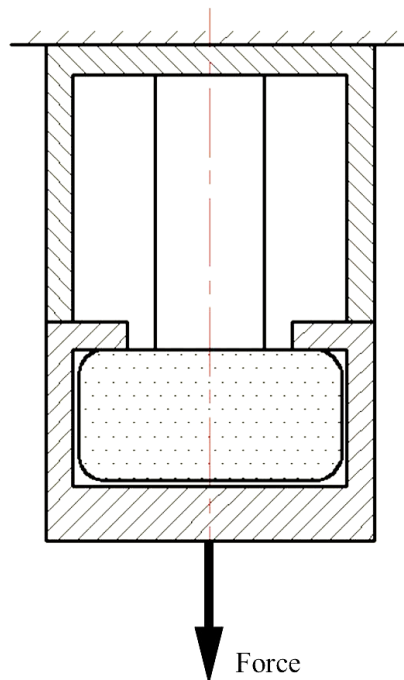
Figure 92: Holding and Vacuum Test for Extension Mechanism

As can be seen in Table 9, the extension mechanism can hold 1.5 N without the help of the vacuum. Then, certain negative pressure is needed to keep the tight

connection. However, when the tensile force reached 4 N and higher, the mechanism will not be able to maintain close connect even with the negative pressure. Figure 93 shows the soft-body interconnect mechanism connection performance when subjected to 2.5 N and 5 N forces.

Table 9: Negative Pressure Needed for Close Connection under Certain Force

Tensile Strength (N)	0	0.5	1	1.5	2	2.5	3	3.5	4
Negative Pressure (psi)	0	0	0	0	-0.16	-0.47	-0.88	-2.62	-9.03
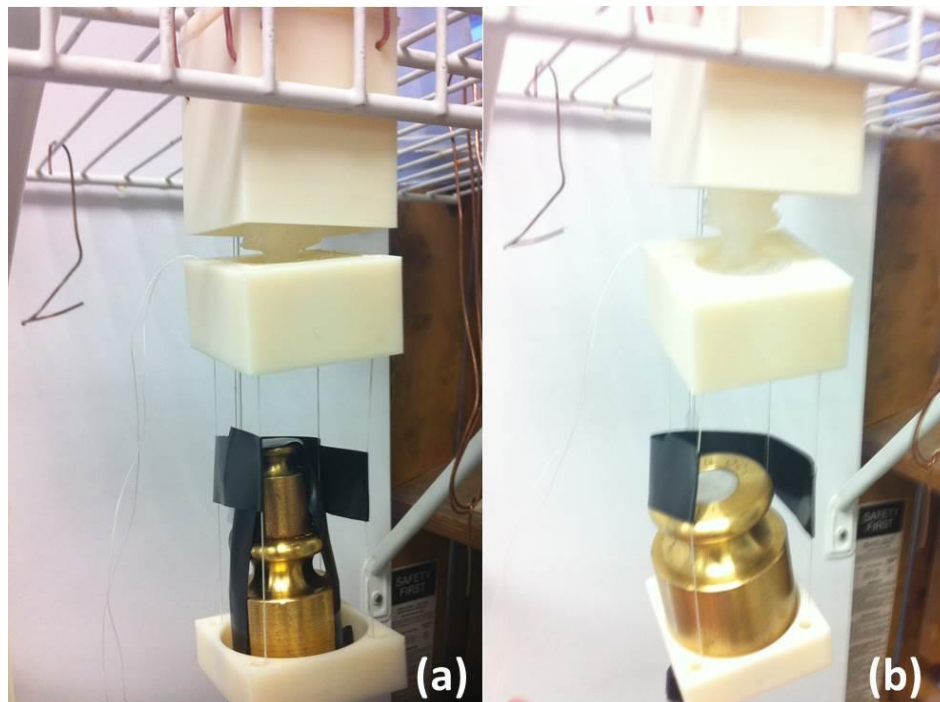
Figure 93: The Soft-Body Mechanism Subjected to Certain Forces, (a) 2.5 N; (b) 5 N

Chapter 7

Discussion and Future Work

The final design of the soft-body interconnection mechanism demonstrates a successful way to intersect the concept of reconfigurable mechanism of modular robotic systems with soft-body materials to create an interconnection mechanism with a long capture range, high misalignment tolerance, and large holding force.

7.1   Discussion

The final version of the soft-body interconnect mechanism can tolerate large misalignments. The 24 mm diameter of the capture mechanism with 27 mm opening of the female port can provide ±9.5 degree angular displacement to the radial direction. The magnet connection method can create large force only when the connecting surfaces are close to each other. The increased distance would largely weaken the connection force

[49]. Therefore, the magnet connection methods do not have a good misalignment tolerance. Some physical latch systems do have certain misalignment tolerance, but limited by the actual size of the latch mechanism, they usually only have a range of ± 1 to 5 degree [27][50].

Since the force generated by magnets is largely depending on the distance between the N and S pole of the magnets, they go not have large capture ability. Some improved version of latch system can reach a 13 mm grasping ability [51]. However, with the length-adjustable functionality of the extension mechanism, the overall elongation of the final soft-body mechanism can reach a maximum of 30 mm while the original size of the extension mechanism is about half of the inflation size to keep to overall mechanism size small.

Just like the magnet system and the latch systems, the soft-body interconnect mechanism can generate enough forces to make the connection as well as to maintain the connection. The mechanism can hold over 1000 grams and can maintain a tight connection with a weight of 350 grams. Furthermore, the soft-body mechanism can handle shear forces.

7.2 Future Work

One future work will be to modify the exterior housing of the interconnect mechanism. The highlighted part in Figure 94a is an idea of enhancing the resistance against bending. The pins and holes highlighted in Figure 94b show in idea of preventing the connected male and female port from twisting when an external torque is applied.
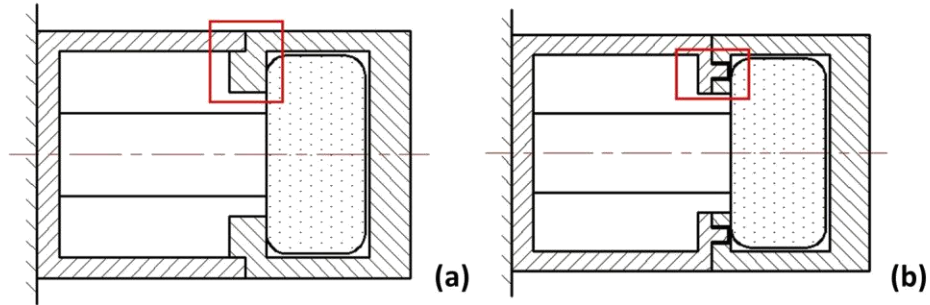
Figure 94: Modification of the Exterior Housing, (a) Bending Resistance; (b) Twisting Resistance

Another future work will be full system integration into a modular robot system. The soft-body mechanism needs a pneumatic actuator to increase the inner pressure to realize the elongation and expansion and needs a vacuum to create negative pressure to maintain the connection. Therefore, a pump and a vacuum should be installed into the robot or a cylinder should be applied as shown in Figure 95. The initial position of the piston of the cylinder should be in the middle for creating either positive or negative pressure when moving to two directions.
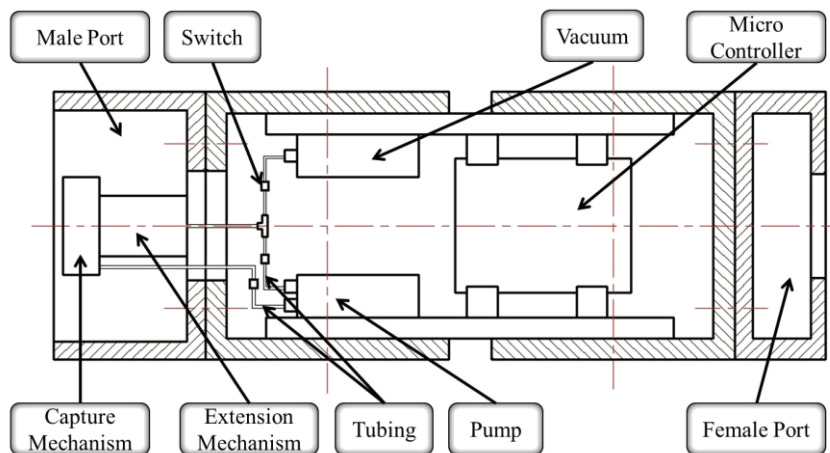
Figure 95: The Conceptual Idea for the Whole System Implementation of the Reconfigurable Modular Robot

For the soft-body interconnect mechanism, one future study would be research on the initial shape and inflated shape of the pneu-rooms. Different pneu-rooms shapes can cause different shapes of overall structure. To design pneu-rooms in different ways to get the equal or unequal distribution when inflated are another point worthy studying. The connection process using adhesive gel between soft-body mechanism and its tubing is complicated. To find an alternative easier way to connect the tubing, either from a design perspective or material selection perspective, will be helpful to simplify the fabrication process. In addition, studying the modeling and simulating way to evaluate the soft-body material will certainly bring huge benefits on the characterization of the soft-body interconnect mechanism.

Chapter 8

Conclusion

To enhance the capabilities of modular robots as support systems for search and rescue operations, a resilient interconnect mechanism is required to allow in-field self-reconfigurability of a modular robot cluster in dangerous environments. Using elastomeric materials, a soft body interconnection mechanism was developed.

The designs of the soft-body interconnection method broke down the mechanism into two separate actuation mechanisms: an extension and capture mechanism. The extension mechanism extends to cross the gap that may exist when two modular robots want to connect together. The capture mechanism, which is attached to the end of the extension mechanism, is inserted into a cavity that exists on the other modular robot. Once the capture mechanism has been inserted into the cavity, the capture mechanism

expands radially to fill the cavity. The expansion of the capture mechanism relies on friction and pressure distribution to securely hold the modular robot. Afterwards, the extension mechanism is collapsed and the modular robots are firmly connected.

An initial study on simulating hypo-elastic materials failed to correlate expected performance results with real-world results. Hence, an iterative design approach was used to determine suitable structural designs for both the extension and capture soft-body mechanisms. The final designs provided the desired 200% deformation of the extension and capture mechanisms along the desired axis. These designs formed the basis for an empirical study to determine how modifications to the structural parameters affect the overall performance of the mechanism.

For the empirical study, an evaluation setup was created to measure the internal pressure of the mechanism sample and the overall deformation of the sample at the given pressure. The results of the empirical study were correlated into diagrams of pressure versus strain. Hence, for a desired elongation or expansion, a designer or engineer can look at the diagrams determine which values should be used for their task. Overall, the diagrams indicate consistent performance outcomes for both the extension and capture mechanisms. For the capture mechanism, the radial deformation scaled with changes to the diameter and height. However, changes to the thickness had drastic effects. Hence, a designer can scale the design to match the constraints of the system. However, care must be taken in the fabrication process to make sure the desired thickness is guaranteed. For the extension mechanism, the axial deformation or axial elongation scaled with the length

and the height/width. Hence, a designer can scale the design to match the constraints of the system.

To demonstrate the use of the diagrams for design, a soft-body interconnection mechanism for in-house designed and fabricated hard shell modular robots was developed. The hard-shell modular robot constrained the overall diameter of the mechanism. The design of the soft-body interconnection mechanism using the diagrams was experimentally validated. The developed soft-body mechanism was able to successfully extend, capture, and lock two hard-shell modular robots together.

References

[1] R. Pfeifer, M. Lungarella, F. Iida, "The Challenges Ahead for Bio-Inspired 'Soft' Robotics," Communications of the ACM, vol. 55, no.11, pp. 76-87, November 2012.

[2] Steltz, E., et al. "Jamming as an enabling technology for soft robotics." SPIE Smart Structures and Materials+ Nondestructive Evaluation and Health Monitoring. International Society for Optics and Photonics, 2010.

[3] Trivedi, Deepak, Christopher D. Rahn, William M. Kier, and Ian D. Walker. "Soft robotics: Biological inspiration, state of the art, and future research." Applied Bionics and Biomechanics 5, no. 3 pp. 99-117, 2008.

[4] Seok, Sangok, Cagdas Denizel Onal, Robert Wood, Daniela Rus, and Sangbae Kim. "Peristaltic locomotion with antagonistic actuators in soft robotics." InRobotics and Automation (ICRA), 2010 IEEE International Conference on, pp. 1228-1233, 2010.

[5] Koichi Suzumori, "Elastic materials producing compliant robots, " Robotics and Autonomous Systems, vol. 18, pp 135-140, 1996.

[6] Chol Kyujin, Chol Yujin, Koh Jesung, Kim Sangwoo, Chu1 Wonshik, Hong Yongtaek , et al., "Review of Manufacturing Processes for Soft Biomimetic Robots ," Iternational Journal of Precision Engineering and Manufaction, vol. 10, no. 3, pp. 171-181, July 2009.

[7] R. F. Shepherda , F. Ilievskia , W. Choia , S. A. Morina , A. A. Stokesa, "Multigait soft robot," in Proceedings of the National Academy of Sciences, vol. 108, no. 51, pp. 20400-20403, December 2011.

[8] E.Yoshida, Satoshi Murata, Shigeru Kokaji, Kohji Tomita, Haruhisa Kurokawa "Micro self-reconfigurable robotic system using shape memory alloy," Distributed Autonomous Robotic Systems 4, pp. 145-154, 2000.

[9] S.Murata, "Hardware Design of Modular Robotic System," in Proceeding of IEEE International Conference of Intelligent Robots and Systems, Takamatsu, Japan, Oct. 30-Nov. 5, pp. 2210-2217, 2000.

[10] K.Hosokawa, "Self-Organizing Collective Robots with Morphogenesis in a Vertical Place," in Proceedings of the IEEE International Conference on Robotics and Automation, Leuven, Belgium, May 16-20, pp. 2858-2863, 1998.

[11] D.Rus and M.Vona, "A basis for self-reconfigurable robots using crystal modules," in Proceeding of IEEE International Conference of Intelligent Robots and Systems, Takamatsu, Japan, Oct. 30-Nov. 5, pp. 2194-2202 ,2000.

[12] Keith Kotay, Daniela Rus Marsette Vona Craig McGray "The self-reconfigurable robotic molecule," in Proceedings of the IEEE International Conference on Robotics and Automation, Leuven, Belgium, May 16-20, pp. 424-431, 1998.

[13] M. Yim, W. Shen, B. Salemi, D. Rus, M. Moll, "Modular Self-Reconfigurable Robot Systems," IEEE Robotics & Automation Magazine, pp. 1070-9932, March 2007.

[14] Wright, Cornell, Aaron Johnson, Aaron Peck, Zachary McCord, Allison Naaktgeboren, et al. "Design of a modular snake robot." In Intelligent Robots and Systems, 2007 IEEE/RSJ International Conference on, pp. 2609-2614, 2007.

[15] Yim, Mark, Kimon Roufas, David Duff, Ying Zhang, Craig Eldershaw, and Sam Homans. "Modular reconfigurable robots in space applications." Autonomous Robots 14, no. 2-3 pp. 225-237, 2003.

[16] Jakopec, M., S. J. Harris, F. Rodriguez y Baena, P. Gomes, J. Cobb, and B. L. Davies. "The first clinical application of a "hands-on" robotic knee surgery system." Computer Aided Surgery 6, no. 6 pp. 329-339, 2001.

[17] Dubowsky, Steven, and D. T. DesForges. "The application of model-referenced adaptive control to robotic manipulators." Journal of Dynamic Systems, Measurement, and Control 101, no. 3 pp. 193-200, 1979.

[18] Şahin, Erol. "Swarm robotics: From sources of inspiration to domains of application." In Swarm robotics, Springer Berlin Heidelberg, pp. 10-20, 2005.

[19] Al-Fahed, A. M., G. E. Stavroulakis, and P. D. Panagiotopoulos. "Hard and soft fingered robot grippers. The linear complementarity approach." ZAMM-Journal of Applied Mathematics and Mechanics/Zeitschrift für Angewandte Mathematik und Mechanik 71, no. 7- 8, pp. 257-265, 1991.

[20] Murakami, Kouji, and Tsutomu Hasegawa. "Novel fingertip equipped with soft skin and hard nail for dexterous multi-fingered robotic manipulation." In Robotics and Automation, 2003. Proceedings. IEEE International Conference on, vol. 1, pp. 708-713, 2003.

[21] Shimoga, K. B., and A. A. Goldenberg. "Soft materials for robotic fingers." InRobotics and Automation, 1992. Proceedings., 1992 IEEE International Conference on, pp. 1300-1305, 1992.

[22] Albu-Schaffer, Alin, Oliver Eiberger, Markus Grebenstein, Sami Haddadin, et al. "Soft robotics." Robotics & Automation Magazine, IEEE 15, no. 3, pp. 20-30, 2008.

[23] Trimmer, Barry A., Ann E. Takesian, Brian M. Sweet, Chris B. Rogers, et al. "Caterpillar locomotion: a new model for soft-bodied climbing and burrowing robots." In 7th International Symposium on Technology and the Mine Problem, Monterey, CA: Mine Warfare Association, vol. 1, pp. 1-10, 2006.

[24] Lee, CS George. "Robot arm kinematics, dynamics, and control." Computer 15, no. 12 (1982): 62-80.

[25] Rolf, Matthias, and Jochen J. Steil. "Efficient exploratory learning of inverse kinematics on a bionic elephant trunk," pp. 1-1, 2002.

[26] H. Kurokawa, K. Tomita, A. Kamimura, S. Murata, Y. Terada, "Distributed metamorphosis control of a modular robotic system M-TRAN," Distributed Autonomous Robotic Systems 7, Springer, pp. 115-124, 2006.

[27] M. Yim, Y. Zhang, K. Roufas, D. Duff, "Connecting and disconnecting for chain self-reconfiguration with PolyBot," IEEE/ASME Transactions on Mechatronics , vol. 7, pp. 422-451, 2002.

[28] A. Kamimura, S. Murata, E. Yoshida, H. Kurokawa, K. Tomita, "Self-Reconfigurable Modular Robot Experiments on Reconfiguration and Locomotion," International Conference on Intelligent Robots and Systems Maui, Hawaii, USA, pp. 606-612, 2001

[29] V. Luboz, E. Promayon, G. Chagnon, T. Alonso, D. Favier, et al., "Validation of a Light Aspiration device for in vivo Soft Tissue Characterization," Soft Tissue Biomechanical Modeling for Computer Assisted Surgery, Yohan Payan (Ed.), pp. 243-256, 2012.

[30] A. Atieh, "Design, Modeling, Fabrication and Testing of a Piezoresistive-Based Tactile Sensor for Minimally Invasive Surgery Applications," Thesis, Mechanical Engineering of Concordia University, Montreal, Quebec, Canada April 2012.

[31] D. Floreano, J.C. Zufferey, M.V. Srinivasan, C. Ellington (Eds.), "Flying insects and Robots," Springer, 2009.

[32] H. T. Lin, G.G. Leisk, B. Trimmer, "GoQBot: A caterpillar-inspired soft-bodied rolling robot," Bioinspiration and Biomimetics, vol.6, no. 2, pp 1-14, 2011.

[33] R. V. Martinez, J. L. Branch, C. R. Fish, L. Jin, R. F. Shepherd, "Robotic Tentacles with Three-Dimensional Mobility Based on Flexible Elastomers," Advanced Materials. Vol. 5, pp 205-212, 2013.

[34] Filip Ilievski, Aaron Mazzeo, Robert Shepherd, Xin Chen, George Whitesides, "Soft Robotics for Chemists," Angewandte Chemie International Edition, Vol. 50, pp 1890-1895, 2011.

[35] C. Laschi, B. Mazzolai, V. Mattoli, M. Cianchetti, P. Dario, "Design of a biomimetic robotic octopus arm," Bioinspiration and Biomimetics," Vol. 4, pp. 1–8, 2009.

[36] H. R. Choi, S. M. Ryew, K. M. Jung, H. M. Kim, J. W. Jeon, "Soft Actuator for Robotic Applications Based on Dielectric Elastomer : Quasi-static Analysis," IEEE lntemational Conference on Robotics and Automation, Washington DC, pp. 3212-3217, May 2002.

[37] F. Daerden, D. Lefeber , "Pneumatic Artificial Muscles: actuators for robotics and automation," European journal of mechanical and environmental engineering, vol. 47, pp 11-21, 2002.

[38] I. Gravagne, I.D. Walker, "On the Kinematics of RemotelyActuated Continuum Robots," IEEE International Conference on Robotics and Automation, San Francisco, CA, USA, April 24-28, pp. 2544-2550, 2000.

[39] Y. Nakabo, T. Mukai, Asaka, "Propulsion model of snake-like swimming artificial muscles," Proceeding of IEEE International Conference on Robotics and Biomimetics, June 18-22, Hong Kong, pp 1855-1861, 2005.

[40] G. S. Chirikjian, "Theory and applications of hyper-redundant robotic manipulators," Ph.D. dissertation, Department of Engineering & Applied Science, Califomia Institute, Technol., Pasadena, May 1992.

[41] F. Boyer, M. Porez, W. Khalil, "Macro-continuous Computed Torque Algorithm for a Three-dimensional Eel-like Robot," IEEE Transactions on Robotics, pp. 563-775, 2006.

[42] Ahmad Atieh, Masoud Kalantari, Roozbeh Ahmadi, Javad Dargahi, Muthukumaran Packirisamy, and Mehrdad Hosseini Zadeh, "FEM Analysis of the Interaction between a Piezoresistive Tactile Sensor and Biological Tissues," World Academy of Science, Engineering and Technology 54, pp 106-110, 2011.

[43] Stephanie M. Shaw, "Frequency Response of Synthetic Vocal Fold Models with Linear and Nonlinear Material Properties," Thesis, Department of Communication Disorders, Brigham Young University, 2009.

[44] Yung-Yu Hsu, Kylie Lucas, Dan Davis, Brian Elolampi, Roozbeh Ghaffari, et al., "Novel Strain Relief Design for Multilayer Thin Film Stretchable Interconnects," IEEE Transactions on Electron Devices, vol. 60, no. 7, pp 2338-2345, 2013.

[45] Vincent Luboz, Emmanuel Promayon, Grégory Chagnon, Thierry Alonso, Denis Favier, "Validation of a Light Aspiration device for in vivo Soft TIssue Characterization (LASTIC)," Soft Tissue Biomechanical Modeling for Computer Assisted Surgery, Yohan Payan (Ed.), pp 243-256, 2012.

[46] R. F. Shepherd, F. Ilievski., W. Choi, S.A. Morin, A.A. Stokes, et al., "A Multi-Gait Soft Robot," Supporting Information, unpublished.

[47] Aidy Ali, M. Hosseini, B.B. Sahari, "A Review of Constitutive Models for Rubber-Like Material," American Journal of Engineering and Applied Sciences vol. 3, no. 1, pp. 232-239, 2010.

[48] A.F.M.S. Amin, M.S. Alam, Y. Okui, "An improved hyperelasticity relation in modeling viscoelasticity response of natural and high damping rubbers in compression: experiments, parameter identification and numerical verification," Mechanics of Materials vol. 34, pp. 75-95, 2002.

[49] Satoshi Murata, Eiichi Yoshida, Akiya Kamimura, Haruhisa Kurokawa, Kohji Tomita, and Shigeru Kokaji. "M-TRAN: Self-reconfigurable modular robotic system." Mechatronics, IEEE/ASME Transactions on 7, no. 4 pp. 431-441, 2002.

[50] Alexander Sproewitz, Masoud Asadpour, Yvan Bourquin, and Auke Jan Ijspeert. "An active connection mechanism for modular self-reconfigurable robotic systems based on physical latching." In Robotics and Automation, IEEE International Conference on, pp. 3508-3513, 2008.

[51] Wei, Hongxing, Youdong Chen, Jindong Tan, and Tianmiao Wang. "Sambot: A self-assembly modular robot system." Mechatronics, IEEE/ASME Transactions on 16, no. 4 pp. 745-757, 2011.